DOCTOR OF PHILOSOPHY

Stability and Instability of Planar Layers of Smectic A Liquid Crystals

Alsuhaimi, Omar Ameer

Award date:
2021

Stability and Instability of Planar Layers of Smectic A Liquid Crystals

Omar Ameer Alsuhaimi

Mathematics

University of Dundee

This dissertation is submitted for the degree of

Doctor of Philosophy

July 2020

Declaration

I declare that the following thesis is my own composition and that it has not been submitted before in application for a higher degree.

Omar Alsuhaimi

Acknowledgements

First, I want to thank my supervisor, Professor Iain W Stewart, for his unstinting patience and support. Through his encouragement and guidance, I was able to maintain a professional approach and stay on course with this work even when the going was hard. Without his assistance at every stage, the goal of this project would not have been attained. I also wish to express my gratitude to Professor Gunnar Hornig for his support during my research at the University of Dundee. Also, thank you to Dr. Geoffrey McKay and Prof. Nigel Mottram for their supervision during my research at the University of Strathclyde. Thanks also to my sponsor, Taibah University in Saudi Arabia for financial support. Last, but by no means least, I wish to express my heartfelt gratitude for the great support of my family, especially my mother, my wife, my children, and my sisters. They kept me going, and this work would not have been possible without their loving presence.

Abstract

We consider the mathematical modelling of smectic A liquid crystals using the continuum dynamic theory for smectic A liquid crystals that has been developed by Stewart [79]. We also examine biaxial nematic liquid crystals using the continuum theory of Leslie and co-workers [50, 51] and the review by Stewart [80].

The Helfrich-Hurault transition is considered in this thesis to study the influence of the compression coefficient B_0 when an electric field is applied. The molecular alignment described by the director $\mathbf{n}$ and the unit layer normal $\mathbf{a}$ of a smectic A sample is considered to be not coincident, unlike the classical smectic A theory where they coincide. Stability and instability in various situations with and without an electric field will be discussed. Finally, the dynamic continuum theory of biaxial nematic liquid crystals is an integral part of this thesis. This theory will be applied to incompressible biaxial nematic liquid crystals to study the linear stability and instability of a planar alignment sample of biaxial nematic under oscillatory shear flow.

Contents

List of Figures

List of Tables

Chapter 1

Introduction

1.1 History of liquid crystals

Matter is commonly classified into three states; solid, liquid and gas. Solids are rigid and have a fixed volume and shape. They do not flow easily due to the immobility of the particles and are not easily compressible due to the close proximity of the particles. In a solid, the molecules are arranged in regular patterns and have fixed positions and directions.

On the other hand, liquids take up space due to their flow and variable shape that conforms to their container. The majority of liquids are incompressible due to the close proximity of the particles but they can move freely. Additionally, because molecules flow easily around one another in liquids, they lose their positions and directions, as illustrated in Figure 1.1.

Reinitzer, an Austrian botanist, discovered a new state of matter called liquid crystals in 1888 when he observed the unusual melting behaviour of cholesteryl benzoate, which he extracted from natural cholesterol in carrots [26, 69, 74]. How-

ever, some scientists observed liquid crystals prior to Reinitzer, but they were unable to explain the phenomenon [44]. Liquid crystals are between the solid crystal state and the isotropic liquid state. Isotropy refers to the property of being uniform in all directions (it derives from the Greek words isos (equal) and tropos (way). *Isotropic* materials exhibit the same physical properties in all directions, whereas anisotropic materials have physical properties that vary according to the direction [78]. Liquid crystals are anisotropic and they flow like fluids but have the molecular alignment characteristics of solid crystals. As a result, they exhibit both liquid and solid crystal properties, hence the name liquid crystals (see Figure 1.2). Reinitzer wrote a letter to Otto Lehmann, a German physicist, on 14 March 1888. This letter served as the catalyst for the discovery and development of thermotropic liquid crystals. After twenty years of research, the existence of the liquid crystals was proved. Reinitzer discovered a new phenomenon involving the two melting points and forwarded his observation to physicist Lehmann for further investigation [26, 41]. Reinitzer observed that there are two melting points with generation of colours when he heated a sample of cholesteryl benzoate. At the first melting point (at 145.5°C), the substance (solid) became a cloudy liquid, then at a second melting point (at 178.5°C), it changed to a clear liquid. Additionally, W. Heintz observed the second point for Stearin materials [41]. Observations of Reinitzer and Heintz guided Lehmann to investigate them experimentally. He used his polarizing microscope to study this strange phenomenon. His research on this phenomenon resulted in the discovery of the fourth state of matter, which is now referred to as liquid crystals [12, 26]. In 1922, Friedel classified liquid crystals into three kinds, nematics, cholesteric and smectic [25, 31].

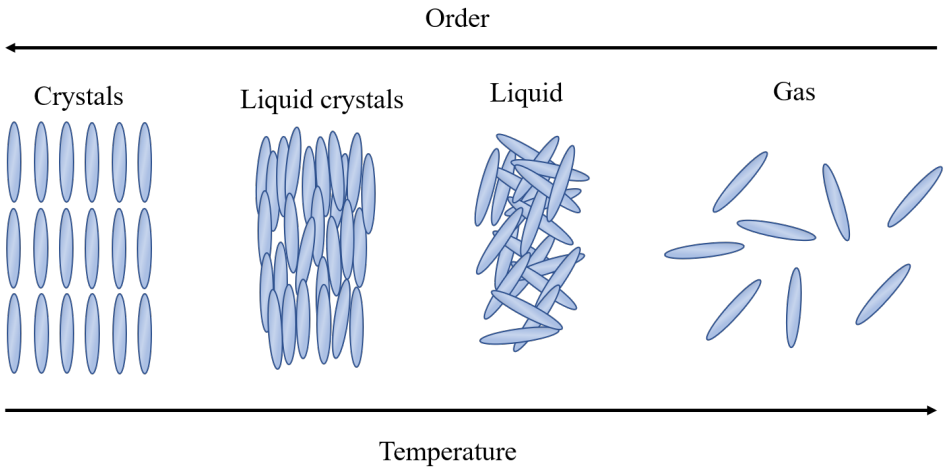

Figure 1.1: This represents the states of matter and their molecules ordering.

In 1962, the research of Richard Williams (from the Princeton Institute of RCA) led to patented light scattering types of electro-optical devices for LCD development. Williams' discovery guided Heilmeier (from RCA) to conduct further investigation on liquid crystals [12, 43]. Major technological breakthroughs were also made in 1970 and 1971 by Schadt and Helfrich [37, 72]. As a result, the new technology piqued the interest of a large number of companies, which worked on the development and application of liquid crystal displays and demonstrated some significant products using liquid crystals, such as LCD televisions, calculators, and computers.

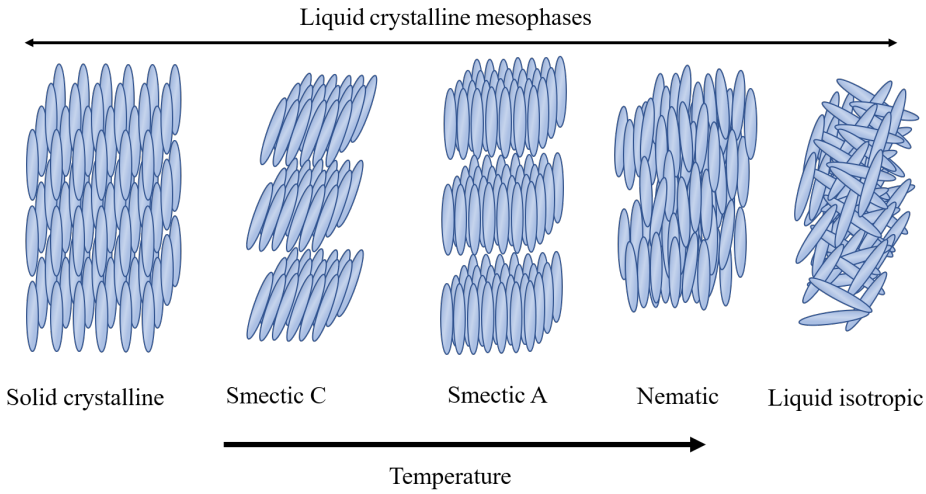

Figure 1.2: Liquid crystals phases.

1.2 What are liquid crystals?

In general, liquid crystals are organic materials that fall between crystalline solids and isotropic materials. Liquid crystals consist of elongated rod-like molecules, called calamitic, or known as discotic when the organic molecules are disk-like. They are also ordered fluid phases [24, 87, 88].

The constituent liquid crystals molecules are measured in nanometres (nm), and the ratio of the length to the diameter in the rod-like molecules or the ratio of the diameter to the thickness of the disk-like molecules is approximately five times larger [21, p. 3], [88]. Typical molecules in a nematic are around 2nm in length and 0.5nm in width. Lengths range from approximately 2nm to 10nm. In liquid crystals, the local direction of average molecular alignment is described by a unit vector $\mathbf{n}$, referred to as the director. As mentioned in the previous section, liquid crystals are classified into three broad fundamental classes: nematics, cholesterics, and smectics. This section will discuss nematics and cholesterics briefly before

delving deeper into smectic liquid crystals.

In general, liquid crystals can also be classified according to their response to temperature changes, referred to as thermotropic liquid crystals, or their response to changes in the concentration of a solvent, referred to as lyotropic liquid crystals. Here, we will focus on thermotropic liquid crystals [20, 87].

1.2.1 Nematic liquid crystals

Nematics are the most widely studied liquid crystals. They are also the most widely used. Nematics are generally regarded as having a crystalline structure. When in equilibrium, an aligned sample can thus be regarded as a single aligned crystal in which the molecules are aligned along the direction defined by the director $\mathbf{n}$. The nematic phase is essentially a one-dimensionally ordered elastic fluid in which the molecules are orientationally ordered, but where there is no long-range positional ordering of the molecules, as illustrated in Figure 1.3. Nematic liquid crystals are mainly used in LCD devices. Their high fluidity and low viscosity make them ideal for the manipulation of electric and magnetic fields [1, 24, 44, 87].

1.2.2 Cholesteric liquid crystals

The cholesteric liquid crystal phase is the counterpart of the nematic phase except that the molecules exhibit a chiral pattern with a given pitch and the alignment can be visualised via cross-sectional layers each with an individual uniform director alignment $\mathbf{n}$ represented in each layer [1, 78], see Figure 1.4. The director changes periodically across these cross-sectional layers as shown. The gradual change in director alignment across layers is described by a helix with a temperature-dependent pitch P [19, 57]; in most cases, the temperature is fixed, and thus P is a constant in the modelling. The pitch of a cholesteric liquid crys-

tals phase is defined as the distance between two layers where the director rotates 360° [57, 78]. Note that the structure of the cholesteric liquid crystals phase is repeated with a period $P/2$ because $\mathbf{n}$ and $-\mathbf{n}$ are indistinguishable [78].

Cholesteric derivatives were the first materials to exhibit the cholesteric phase [19], and thus the chiral nematic phase was named the cholesteric phase. In fact, a cholesteric liquid crystal can be obtained either naturally or by adding a trace amount of chiral material to nematic material [19, 57]. Moreover, the helical structure has the ability to reflect light of a wavelength similar in magnitude to P [25,44]. Suppose that the helix is parallel to the z direction, the director $\mathbf{n}(\mathbf{r})$ can be described by [25]

$$\mathbf{n}(\mathbf{r}) = \begin{pmatrix} \cos\left(\frac{2\pi}{P}z + \varphi_0\right) \\ \sin\left(\frac{2\pi}{r}z + \varphi_0\right) \\ 0 \end{pmatrix}, \tag{1.1}$$

where we assume that P is the constant temperature-dependent pitch of the helical superstructure and φ_0 is a constant that depends on the boundary conditions.

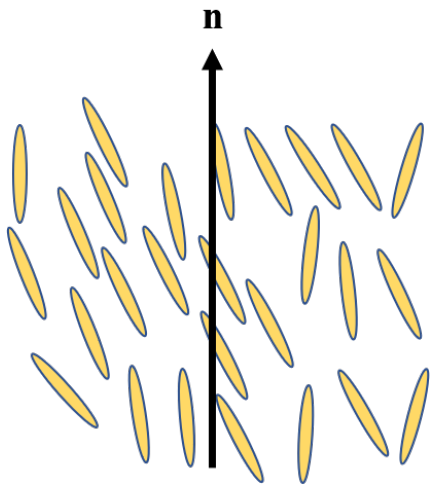

Figure 1.3: The structure of the nematic phase [35].

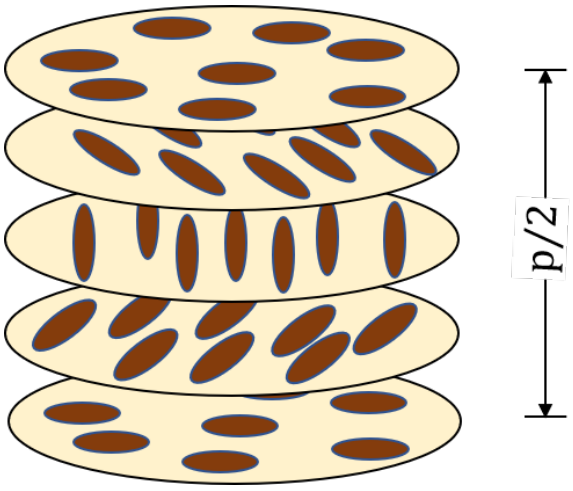

Figure 1.4: The structure of the cholesteric phase [57].

1.2.3 Smectic liquid crystals

Smectic liquid crystals are liquids in which the molecules form layered structures with a well-defined interlayer distance, resulting in their long axes being perpendicular to the layer planes on average. In general, the molecules in a nematic tend to be aligned on average with a unit vector $\mathbf{n}$ which is called the director [24, 63]. Smectics, on the other hand, are more ordered than nematics, as seen in Figure 1.5. Here we consider only the smectic A liquid crystal phases. For other smectic liquid crystal phases, details can be found in de Gennes and Prost [21]. For the smectic A phase, the molecules are arranged in layers where their alignment is perpendicular to these layers and parallel to the layer normal; see Figure 1.5a. Whereas, in smectic C liquid crystals, the director makes an angle θ with the layers; see Figure 1.5b. Note that the director $\mathbf{n}$ is the average direction of the molecular alignment, where $\mathbf{n}$ and $-\mathbf{n}$ represent identical directions due to the symmetry of the nematic phase.

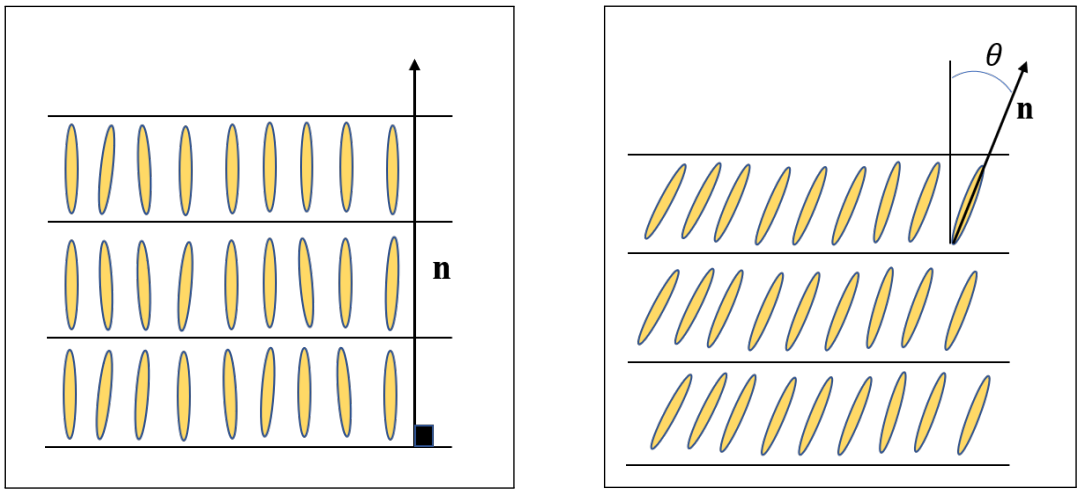

(a) Smectic A (b) Smectic C

Figure 1.5: The structure of the smectic A and smectic C phase [62].

In SmC liquid crystals, the layer normal **a** in the Cartesian coordinates is a unit vector that is perpendicular to the liquid crystal sample layers. By contrast, the vector **c** is the unit orthogonal projection of **n** onto the smectic planes [21,78]. For more information, consult the books [3, 21, 63]. In Smectic A, we will use these ideas for **n** and **a** in Chapters 3-5.

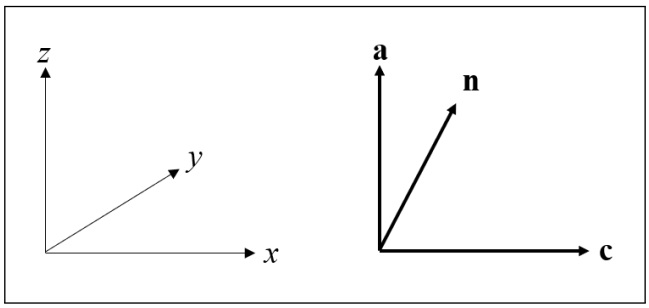

Figure 1.6: The unit vectors **a** and **c** that describe the arrangement of a planar aligned sample of SmC liquid crystal in Cartesian coordinates [78]. Note that **c** is the unit orthogonal projection of the director **n** onto the xy-plane.

1.3 Viscosity in liquid crystals

Viscosity is the one of the most important concepts in liquid crystals. It is related to the measurement of a fluid's resistance to motion when the frictional force between adjacent fluid layers in a liquid crystal. The viscosity in liquid crystals is generally described in terms of numerous viscosity coefficients (e.g., five in the usual nematic phase, cf. Appendix A and section A.3). Moreover, viscosity is dependent on temperature by the given relation

$$\eta = \eta_0 \exp\left(\frac{E}{k_{\mathrm{B}}T}\right)$$

where $E > 0$ is activation energy for the diffusion molecular motion and η_0 is a constant, and k_B is the well-known Boltzmann constant of statistical physics. It clear that from the equation above that viscosity decreases as temperature increases [12, 13, 22, 64, 87].

1.4 Elasticity in liquid crystals

Elasticity means that the shape of body can be changed in response to external forces and then revert to its original shape. It is well known that solids have elasticity, whereas liquids do not. By contrast, liquid crystals exhibit elasticity. This means that when an external force (an electric or magnetic field) acts on a liquid crystal sample, its director orientation changes. As a result, for example, a nematic liquid crystal can be distorted and one of three possible deformation types occurs (the presence of these deformation types depends on the type of liquid crystal). These three types of distortion are referred to as splay, twist, and bend, and are represented by the K_{11}, K_{22} and K_{33} (collectively referred to as elastic constants), respectively. These elastic constants have a range of magnitudes.

Additionally, this deformation generates energy. [12, 25, 26, 82, 88].

In the nematic liquid crystal phase, for example, the three basic elastic deformations that can occur are shown in Figure 1.7 below, and the energy produced is called Frank free-energy density, see Appendix A. For more details on elasticity in liquid crystals, see, [1, 20, 22, 42, 64]

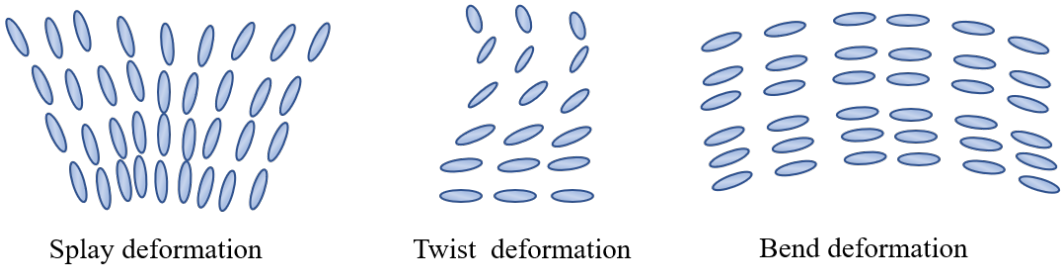

Figure 1.7: The three possible deformation types in nematic liquid crystals.

1.5 Liquid crystals and disease

Biological cells are surrounded by a liquid crystal membrane. It allows the transport of various biomolecules through the cell membranes [26]. A group of researchers at the University of Chicago's Institute for Molecular Engineering are putting liquid crystals to work as detectors for protein fibres. This is an advanced step using liquid crystals in medicine. Liquid crystals could be used to monitor the development of protein fibres that are implicated in the development of Alzheimers and other neuro-degenerative diseases [70].

1.6 Outline of thesis

This mathematics-based mechanics research project is to apply nonlinear smectic A liquid crystal dynamic theory to some unexpected and novel fluid flow effects which have been observed by various researchers, especially in relation to the mechanics of transverse flow and transient two-dimensional instability patterns induced by electric or magnetic fields. Other effects will then be investigated, especially those relating to defects and disclinations in smectic liquid crystals, which have been examined experimentally, where it is known that stable and transient pattern formation states can be induced. It is also known that smectic A liquid crystals behave in unusual ways in simple shear experiments and that these effects are highly nonlinear and remain to be understood and explored. The solutions to the mathematical equations that arise from applications of the dynamic theory will provide qualitative results that will be central to the understanding of all these phenomena and will form the major part of the research. The consequences will then be investigated further in relation to other aspects of these highly complex non-Newtonian fluids.

Chapter 1 starts with a brief history and explanation of liquid crystals and their development. It also provides a description of the liquid crystalline phases, nematic, cholesteric and smectic liquid crystals. Also, we a give brief review of viscosity and elasticity in liquid crystals. Appropriate summaries of relevant results and mathematical notation from the continuum theory of liquid crystals literature are contained in the Appendices, for the convenience of the reader, and are referred to at various parts of the thesis.

The dynamic continuum theory of nematics (established by Ericksen and Leslie) and smectics (developed by Leslie and co-workers) [21,78] will be explained in detail

in Chapter 2 and Chapter 4, respectively. We also outline the classical Freedericksz transition and Frank defect structures.

In Chapter 3, the Helfrich-Hurault transition effect in SmA will be considered. In this case, the director $\mathbf{n}$ and the layer normal $\mathbf{a}$ are no longer coincident. An electric field is applied to the SmA sample. This will lead to a transition which is called the Helfrich-Hurault transition. This transition occurs at a critical value of the electric field. The influence of the compression coefficient B_0 upon the critical electric field strength and also upon the wave number will be discussed.

Chapter 4 focuses on applying dynamic theory for SmA liquid crystals, which was developed by Stewart [79]. The energy density was used to discuss the stability of SmA's initial planar alignment when no external field is applied.

In Chapter 5, the dynamic continuum theory of liquid crystals will be used to seek the stability and instability of the planar alignment of a SmA liquid crystal sample when an electric field is applied. Moreover, it is worth studying response times in this chapter.

In Chapter 6, the dynamic continuum theory of biaxial nematic liquid crystals will be applied to an incompressible biaxial nematic liquid crystal sample to study the linear stability and instability. The influence of an induced oscillatory shear flow on biaxial nematic liquid crystals will be considered. The relation between Lagrange multipliers will be discussed as well. This chapter concludes by looking at the viscous dissipation of biaxial nematic liquid crystals, which is convenient for studying nonlinear stability and instability in fundamental problems. We show that the nonlinear stability analysis is complicated for biaxial nematics, and it is beyond the scope of this thesis; despite this, some exploratory work has been carried out here.

Chapter 2

Continuum theory of liquid crystals

As outlined by Stewart [78], the beginning of continuum theory for liquid crystals is attributed to the work of Oseen [60, 61] and Zocher [91] in the 1920s. The derivation of the static version of the continuum theory for nematics was the starting point for developing the continuum theory of liquid crystals. Oseen's work was adequate for Frank [30] to develop and formulate the classical static theory for basic liquid crystals in 1958. In 1933, Zocher [92] succeeded in applying static continuum theory to a phenomenon which is known as Freedericksz transition [24, 91].

Another successful work for developing the continuum theory of liquid crystals was by Ericksen [27] in 1961, when he employed the static theory of nematic liquid crystals to propose balance laws for dynamical behaviour. The most important work in the continuum theory of liquid crystals was in 1966 and 1968 when Leslie [45, 46] successfully used Ericksen's ideas of the general static theory of nematics to formulate constitutive equations and this is adequate to complete the dynamic theory for nematic liquid crystals. Thus, it is known as the Ericksen-Leslie dynamic theory for nematic liquid crystals [21, 78], and the textbooks by Collings [17],

Collings and Hird [18] and Dunmer [26]. The static and dynamic theory accounts and their applications are detailed in [7,11,21,83] and also in the reviews [28,40,47, 76]. Leslie, Stewart and Nakagawa [52] introduced an important work on smectic C liquid crystals to develop the continuum theory for liquid crystals when they used the earlier work by the Orsay Group [59], Rapini [66] and Martin, Parodi and Pershan [55]. In this work, a non-linear static and dynamic theory is employed for non-chiral smectic C, which is based upon the same types of balance laws used to model nematic liquid crystals [78].

2.1 Theory of nematics

We use the book by Stewart [78] as a main resource for a review of the continuum theory of liquid crystals in this chapter. Here, we introduce the theory of nematics. The textbooks by de Gennes and Prost [21], Blinov [7] and Chandrasekhar [11] have also been consulted, as well as the original research papers by Leslie [45, 46]. For a more general overview of the theory and the physics and applications of liquid crystals, the reader is referred to the Handbook of Liquid Crystals [34]. Firstly, we consider static theory of nematics, which leads naturally towards the dynamic theory of nematics.

2.1.1 Static theory of nematic liquid crystals

The static theory involves two crucial steps. Firstly, construction of an energy based upon possible distortions of the director $\mathbf{n}$. Secondly, minimising of this energy which leads to equilibrium equations in $\mathbf{n}$. The solutions of these differential equations yield possible equilibrium orientations for $\mathbf{n}$: it is these alignments of $\mathbf{n}$ that are the ultimate goal of static continuum theory since they indicate the director alignment within a sample of liquid crystal. The solutions with the least

energy are interpreted as the physically relevant ones. As we introduced in the previous chapter, the director $\mathbf{n}$ is used to describe locally the average molecular alignment in liquid crystals. This director will be employed in the static theory of nematics.

We now summarise the basic theory following extracts from Stewart [78] in the subsequent descriptions in this chapter. Let $\mathbf{x}$ be a general point in a given sample volume V. Then $\mathbf{n}$ takes the form

$$\mathbf{n} = \mathbf{n}(\mathbf{x}), \quad \mathbf{n} \cdot \mathbf{n} = 1, \tag{2.1}$$

where the second equation is the standard constraint for a unit vector. This alignment displays a certain elasticity and it is known that an initial uniform alignment of a nematic liquid crystal commonly returns after the removal of any disturbing influences. It is therefore assumed that there is a free energy density, also called the free energy integrand, associated with distortions of the anisotropic axis of the form

$$w = w(\mathbf{n}, \nabla\mathbf{n}), \tag{2.2}$$

with the total elastic Helmholtz free energy (assuming that the liquid crystal sample is incompressible), being given by

$$W = \int_V w(\mathbf{n}, \nabla\mathbf{n}) dV. \tag{2.3}$$

Note in this case that the mass density is an assumed constant. The liquid crystal sample is in the natural orientation ($w = 0$) when forces, fields and boundary conditions are absent. It is worthwhile to suppose that the energy which is produced upon the sample by configuration is greater than or equal to that for a completely relaxed natural orientation. Consequently, we suppose that

$$w(\mathbf{n}, \nabla\mathbf{n}) \geq 0. \tag{2.4}$$

As mentioned in the previous chapter, the vectors $\mathbf{n}$ and $-\mathbf{n}$ are physically indistinguishable for nematics, thus we require

$$w(\mathbf{n}, \nabla\mathbf{n}) = w(-\mathbf{n}, -\nabla\mathbf{n}). \tag{2.5}$$

The free energy per unit volume must also be the same when described in any two frames of reference, that is, it must be frame-indifferent. This means that the energy density must be invariant to arbitrary superposed rigid body rotations and consequently, we require

$$w(\mathbf{n}, \nabla\mathbf{n}) = w\left(Q\mathbf{n}, Q\nabla\mathbf{n}Q^T\right), \tag{2.6}$$

where Q is any proper orthogonal matrix (det $Q = 1$), Q^T being its transpose. Under these conditions, the free energy density for nematics is given in the form

$$\begin{aligned} w_F =& \frac{1}{2}K_1(\nabla\cdot\mathbf{n})^2 + \frac{1}{2}K_2(\mathbf{n}\cdot\nabla\times\mathbf{n})^2 + \frac{1}{2}K_3(\mathbf{n}\times\nabla\times\mathbf{n})^2 \\ &+ \frac{1}{2}\left(K_2 + K_4\right)\nabla\cdot[(\mathbf{n}\cdot\nabla)\mathbf{n} - (\nabla\cdot\mathbf{n})\mathbf{n}], \end{aligned} \tag{2.7}$$

where the K_i are often referred to as the Frank elastic constants. K_1, K_2 and K_3 are called the splay, twist and bend constants, respectively, while the combination $(K_2 + K_4)$ is called the saddle-splay constant. The saddle-splay term in w_F is often omitted since it does not contribute to the bulk equilibrium equations for problems involving strong anchoring. Calculations reveal that, under strong anchoring conditions, the saddle-splay term is actually a null Lagrangian because it cannot contribute to the equilibrium equations in the bulk (see Stewart [78] for details). These constants satisfy the inequalities (called Ericksen's inequalities)

$$K_1 \geq 0, \quad K_2 \geq 0, \quad K_3 \geq 0, \quad K_2 \geq |K_4|, \quad 2K_1 \geq K_2 + K_4 \geq 0. \tag{2.8}$$

Note that the free density energy in (2.7) can be simplified by using the one-constant approximation when K_i values are unknown or when the resulting equi-

librium equations are complicated, we set

$$K \equiv K_1 = K_2 = K_3, \quad K_4 = 0, \tag{2.9}$$

therefore the equation (2.7) becomes in the form

$$w_F = \frac{1}{2} K n_{i,j} n_{i,j} = \frac{1}{2} K \|\nabla \mathbf{n}\|^2. \tag{2.10}$$

We summarise the equilibrium equations for the static theory of nematics (for more detail see [78, pp.34-42]), in the volume V with boundary surface S, the differential equations for equilibrium are given by

$$\left(\frac{\partial w}{\partial n_{i,j}}\right)_{,j} - \frac{\partial w}{\partial n_i} + G_i + \lambda n_i = 0, \tag{2.11}$$

$$t_{ij,j} + F_i = 0, \tag{2.12}$$

where $\mathbf{F}$ represents the body force per unit volume, $\mathbf{G}$ is the generalised body force (e.g., electric or magnetic fields), λ is the scalar function Lagrange multiplier which arises from the unit vector constraint and $\mathbf{t}$ is the stress vector that takes the form

$$t_i = t_{ij} \nu_j, \tag{2.13}$$

and the generalised stress vector $\mathbf{s}$ is given by

$$s_i = s_{ij} \nu_j + \beta n_i, \tag{2.14}$$

with $\boldsymbol{\nu}$ as the unit outward normal to the surface S and β is an arbitrary scalar.

We summarise the Freedericksz transition, defects and the dynamic theory of nematics liquid crystals because they are basic to the ideas and structures of the other liquid crystals phases we explore (e.g., transitions, possible defects and complex dynamics). Smectic A defect structures, such as the Dupin cyclides, are directly relevant to bovine brain structures (see Zasadzinski et al. [90]).

2.1.2 Dynamic theory of nematic liquid crystals

We begin by summarising the basic continuum theory balance laws in relation to nematic liquid crystals. These were derived by Leslie [45,46] to which the reader is referred if more details are required. For more details on the applications and developments of the continuum theory, the reader should consult the reviews and textbooks cited above at the beginning of Section 2.1.

2.1.2.1 Balance laws

Let D/Dt represent the usual material time derivative defined by

$$\frac{D}{Dt} = \frac{\partial}{\partial t} + \mathbf{v} \cdot \frac{\partial}{\partial \mathbf{x}}, \tag{2.15}$$

where $\mathbf{x}$ is the position vector and $\mathbf{v}$ is the velocity of the fluid. As before, we follow Stewart [78]. Suppose that V is a volume of liquid crystal bounded by the surface S, then the conservation laws for mass, linear momentum and angular momentum are, respectively, given by (cf. [2]),

$$\frac{D}{Dt}\int_V \rho dV = 0, \tag{2.16}$$

$$\frac{D}{Dt}\int_V \rho \mathbf{v} dV = \int_V \rho \mathbf{F} dV + \int_S \mathbf{t} dS, \tag{2.17}$$

$$\frac{D}{Dt}\int_V \rho(\mathbf{x} \times \mathbf{v}) dV = \int_V \rho(\mathbf{x} \times \mathbf{F} + \mathbf{K}) dV + \int_S (\mathbf{x} \times \mathbf{t} + \mathbf{l}) dS, \tag{2.18}$$

where ρ denotes the density, $\mathbf{F}$ is the external body force per unit mass, $\mathbf{t}$ is the surface force per unit area, $\mathbf{K}$ is the external body moment per unit mass and $\mathbf{l}$ is the surface moment per unit area, where the components t_i and l_i of the surface force and surface moment take the forms respectively,

$$t_i = t_{ij}\nu_j, \quad l_i = l_{ij}\nu_j, \tag{2.19}$$

where ν is the outward unit normal to the surface S. If the sample is assumed to be incompressible, then standard results show that the three balance laws equations

(2.16)-(2.18) can be reduced to the forms [51, 80]

$$v_{i,i} = 0, \tag{2.20}$$

$$\rho \dot{v}_i = \rho F_i + t_{ij,j}, \tag{2.21}$$

$$0 = \rho K_i + \epsilon_{ijk} t_{kj} + l_{ij,j}. \tag{2.22}$$

A virtual work hypothesis is given by the form [51, 80]

$$\int_V \rho(\mathbf{F}\cdot\mathbf{v} + \mathbf{K}\cdot\mathbf{w})dV + \int_S (\mathbf{t}\cdot\mathbf{v} + \mathbf{l}\cdot\mathbf{w})dS = \frac{D}{Dt}\int_V \left(\frac{1}{2}\rho\mathbf{v}\cdot\mathbf{v} + w_{el}\right) dV + \int_V \mathcal{D}\, dV, \tag{2.23}$$

where $\mathbf{w}$ is the local angular velocity of the liquid crystal material element, $\mathcal{D}$ is the rate of viscous dissipation per unit volume and w_{el} is the elastic energy density

$$t_{ij}v_{i,j} + l_{ij}w_{i,j} - w_i\epsilon_{ijk}t_{kj} = \dot{w}_{el} + \mathcal{D}. \tag{2.24}$$

Suppose that there is no supposed dependence upon the derivatives of the local angular velocity; then the rate of viscous dissipation per unit volume $\mathcal{D}$ is positive which is given by [51, 80]

$$\mathcal{D} = \tilde{t}_{ij}v_{i,j} - w_i\epsilon_{ijk}\tilde{t}_{kj}. \tag{2.25}$$

2.2 Dynamic theory of smectic A

The dynamic theory of smectic A is discussed in Chapter 4. This theory is based upon the classical balance laws outlined above for nematics and and is explored in further detail as required later in this thesis. Many of the feature of the nematic theory appear in the SmA theory, but in a different setting that is intertwined with other novel features because of the biaxiality of this specialised phase of liquid crystals.

2.3 Dissipation functions

The dissipation function $\mathcal{D}$ is a function used to take into account the effect of the forces of viscous friction on the motion of a mechanical system. It is the rate of viscous dissipation per unit volume. It will be assumed that, as common, it is always positive. The dissipation function is employed to describe the effect of the resistance to small vibrations of the mechanical energy of the system around its equilibrium position.

The positivity of the dissipation function allows the rigorous construction of constitutive equations to be carried out, leading to necessary conditions on the relative magnitudes and signs of viscosity coefficients, for example. This has been extensively exploited in deriving constitutive equations for liquid crystals [45, 46, 78]. The dissipation function is often introduced in a fundamental balance of work postulation which then allows the derivation of the dissipation function explicitly (see [51]) using the standard balance laws of continuum mechanics for deriving the continuum theory of nematic liquid crystals, for example (this was the first publication of this method used in liquid crystal theory - historically important because the original Ericksen-Leslie theory did not employ this technique).

2.4 The Routh-Hurwitz linear stability criterion

This is the criterion theory that is used to study the stability and instability in this thesis. Let A be an $m \times m$ matrix, the eigenvalues λ of the matrix A is governed by the polynomial equation

$$\lambda^m + a_1\lambda^{m-1} + a_2\lambda^{m-2} + \cdots + a_m = 0. \tag{2.26}$$

Giving constraints on the coefficients $a_1, a_2, \ldots, a_m$ which are necessary and sufficient to ensure all eigenvalues are negative [56]. The explicit Routh-Hurwitz

stability conditions ($\Re(\lambda) < 0$) for $m = 2$ and 3 . If $m = 2$, then $\Re(\lambda) < 0$ if $a_1 > 0$ and $a_2 > 0$. If $m = 3$ then $\Re(\lambda) < 0$ if $a_1 > 0$, $a_3 > 0$ and $a_1 a_2 > a_3$.

Chapter 3

Helfrich-Hurault effect in SmA

3.1 Introduction

A summary of the problems in each section will be provided, along with comments on the equations that will be used, with suitable citations and comments on the fact that the technical details are omitted due to their extensive length. Many hundreds of mathematical derivations in some instances are required; for example, the dynamic theory of nematics is very sophisticated and the content of these details would be far too extensive for this thesis. The reader is referred to the books by Virga [83] and Stewart [78] for pointers in the associated derivations (or, of course, to the original research papers referred to in these books).

In Section 3.2, we introduce the Helfrich-Hurault transition. In Section 3.3, we summarise and explore some previous results for SmA before exploring novel directions and results that involve electric fields and smectic layer compression effects.

3.2 The Helfrich-Hurault transition

There is a well-known effect in liquid crystals (biaxial and smectic) called the Helfrich-Hurault effect. Consider the diagram, which is shown in Figure 3.1. An electric field $\mathbf{E}$ is applied in the x-direction parallel to SmA liquid crystal layers. We assume that the dielectric anisotropy ϵ_a is positive. This means that the director attempts to be parallel to the electric field $\mathbf{E}$. Increasing the magnitude $E = |\mathbf{E}|$ will induce a critical value $E = E_c$. At the value $E_c > 0$, the smectic layers start to undulate as the director $\mathbf{n}$ attempts to be parallel to the electric field. This transition in which the layers begin to be distorted is called the Helfrich-Hurault transition, see Figure 3.1 [77, 78]. Helfrich [36] and Hurault [38] have examined those effects in cholesteric liquid crystals by applying a magnetic field. Moreover, the Helfrich-Hurault transition in SmA has been reviewed by Chandrasekhar [11] and de Gennes and Prost [21]. There are also some electric field results for SmA undergoing such transitions in relation to chiral smectic C liquid crystals by Selinger et al. [73]; such transitions are dependent on the material properties of the original SmA liquid crystal. In the cases presented in this thesis, it is presumed that there is no chirality to be expected or induced, and that chirality is absent in the effects discussed, that is, there is no inherent chirality present in the original SmA phase being modelled.

In the next section, we will seek the critical value E_c for the onset of the Helfrich-Hurault transition by studying the case which is described in [77], in SmA. This will involve exploring how the electric field transition threshold is affected as the key material parameters are varied, especially the smectic layer compression constant B_0, the SmA elastic constant K_1 and the coupling constant B_1 (which is a measure of the separation between molecular alignment relative to the smectic layer alignment). Results will also be presented graphically.

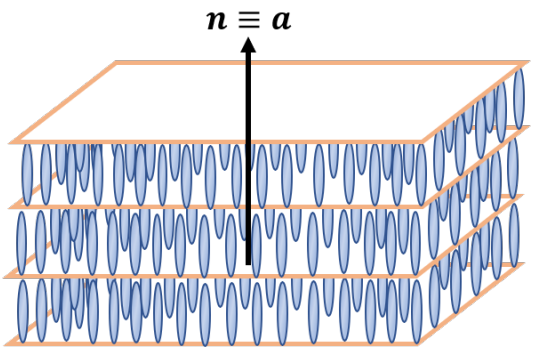

(a) Undistorted SmA

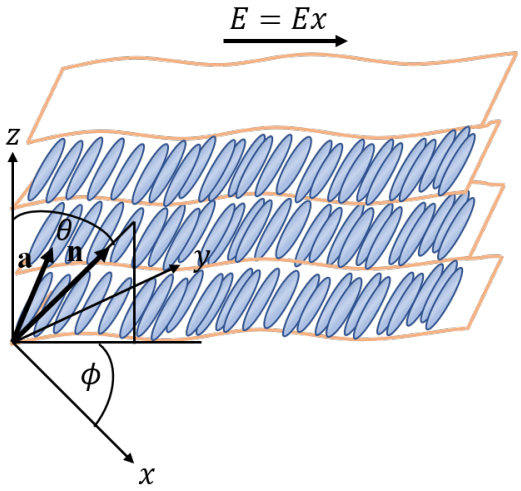

(b) Locally distorted SmA

Figure 3.1: (a) A planar aligned sample of SmA liquid crystals in Cartesian coordinates. (b) When an electric field is applied to the sample in the x-direction, the smectic layers will start to distort when $\epsilon_a > 0$. Initially, **n** is parallel to the layer normal **a**, and then **n** and **a** may separate under the influence of **E** (cf. [77]).

3.3 The Helfrich-Hurault effect in SmA

The smectic layers and the director distort and undulate to get the known transition, which is called the Helfrich-Hurault transition [77]. We follow the work

of Stewart and Stewart [77] to study the influence of the compression coefficient B_0 on the applied electric field threshold. Our aim in this study is to investigate how the critical threshold for the onset of the Helfrich-Hurault transition is reduced as $\mathbf{n}$ and $\mathbf{a}$ are allowed to separate (see Figure 3.1). When an electric field $\mathbf{E}$ is applied parallel to the smectic layers, the energy density can be written in the form (this form is not the only one, but it is the most basic one) [23, 77]

$$w_A = \frac{1}{2}K_1^a(\nabla\cdot\mathbf{a})^2 + \frac{1}{2}K_1^n(\nabla\cdot\mathbf{n})^2 + \frac{1}{2}B_1\Big(1-(\mathbf{n}\cdot\mathbf{a})^2\Big) + \frac{1}{2}B_0\Big(|\nabla\Phi|+(\mathbf{n}\cdot\mathbf{a})-2\Big)^2 - \frac{1}{2}\epsilon_0\epsilon_a(\mathbf{n}\cdot\mathbf{E})^2, \tag{3.1}$$

where K_1^n and K_1^a are positive elastic constants; the positive constant B_0 is the layer compression constant and the positive constant B_1 is a measure of the coupling strength between $\mathbf{n}$ and $\mathbf{a}$, and $\Phi = z - u(x,y,z)$ is the function which describes the smectic layers (surfaces), and $u(x,y,z)$ is the displacement of the layers from their original alignment at $\mathbf{a}_0 = (0,0,1)$. The unit layer normal $\mathbf{a}$ and the director $\mathbf{n}$ in the distorted case, in general, is defined, respectively, by the forms

$$\mathbf{a} = \frac{\nabla\Phi}{|\nabla\Phi|}, \tag{3.2}$$

$$\mathbf{n} = (\sin\theta\cos\phi, \sin\theta\sin\phi, \cos\theta), \tag{3.3}$$

where $\mathbf{n}$ and $\mathbf{a}$ satisfy the two following constraints

$$\mathbf{n}\cdot\mathbf{n} = 1, \quad \mathbf{a}\cdot\mathbf{a} = 1. \tag{3.4}$$

It is well known that the gradients in $\mathbf{a}$ and $\mathbf{n}$ only occur as divergence terms in the simplified theories for smectic liquid crystals [30]. Of course, there are more terms available, in general, as the smectic A layers compress and flex, especially if they transition to smectic C layers of liquid crystals; there are variants that extend w_A to include other gradient terms [4–6, 23] that are especially important

in analysing and modelling non-linear phenomena. Following [77], $\nabla\Phi$ and $|\nabla\Phi|$ can be approximated to second order in u, and then the unit layer normal $\mathbf{a}$ can be expressed as

$$\mathbf{a} = \left(-u_x(1+u_z), 0, 1 - \frac{1}{2}u_x^2\right). \tag{3.5}$$

For small disturbances to the director ($|\theta| << 1$ and $|\phi| << 1$), the director in (3.3) can be approximated to second order by

$$\mathbf{n} = \left(\theta, 0, 1 - \frac{\theta^2}{2}\right), \tag{3.6}$$

where we have, as in [47], assumed that neither $\mathbf{a}$ nor $\mathbf{n}$ have any y-component to this order of approximation.

The electric field $\mathbf{E}$, which is applied in the x-direction, can be given in the form

$$\mathbf{E} = (E, 0, 0), \qquad E = |\mathbf{E}|. \tag{3.7}$$

Also, ϵ_0 is the permittivity of free space and ϵ_a is a dimensionless parameter which is called the dielectric anisotropy of the liquid crystal. $\epsilon_a > 0$ means the director will prefer to be aligned with $\mathbf{E}$ while $\epsilon_a < 0$ means the director will prefer to be orthogonal to $\mathbf{E}$.

It is worth comparing the classical case, when $\mathbf{a} \equiv \mathbf{n}$, with the uncoupled case, when $\mathbf{a}$ and $\mathbf{n}$ are no longer coincident. Ignoring electric field effects and setting $\mathbf{a} = \mathbf{n}$ and $K_1 = K_1^a + K_1^n$, the energy density can be written in the form (called the classical form of the energy density) [77, 85]

$$w = \frac{1}{2}K_1(\nabla.\mathbf{n})^2 + \frac{1}{2}B_0(|\nabla\Phi| - 1)^2. \tag{3.8}$$

We consider the critical electric field strength required for the Helfrich-Hurault transition to occur. To obtain this, we need to consider averaging the energy

density [77]. The average of a function f is defined by

$$\langle f\rangle = \frac{1}{P}\int_0^P f(m)dm, \tag{3.9}$$

where $P>0$ is the period of the function f. We introduce q_x, q_z, θ_0 and u_0 which are constants given in sinusoidal ansatz of the form

$$u = u_0\sin(q_x x)\sin(q_z z),\ \theta = \theta_0\cos(q_x x)\sin(q_z z),\ q_z = \frac{\pi}{d},$$

where $|u_0|<<1, |\theta_0|<<1$ and d is the sample thickness.

As an overview of some previous results that we will develop and extend later in this chapter, we briefly summarise some results from [77] that will allow us to display new graphs. The results in [77] were the first in the field for SmA when **a** and **n** were allowed to separate during the Helfrich-Hurault transition and for this reason these first results in the literature are worthy of quoting here in detail and it is also appropriate to comment on them too. Following the method deployed by de Gennes and Prost [21, p.363] , to average w_A using (3.9), the result can be taken in the form

$$\langle w(u,\theta)\rangle = \frac{1}{8}\left[K_1^a u_0^2 q_x^4 + K_1^n\theta_0^2 q_x^2 + B_1\left(u_0 q_x+\theta_0\right)^2 + B_0 u_0^2 q_z^2 - \epsilon_0\epsilon_a E^2\theta_0^2\right]. \tag{3.10}$$

To compare the distorted state and undistorted state, we consider the change in the average energy density $\Delta\langle w\rangle$ which is defined by [77]

$$\Delta\langle w\rangle = \langle w(u,\theta)\rangle - \langle w(u\equiv 0,\theta\equiv 0)\rangle = \langle w(u,0)\rangle.$$

Following [77], the critical electric field strength satisfies $\Delta\langle w\rangle = 0$, which results in the relation

$$\epsilon_0\epsilon_a E^2\theta_0^2 = K_1^n q_x^2\theta_0^2 + B_1\theta_0^2 + \left[K_1^a u_0^2 q_x^4 + B_1(u_0^2 q_x^2 + 2u_0 q_x\theta_0) + B_0 u_0^2 q_z^2\right]. \tag{3.11}$$

Remark. $\theta_0 = 0$ does not make physical sense in this particular case; there would

be no separation of **n** and **a**.

For non-zero θ_0, we can rewrite (3.11) in the form

$$\epsilon_0\epsilon_a E^2 = K_1^n q_x^2 + B_1 + \frac{1}{\theta_0^2}\left[K_1^a u_0^2 q_x^4 + B_1(u_0^2 q_x^2 + 2u_0 q_x \theta_0) + B_0 u_0^2 q_z^2\right]. \tag{3.12}$$

To find the critical electric field E_c, we need to minimise the right-hand side of (3.12) with respect to non-zero θ_0 and non-zero q_x. Firstly, by minimising with respect to θ_0, we obtain the critical threshold that is given by

$$\theta_0 = -\frac{\left(K_1^a q_x^4 + B_1 q_x^2 + B_0 q_z^2\right) u_0}{B_1 q_x}. \tag{3.13}$$

Substitution of equation (3.13) into equation (3.12), we get

$$\epsilon_0\epsilon_a E^2 = K_1^n q_x^2 + B_1 - \frac{B_1^2 q_x^2}{B_1 q_x^2 + K_1^a q_x^4 + B_0 q_z^2}. \tag{3.14}$$

Notice that u_0 is absent in this final critical threshold expression. This is typical and characteristic of thresholds in nematics too, where the critical threshold is independent of the presumed small magnitude of the assumed disturbance [cf. [78], p. 81]. Now, minimising this result with respect to q_x, we obtain the expression [77]

$$\begin{aligned} K_1^n (K_1^a)^2 q_x^8 + 2K_1^n K_1^a B_1 q_x^6 + (K_1^n B_1^2 + 2K_1^n K_1^a B_0 q_z^2 + B_1^2 K_1^a) q_x^4 \\ + 2K_1^n B_1 B_0 q_z^2 q_x^2 = B_1^2 B_0 q_z^2 - K_1^n B_0^2 q_z^4. \end{aligned} \tag{3.15}$$

The left-hand side of (3.15) is a polynomial in q_x and it is clear that for $q_x > 0$ the polynomial is increasing. Therefore, for a non-zero real solution for $q_x > 0$, we must have the following condition

$$B_0 < \frac{B_1^2}{K_1^n q_z^2} \equiv B_0^c. \tag{3.16}$$

The positive value q_x, say, q_x^c which satisfied the equation(3.15) under the condition (3.16) is unique (because there is a polynomial with positive coefficients) [77] and

we can then write (3.12) for the critical threshold E_c in the form

$$\epsilon_0\epsilon_a E_c^2 = K_1^n(q_x^c)^2 + B_1 - \frac{B_1^2(q_x^c)^2}{K_1^a(q_x^c)^4 + B_1(q_x^c)^2 + B_0 q_z^2}. \tag{3.17}$$

Notice that in (3.14), when q_x is very large, then

$$\epsilon_0\epsilon_a E^2 \approx K_1^n(q_x)^2 + B_1, \tag{3.18}$$

a novel result that was not observed in [77]. This shows that for large q_x, the critical behaviour is governed by a square root relation in B_1, q_x and K_1^n, with B_0 not playing a key role in the value of the threshold, i.e., layer compression is less evident than splay of the director $\mathbf{n}$ and separation of the directors $\mathbf{n}$ and $\mathbf{a}$. This is evident in the numerically derived behaviour in Figure 3.2 (a) when K_1^n and B_1 are given fixed material parameters.

For the classical Helfrich-Hurault transition case, setting $\theta = -u_{,x}$ and $K_1^a + K_1^n = K_1$, the average energy (3.10) takes the form [77]

$$\langle w(u)\rangle = \frac{u_0^2}{8}\Big[K_1 q_x^4 + B_0\frac{\pi^2}{d^2} - \epsilon_0\epsilon_a E^2 q_x^2\Big]. \tag{3.19}$$

Therefore, the classical Helfrich-Hurault transition threshold for an electric field (which we will use to compare it with the uncoupled case (3.17)) which is given in [77]

$$\epsilon_0\epsilon_a E_{cc}^2 = 2\pi\frac{K_1}{\lambda d}, \quad \lambda = \sqrt{\frac{K_1}{B_0}}, \tag{3.20}$$

and the critical wave number given by

$$q_x^{cc} = \sqrt{\frac{\pi}{\lambda d}}. \tag{3.21}$$

The dependence of B_1 was considered in [77]; as an alternative here, we consider the dependence of E_c on B_0 from (3.17), especially in comparison with the classical threshold E_{cc} that can be seen in Figure 3.2, while the dependence of q_x^c on B_0 from equation (3.15) in relation to the classical threshold q_x^{cc} is shown in Figure

3.3.

q_x is determined numerically as a solution for equation (3.15) by Mathematica for the given fixed values of material parameters in Table 3.1. This value is then substituted into (3.17) to allow E_c and E_{cc} to be plotted as functions for the chosen 'variable' material parameter B_0, as shown in Figure 3.3.

d	10^{-4} m
q_z	31415.9m^{-1}
K_1^a	5×10^{-12} N
K_1^n	5×10^{-12} N
B_1	4×10^7 N m^{-2}
ϵ_0	8.854×10^{-12} F m^{-1}
ϵ_a	0.7

Table 3.1: The material parameters used to obtain the results displayed in Figures 3.2 and 3.3 are given by [78, p.330] and [81]. Note: ϵ_a is a dimensionless parameter whose magnitude is a measure of the propensity for the alignment of the director (either parallel or perpendicular, according to its sign). Note that q_z represents a basic first mode solution in the z-direction.

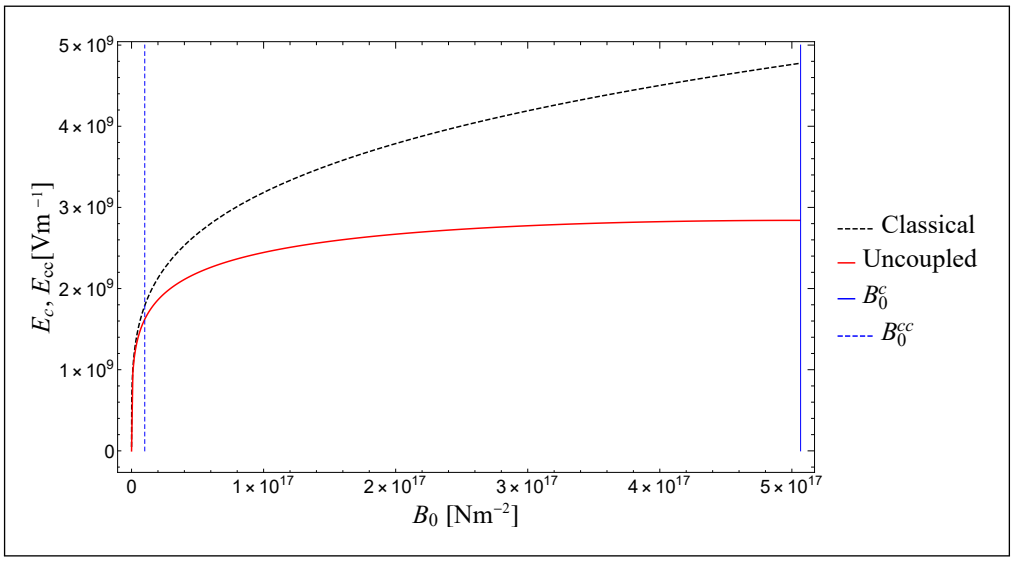

(a) $B_0 \leq B_0^c$.

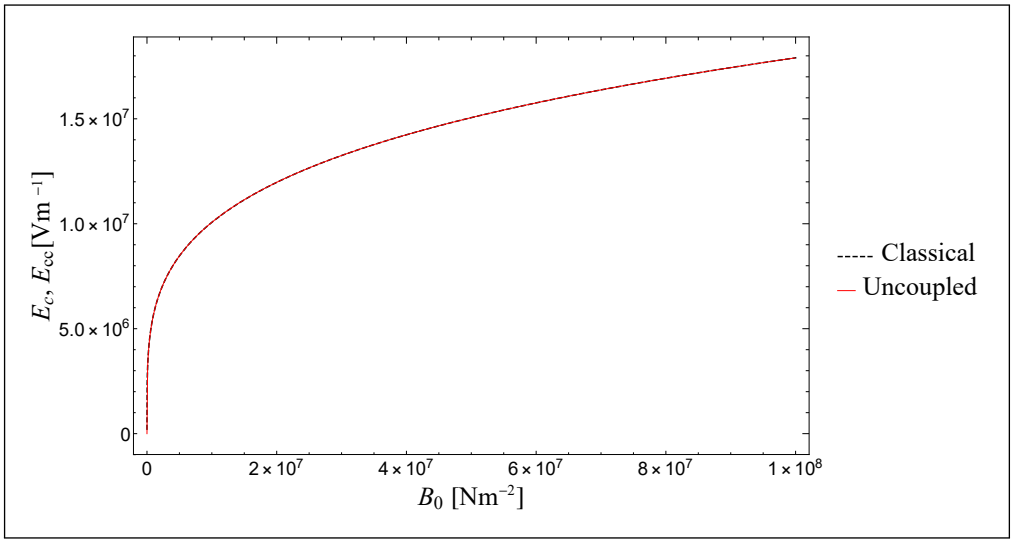

(b) $B_0 \leq 10^8$

Figure 3.2: The graph obtained from equation (3.17) and equation (3.20) showing the influence of the layer compression coefficient B_0 upon the critical electric field strength E_c and the classical Helfrich-Hurault transition threshold E_{cc} when (a) $B_0 \leq B_0^c$, and (b) $B_0 \leq 10^8\ N\ m^{-2}$. B_0^{cc} is an approximate value where the separation between the thresholds becomes apparent.

From Figure 3.2, the uncoupled and classic curves separate markedly at approximately $B_0 \approx 1 \times 10^{16}$ N m^{-2}. In the literature, B_0 is often estimated (an experimental measurement) at around $10^5 \sim 10^8$ N m^{-2} [16]; for significant differences between the coupled and uncoupled models, the values of B_0 would need to be correspondingly much larger in magnitude. Since physical estimates are frequently assumed in such a way that $B_1 \leqslant B_0$, despite the fact that the physical reality of such a range of magnitude is currently unknown. The difference between the classical and uncoupled thresholds becomes particularly evident around the value B_0^{cc}, as indicated in Figures 3.2a and 3.3a.

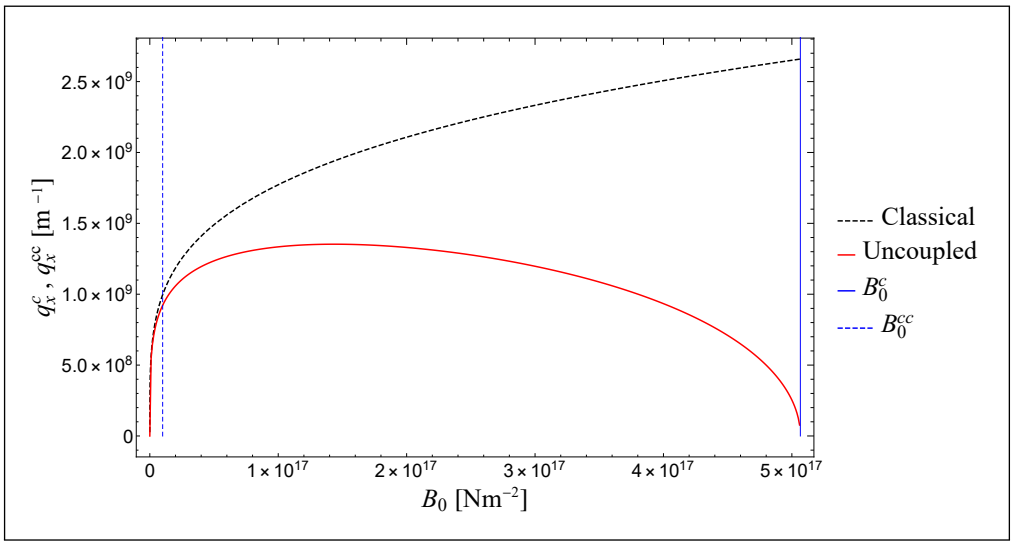

(a) $B_0 \leq B_0^c$.

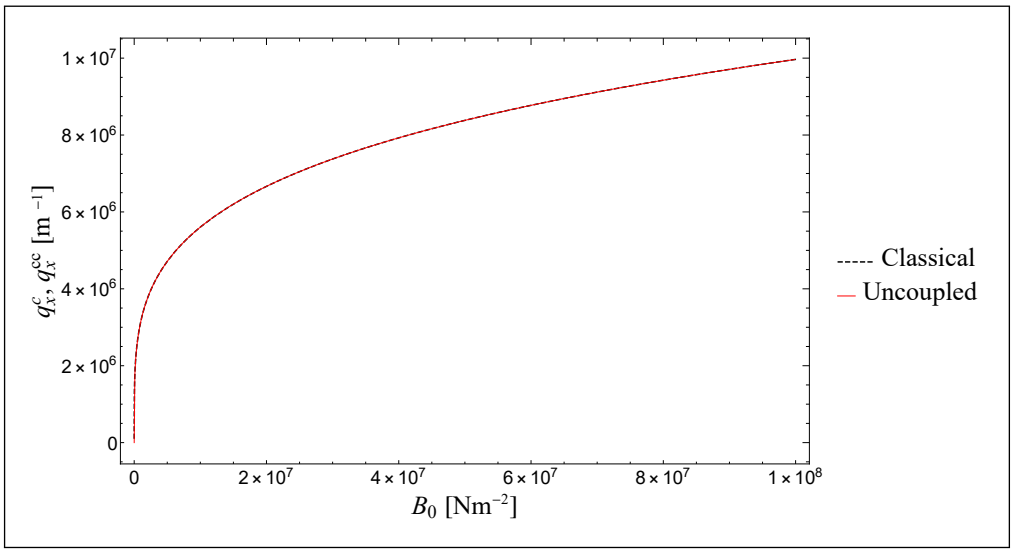

(b) $B_0 \leq 10^8$

Figure 3.3: The graph obtained from equations (3.15) and (3.21). This result shows the influence of the layer compression coefficient B_0 upon q_x^c and q_x^{cc} when (a) $B_0 \leq B_0^c$; (b) $B_0 \leq 10^8$ $N\ m^{-2}$. B_0^{cc} is an approximate value where the separation between the thresholds becomes apparent.

Similarly to Figure 3.2, Figure 3.3 shows a marked separation at $B_0 \approx 1 \times 10^{16}$ N m^{-2}. As mentioned previously, it has been estimated that $B_1 \leqslant B_0$ [71]. We note that this value of B_0 is the same magnitude in both Figures. We can see from Figure 3.3 that the classical critical wave number in (3.21) always increases as B_0 increases. However, when **n** and **a** decouple, the critical wave number q_x, remarkably, begins to decrease as B_0 increases after reaching a local maximum value. The behaviour of the uncoupled curves in these two figures is significantly different for large values of B_0; they reflect different types of responses (critical field and critical wave numbers) and, in particular, Figure 3.3 demands more exploration.

From the condition (3.16), we have $B_1 \leqslant B_0 < B_0^c \approx 10^{17}$ N m^{-2}. By the physically restricted realistic values, $B_0 \approx 10^5$ N m^{-2} $\sim 10^8$ N m^{-2}, we can see graphically that the classical and uncoupled are virtually coincident. This is unexpected and requires further investigation; for example, an asymptotic analysis of the large B_0 dependent behaviour should be carried out. Furthermore, there is a very clear separation in the predictive properties of these models for large B_0 that requires further study. It should be noted that 10^{17}N m^{-2} is excessively high as a model but does reveal novel behaviour dependent on B_0.

3.4 Conclusions and comments

We have summarised the Helfrich-Hurault transition and developed novel results in Section 3.2. In Section 3.3, we found that for large q_x, the layer compression B_0 does not play a key role in the value of the threshold, while the influence of q_x, B_1 and K_1^n are evident in the final value of the threshold. We compared the uncoupled case and the classical case by considering the dependence of E_c and E_{cc} on B_0, respectively. We also considered the dependence of q_x^c on B_0 in the

uncoupled case and compared this to the dependence of q_x^{cc} on B_0 in the classical case. We note that for physical reality (which $B_0 \leqslant B_0^{cc} \approx 10^5 \sim 10^8$ N m^{-2} and $B_1 \leqslant B_0$) that the uncoupled and classical curves are increased and coincident, see Figures 3.2b and 3.3b.

The above analysis is for an infinite sample of SmA. Nevertheless, we now mention that a novel investigation using the foregoing analysis could also be applied to a standard finite sample of "bookshelf" SmA alignment (cf. [78, p.276]), with the field perpendicular to the boundary plates:

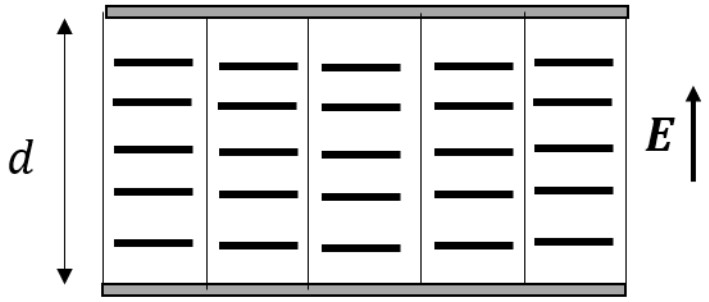

Figure 3.4: This is a more intricate geometry because of the fixed boundaries and is beyond the scope of this thesis, but is worthy of future investigation for $\epsilon_a > 0$.

However, we merely note this as a possibility, having concentrated on the above analysis which would be similar in style. In physical experiments, the depth d is usually small [39]. Moreover, the wedge geometry could equally be investigated by this approach, too (cf. [9]).

Chapter 4

Dynamic theory for SmA liquid crystals

4.1 Introduction

Following the comments and description of smectic liquid crystals in Chapter 1, we shall consider the smectic A (SmA) liquid crystal phase in which the molecules are normally arranged in equidistantly spaced layers with **n** parallel to the layer normal **a**, as shown in Figure 4.1a. Also, we consider a mathematical analysis of the phase when the layer normal **a** and the director **n** are allowed to be non-parallel. The dynamic continuum theory for the dynamics of SmA that was developed by Stewart [79] will also be considered when flow and more viscosities are included to extend the problem in Stewart's work [79]. After a brief review of the SmA continuum theory in Section 4.2, we then begin, in Subsection 4.2.2, to simplify the problem by ignoring the flow to illustrate that planar alignments of samples of SmA are stable. Then, we will study the stability when flow and more viscosities are included in Subsections 4.2.3 and 4.2.4. The reader should consult references

[15, 29, 32, 65, 84] for details on the applications and analysis of the smectic theory that is deployed in this chapter; these papers also show many of the methods used to obtain results for different experimental and numerical setups, with a guide to the necessary calculations when required.

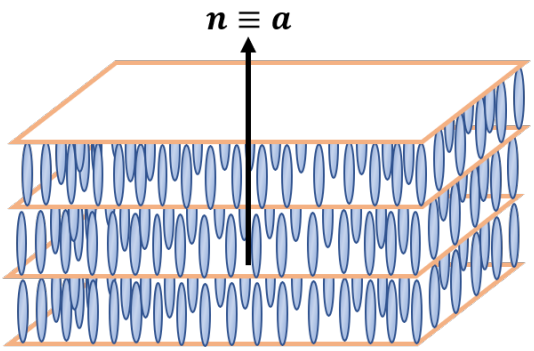

(a) Undistorted SmA dynamic

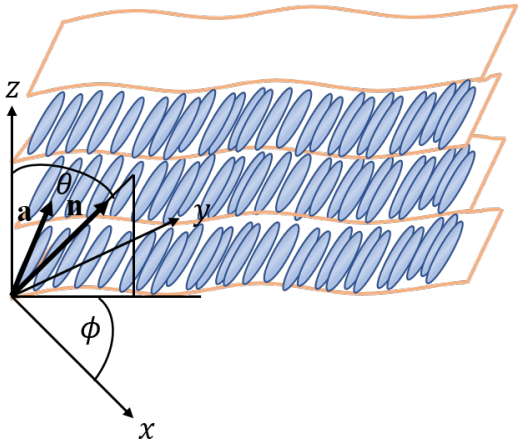

(b) locally distorted SmA dynamic

Figure 4.1: (a) The rod-like molecular structures within the layers are illustrated by the short blue ellipses, while the layer alignment of the SmA phase is represented by the planes. The director $\mathbf{n}$ coincides with the layer normal $\mathbf{a}$. In this scenario, the scalar layer function $\Phi = z$ and $\mathbf{a} = \nabla\Phi/|\nabla\Phi|$. (b) Small deformations of the SmA induce biaxiality and the behaviour of the director $\mathbf{n}$ may separate from that of $\mathbf{a}$, the layer normal. The angle θ measures the director tilt from the z-axis and ϕ is the orientation angle of the orthogonal projection of $\mathbf{n}$ onto the smectic layers [79].

4.2 Dynamic theory for SmA liquid crystals

We will use the continuum theory for the dynamics of SmA that was developed by Stewart [79] using the classical balance laws of continuum mechanics (cf. [79] and equations (2.15)-(2.18) in the nematics section in Chapter 2 of this thesis). This theory does not need $\mathbf{n}$ and $\mathbf{a}$ to be equal as there is a study [71] that indicates that samples of SmA under simple shear may exhibit a decoupling between $\mathbf{n}$ and $\mathbf{a}$ (see Figure 4.1b). We can describe the smectic layer by a scalar function Φ and then $\mathbf{a} = \nabla\Phi/|\nabla\Phi|$. For general disturbances to the smectic layers, $|\nabla\Phi|$ is generally not constant and therefore $\nabla \times \mathbf{a} \neq \mathbf{0}$. Consequently, the Oseen [61] constraint ($\nabla \times \mathbf{a} = \mathbf{0}$) for smectic liquid crystals will not necessarily be required in the dynamic theory. The motion of fluid through the smectic layers in the direction of the layer normal $\mathbf{a}$ is called permeation. We follow the work of Stewart [79], where the effect of the permeation is included, to study the stability of planar aligned layers of SmA for the energy density model, which is given in [79]. It is important to mention here that an incompressible fluid possessing compressible smectic layers are assumed and thermal effects are ignored. Suppose a volume V of SmA liquid crystal bounded by the surface S satisfies the equations (2.15)-(2.18).

Now, consider the energy density, which is given by the following form [77, 79]

$$\begin{aligned} w_A =& \frac{1}{2}K_1^n(\nabla \cdot \mathbf{n})^2 + \frac{1}{2}K_1^a(\nabla \cdot \mathbf{a})^2 + \frac{1}{2}B_0\Big(|\nabla\Phi| + \mathbf{n} \cdot \mathbf{a} - 2\Big)^2 \\ &+ \frac{1}{2}B_1\Big(1 - (\mathbf{n} \cdot \mathbf{a})^2\Big). \end{aligned} \tag{4.1}$$

Emphasis is placed on the fact that this form of the energy density segregates the effects of the director from the layer normal [77]. Consider a sample of SmA liquid crystal that is initially in an undistorted state as shown in Figure 4.1a, when

$\mathbf{n} \equiv \mathbf{a} = (0, 0, 1)$ and the compressible smectic layers are subjected to the function

$$\Phi = z. \tag{4.2}$$

In a distorted SmA, see Figure 4.1b, the layer normal $\mathbf{a}$ and the director $\mathbf{n}$ do not necessarily need to be equal. In general, the director takes the form

$$\mathbf{n} = (\sin\theta\cos\phi, \sin\theta\sin\phi, \cos\theta), \tag{4.3}$$

where the angle θ represents the director tilt from the z-axis and ϕ is the orientation angle of the orthogonal projection of $\mathbf{n}$ onto the smectic layers. Note that $\mathbf{n}$ and $\mathbf{a}$ must fulfil the constraints

$$\mathbf{n} \cdot \mathbf{n} = 1, \quad \mathbf{a} \cdot \mathbf{a} = 1. \tag{4.4}$$

The vectors $\mathbf{n}$ and $\mathbf{a}$ are unit vectors and describe average directions of alignment and so, as such, their magnitudes are not relevant and are always considered to be of fixed modulus; for simplicity, the magnitudes are therefore taken as unity in order to simplify the mathematical models.

Following [79], for small disturbances ($|\theta| << 1$ and $|\phi| << 1$), consider y-independent distortion to the initial state, the director $\mathbf{n}$, the layer normal $\mathbf{a}$, the velocity and the layer function. These can be approximated to first order by

$$\begin{aligned} \mathbf{n} &= (\theta(x, z, t), 0, 1), \\ \Phi &= z - u(x, z, t), \\ \mathbf{a} &= (-u_{,x}, 0, 1), \\ \boldsymbol{v} &= (v_1(x, z, t), 0, v_3(x, z, t)), \end{aligned} \tag{4.5}$$

and

$$\begin{aligned} |\nabla\Phi| &= 1 - u_{,z}, \\ |\nabla\Phi|^{-1} &= 1 + u_{,z}, \end{aligned} \tag{4.6}$$

where $|u|<<1$ represents the displacement of the smectic layers from their initial planar arrangement and $\boldsymbol{v}$ is the velocity with $|v_1|<<1$ and $|v_3|<<1$. We are now in a position to summarise in the next subsection, the SmA dynamic theory that will use the above modelling functions and variables that have been introduced here.

4.2.1 The dynamic equations

The incompressibility condition is given by

$$v_{i,i} = 0, \tag{4.7}$$

where $\mathbf{v}$ is the velocity. In absence of body forces, the balance law for linear momentum gives the following equations

$$\rho \dot{v}_i = -\tilde{p}_{,i} + \tilde{g}_j n_{j,i} + |\nabla\Phi| a_i J_{j,j} + \tilde{t}_{ij,j}, \tag{4.8}$$

where ρ is the density, $\tilde{p} = p + w_A$ and where p is the pressure; $\mathbf{J}$, sometimes referred to as the "phase flux" term (cf, [79]) and $\tilde{g}_i$ are defined by

$$\tilde{g}_i = -(\alpha_3 - \alpha_2)N_i - (\alpha_2 + \alpha_3)A_{ip}n_p - 2\kappa_1 A_{ip}a_p, \tag{4.9}$$

$$J_i = -\frac{\partial w_A}{\partial \phi_{,i}} + \frac{1}{|\nabla\phi|}\left[\left(\frac{\partial w_A}{\partial a_{p,k}}\right)_{,k} - \frac{\partial w_A}{\partial a_p}\right](\delta_{pi} - a_i a_p). \tag{4.10}$$

The term $\mathbf{J}$ can be calculated via (4.5) and (4.6) to first order

$$\mathbf{J} = (-K_1^a u_{,xxx} + B_1(\theta + u_{,x}), 0, B_0 u_{,z}). \tag{4.11}$$

In the absence of body forces, the balance of angular momentum gives the following equations

$$\left(\frac{\partial w_A}{\partial n_{i,j}}\right)_{,j} - \frac{\partial w_A}{\partial n_i} + \tilde{g}_i = \lambda n_i, \tag{4.12}$$

where the scalar function λ is a Lagrange multiplier. The permeation equation is

$$\dot{\Phi} = -\lambda_p J_{i,i}, \quad \lambda_p \geq 0, \tag{4.13}$$

where λ_p is called the permeation coefficient, based upon concepts originally discussed by Helfrich [18] for cholesteric and smectic liquid crystals. Permeation occurs when molecules diffuse from one smectic layer to the next without changing the average periodic layer structure of the smectic layers (cf. Chaikin and Lubensky [10, p.458]).

The viscous stress is given by the form

$$\tilde{t}_{ij} = \alpha_4 A_{ij} + \tau_1 \left(a_k A_{kp} a_p\right) a_i a_j + \tau_2 \left(a_i A_{jp} a_p + a_j A_{ip} a_p\right), \tag{4.14}$$

where the coefficients viscosities α_2, α_3 and α_4 represent the usual Leslie viscosities, while τ_1 and τ_2 are SmA-like and κ occurs in contributions that depend upon both $\mathbf{a}$ and $\mathbf{n}$. The co-rotational time flux of the director $\mathbf{n}$, the rate of strain tensor and vorticity tensor are respectively given by

$$N_i = \dot{n}_i - W_{ij} n_i, \tag{4.15}$$

$$A_{ij} = \frac{1}{2}\left(v_{i,j} + v_{j,i}\right), \tag{4.16}$$

$$W_{ij} = \frac{1}{2}\left(v_{i,j} - v_{j,i}\right). \tag{4.17}$$

4.2.2 No flow included

Note: When there is no flow, we then have hydrostatics ($v \equiv 0$). Note that the director will still be time-dependent and, unlike classical hydrostatics, the time-dependent motion of the director can still take place. To extend Stewart's problem in [79], we first ignore flow to see what basic terms and properties arise. So, the balance of angular momentum and the permeation equations are given in

the following forms respectively:

$$\left(\frac{\partial w_A}{\partial n_{i,j}}\right)_{,j} - \frac{\partial w_A}{\partial n_i} = \lambda n_i, \tag{4.18}$$

$$\dot{\Phi} = -\lambda_p J_{i,i}. \tag{4.19}$$

Now we substitute (4.5) and (4.6) into the dynamic equations (4.18) and (4.19). Firstly, for the equation (4.18)

$$L.H.S = \left(\frac{\partial w_A}{\partial n_{i,j}}\right)_{,j} - \frac{\partial w_A}{\partial n_i} = K_1^n(\nabla \cdot \mathbf{n})_{,i} - B_0(|\nabla\Phi| + \mathbf{n}\cdot\mathbf{a} - 2)a_i + B_1(\mathbf{n}\cdot\mathbf{a})a_i,$$

$$= K_1^n\theta_{,xi} + (B_0 u_{,z} + B_1)a_i. \tag{4.20}$$

Substituting (4.20) into the equation (4.18) gives a system of three equations: for $i = x$,

$$K_1^n\theta_{,xx} + (B_0 u_{,z} + B_1)a_1 = \lambda n_1, \tag{4.21}$$

therefore,

$$K_1^n\theta_{,xx} - (B_0 u_{,z} + B_1)u_{,x} = \lambda\theta. \tag{4.22}$$

For $i = y$,

$$K_1^n\theta_{,xy} + (B_0 u_{,z} + B_1)a_2 = \lambda n_2, \tag{4.23}$$

therefore,

$$K_1^n\theta_{,xy} = 0. \tag{4.24}$$

For $i = z$,

$$K_1^n\theta_{,xz} + (B_0 u_{,z} + B_1)a_3 = \lambda n_3, \tag{4.25}$$

therefore,

$$K_1^n\theta_{,xz} + (B_0 u_{,z} + B_1) = \lambda. \tag{4.26}$$

We can rewrite the equations (4.22), (4.24) and (4.26) in the matrix form

$$M = \lambda \mathbf{n}, \tag{4.27}$$

where

$$M = \begin{pmatrix} K_1^n \theta_{,xx} - B_1 u_{,x} \\ K_1^n \theta_{,xy} \\ K_1^n \theta_{,xz} + B_1 + B_0 u_{,z} \end{pmatrix}. \tag{4.28}$$

Taking the scalar product of (4.27) by $\mathbf{n}$

$$\lambda = M \cdot \mathbf{n} = (K_1^n \theta_{,xx} - B_1 u_{,x})\theta + (K_1^n \theta_{,xz} + B_1 + B_0 u_{,z}). \tag{4.29}$$

As we work to the first order, we obtain

$$\lambda = K_1^n \theta_{,xz} + B_1 + B_0 u_{,z}. \tag{4.30}$$

So, the equations system (4.27) can be written as

$$\begin{pmatrix} K_1^n \theta_{,xx} - B_1 u_{,x} \\ K_1^n \theta_{,xy} \\ K_1^n \theta_{,xz} + B_1 + B_0 u_{,z} \end{pmatrix} = \begin{pmatrix} B_1 \theta \\ 0 \\ K_1^n \theta_{,xz} + B_1 + B_0 u_{,z} \end{pmatrix}, \tag{4.31}$$

and the system of three equations (4.31) then reduce to the following equation

$$K_1^n \theta_{,xx} = B_1(\theta + u_{,x}). \tag{4.32}$$

Secondly, for the equation (4.19),

$$L.H.S. = \dot{\Phi} = \frac{d\Phi}{dt} + v \cdot \nabla \Phi = -u_{,t}, \tag{4.33}$$

therefore

$$u_{,t} = \lambda_p J_{i,i}, \tag{4.34}$$

where

$$J_{i,i} = \nabla \cdot \mathbf{J} = -K_1^a u_{,xxxx} + B_1(\theta_{,x} + u_{,xx}) + B_0 u_{,zz}. \tag{4.35}$$

We then have a linear system of two equations in the two unknown θ and u, namely,

$$K_1^n \theta_{,xx} = B_1(\theta + u_{,x}), \tag{4.36}$$

$$u_{,t} = -\lambda_p \Big[K_1^a u_{,xxxx} - B_1(\theta_{,x} + u_{,xx}) - B_0 u_{,zz} \Big]. \tag{4.37}$$

We are looking for non-zero solutions which are given by the spatially periodic forms

$$\theta = \theta_0 e^{\omega t + i(q_x x + q_z z)}, \tag{4.38}$$

$$u = u_0 e^{\omega t + i(q_x x + q_z z)}, \tag{4.39}$$

where θ_0 and u_0 are small constants and q_x and q_z are wave numbers. By simple calculations, we get the matrix system

$$\begin{pmatrix} S & iB_1 q_x \\ -i\lambda_p q_x B_1 & \omega + \lambda_p Q \end{pmatrix} \begin{pmatrix} \theta_0 \\ u_0 \end{pmatrix} = \begin{pmatrix} 0 \\ 0 \end{pmatrix}, \tag{4.40}$$

where

$$S = K_1^n q_x^2 + B_1, \tag{4.41}$$

$$Q = K_1^a q_x^4 + B_0 q_z^2 + B_1 q_x^2. \tag{4.42}$$

The non-zero solutions of the system equations (4.40) are subjected to the condition that determinant of the matrix (4.40) must equal zero, which is given by the following linear equation for ω

$$S\omega + \lambda_p R = 0, \tag{4.43}$$

where,

$$R = SQ - B_1^2 q_x^2 = B_1 q_x^4 \left(K_1^a + K_1^n\right) + K_1^a K_1^n q_x^6 + B_0 \left(B_1 + K_1^n q_x^2\right) q_z^2. \tag{4.44}$$

It is clear that S and R are positive. Thus, ω is real and negative for all wave numbers q_x and q_z and therefore the initial planar alignment of SmA is linearly

asymptotically stable to small perturbations.

4.2.2.1 $\tilde{g}_i$ included for director dynamics

Here, we include $\tilde{g}_i$ to extend the problem that is given by equations (4.18) and (4.19) to include viscosities and the possibility of director dynamics. So, the balance of angular momentum and the permeation equations take the forms

$$\left(\frac{\partial w_A}{\partial n_{i,j}}\right)_{,j} - \frac{\partial w_A}{\partial n_i} + \tilde{g}_i = \lambda n_i, \tag{4.45}$$

$$\dot{\Phi} = -\lambda_p J_{i,i}. \tag{4.46}$$

As there is no velocity included in this case, we have

$$A_{ij} = W_{ij} = 0, \tag{4.47}$$

$$\tilde{g}_i = (\alpha_2 - \alpha_3) N_i. \tag{4.48}$$

To find $\mathbf{N}$, we have

$$\begin{aligned} \mathbf{N} &= \dot{\mathbf{n}} \\ &= \frac{\partial \mathbf{n}}{\partial t} + v_i \frac{\partial \mathbf{n}}{\partial x_i}. \end{aligned} \tag{4.49}$$

Note that $v_i \dfrac{\partial \mathbf{n}}{\partial x_i} = 0$ because we work to the first order. Thus

$$N_i = \frac{\partial n_i}{\partial t}. \tag{4.50}$$

Therefore,

$$\tilde{g}_i = (\alpha_2 - \alpha_3) n_{i,t}. \tag{4.51}$$

Hence, the balance of the angular momentum equation gives

$$\left(\frac{\partial w_A}{\partial n_{i,j}}\right)_{,j} - \frac{\partial w_A}{\partial n_i} + \tilde{g}_i = K_1^n(\nabla\cdot\mathbf{n})_{,i} - B_0(|\nabla\Phi|+\mathbf{n}\cdot\mathbf{a}-2)a_i + B_1(\mathbf{n}\cdot\mathbf{a})a_i + (\alpha_2-\alpha_3)n_{i,t}$$
$$= K_1^n\theta_{,xi} + (B_0u_{,z}+B_1)a_i + (\alpha_2-\alpha_3)n_{i,t}. \tag{4.52}$$

Following the same procedure in the previous section, we get the matrix system in θ_0 and u_0

$$\begin{pmatrix} S+\gamma_1\omega & iB_1q_x \\ -i\lambda_pq_xB_1 & \omega+\lambda_pQ \end{pmatrix}\begin{pmatrix}\theta_0\\ u_0\end{pmatrix} = \begin{pmatrix}0\\0\end{pmatrix}, \tag{4.53}$$

where $\gamma_1 = \alpha_3 - \alpha_2$ is positive.

As before, non-zero solutions, the determinant of the square matrix on the left-hand side of (4.53) must equal zero. This condition is given by the following quadratic equation for ω:

$$\gamma_1\omega^2 + (S+\lambda_p\gamma_1Q)\omega + \lambda_pR = 0. \tag{4.54}$$

It is clear that all coefficients in equation (4.54) are positive; therefore, by the Routh-Hurwitz stability criterion [56]

$$\Re(\omega) < 0, \tag{4.55}$$

for all wave numbers q_x and q_z and therefore the initial planar alignment of SmA is linearly asymptotically stable to small perturbations.

4.2.3 Flow included

Here, we extend Stewart's problem in [79], which includes flow and the dynamic term $\tilde{g}_i$. In this problem, κ_1 is ignored; this is a "coupling viscosity" that is commonly neglected in elementary investigations. Substituting the results in (4.35) and (4.52) into the dynamic equations (4.7)-(4.13), they are given explicitly to first

order as

$$v_{1,x} + v_{3,z} = 0, \tag{4.56}$$

$$\rho v_{1,t} = -\tilde{p}_{,x} + \frac{1}{2}(\alpha_4 - \tau_2)v_{1,xx} + \frac{1}{2}(\alpha_4 + \tau_2)v_{1,zz}, \tag{4.57}$$

$$\rho v_{3,t} = -\tilde{p}_{,z} - K_1^a u_{,xxxx} + (B_1 u_{,xx} + B_0 u_{,zz}) + B_1\theta_{,x} + \frac{1}{2}(\alpha_4 + \tau_2)v_{3,xx} + \frac{1}{2}(\alpha_4 + 2\tau_1 + 3\tau_2)v_{3,zz}, \tag{4.58}$$

$$K_1^n\theta_{,xx} = B_1(\theta + u_{,x}) + (\alpha_3 - \alpha_2)\theta_{,t}, \tag{4.59}$$

$$v_3 - u_{,t} = \lambda_p[K_1^a u_{xxxx} - B_1(\theta_{,x} + u_{,xx}) - B_0 u_{,zz}]. \tag{4.60}$$

where the unknown functions $\tilde{p}$, θ, u, v_1 and v_3 are given in the spatially periodic forms

$$\begin{aligned} \tilde{p} &= P + p_0 e^{\omega t + i(q_x x + q_z z)}, \\ \theta &= \theta_0 e^{\omega t + i(q_x x + q_z z)}, \\ u &= u_0 e^{\omega t + i(q_x x + q_z z)}, \\ v_1 &= v_{10} e^{\omega t + i(q_x x + q_z z)}, \\ v_3 &= v_{30} e^{\omega t + i(q_x x + q_z z)}, \end{aligned} \tag{4.61}$$

where P is a constant, p_0, θ_0, u_0, v_{10} and v_{30} are small constants. Inserting (4.61) into (4.56)-(4.60) we get the matrix system

$$\begin{pmatrix} 0 & 0 & 0 & q_x & q_z \\ iq_x & 0 & 0 & \rho\omega + X & 0 \\ iq_z & -iB_1 q_x & Q & 0 & \rho\omega + Z \\ 0 & S + \gamma_1\omega & iB_1 q_x & 0 & 0 \\ 0 & i\lambda_p B_1 q_x & -\omega - \lambda_p Q & 0 & 1 \end{pmatrix} \begin{pmatrix} p_0 \\ \theta_0 \\ u_0 \\ v_{10} \\ v_{30} \end{pmatrix} = \begin{pmatrix} 0 \\ 0 \\ 0 \\ 0 \\ 0 \end{pmatrix}, \tag{4.62}$$

where,

$$\gamma_1 = \alpha_3 - \alpha_2, \tag{4.63}$$

$$X = \frac{1}{2}\left[qx^2(\alpha_4 - \tau_2) + qz^2(\alpha_4 + \tau_2)\right], \tag{4.64}$$

$$Z = \frac{1}{2}\left[qx^2(\alpha_4 + \tau_2) + qz^2(\alpha_4 + 2\tau_1 + 3\tau_2)\right]. \tag{4.65}$$

For non-zero solutions, the determinant of the square matrix on the left-hand side of (4.62) must equal zero. This condition results in the following cubic equation for ω:

$$a_0\omega^3 + a_1\omega^2 + a_2\omega + a_3 = 0, \tag{4.66}$$

where,

$$\begin{aligned}
a_0 &= \rho(q_x^2 + q_z^2)\gamma_1, \\
a_1 &= \gamma_1 T + \rho(q_x^2 + q_z^2)(S + \lambda_p\gamma_1 Q), \\
a_2 &= \gamma_1 q_x^2 Q + (S + \lambda_p\gamma_1 Q)T + \rho\lambda_p(q_x^2 + q_z^2)R, \\
a_3 &= (q_x^2 + \lambda_p T)R,
\end{aligned}$$

and

$$T = q_z^2 X + q_x^2 Z = \frac{1}{2}\left[2\left(\alpha_2 + \tau_1 + \tau_2\right)q_x^2 q_z^2 + \left(\alpha_4 + \tau_2\right)\left(q_x^4 + q_z^4\right)\right] > 0. \tag{4.67}$$

Since *a priori*, we have $\alpha_4 + \tau_2 > 0$ and $2\alpha_4 + \tau_1 + 2\tau_2 > 0$ [79], we additionally impose the further modelling restriction $\alpha_4 + \tau_1 + \tau_2 > 0$ as supposed by Stewart [79]. The dissipation function (equation (5.4) and Appendix A equation (1.4) in Stewart [79]) can be calculated explicitly for the case of $\mathbf{a} = \hat{\mathbf{z}}$ to reveal the aforementioned inequalities, for more details, see Appendix D. These are actually necessary conditions, with no further assumptions required to reach this conclusion. For stability, we can see clearly that a_0 is always positive; therefore, using Routh-Hurwitz stability criterion [56], the equation (4.66) must satisfy the

following conditions

$$a_1 > 0, \tag{4.68}$$

$$a_3 > 0, \tag{4.69}$$

$$\Delta = a_1 a_2 - a_0 a_3 > 0. \tag{4.70}$$

See Section 2.4 for the explicit criteria used in the cubic case. We need the real part of ω to be negative. It is clear that the coefficients a_0, a_1 and a_3 are positive. Also, we can write

$$\Delta = r_1 \gamma_1^2 + r_2 \gamma_1 + r_3, \tag{4.71}$$

where,

$$r_1 = Q\left(q_x^2 + \lambda_p T\right)\left[T + \rho\lambda_p Q(q_z^2 + q_x^2)\right] > 0,$$
$$r_2 = ST^2 + \rho^2\lambda_p^2(q_x^2 + q_z^2)^2 QR + 2\rho\lambda_p(q_x^2 + q_z^2)SQT + \rho B_1^2 q_x^4(q_x^2 + q_z^2) > 0,$$
$$r_3 = \rho S(q_x^2 + q_z^2)\left[ST + \rho\lambda_p R(q_x^2 + q_z^2)\right] > 0.$$

It is clear that $\Delta > 0$. We can therefore conclude that

$$\Re(\omega) < 0,$$

for all wave numbers q_x and q_z and therefore the initial planar alignment of SmA is linearly asymptotically stable to small perturbations.

4.2.4 Flow included, κ_1 included

It is known that stability versus instability in applications is important and we look at the effect of including a particular viscosity. Here, we extend the problem in the previous subsection by including the coupling viscosity κ_1. Therefore, the dynamic equations are given explicitly to first order as

$$v_{1,x} + v_{3,z} = 0, \tag{4.72}$$

$$\rho v_{1,t} = -\tilde{p}_{,x} + \frac{1}{2}(\alpha_4 - \tau_2)v_{1,xx} + \frac{1}{2}(\alpha_4 + \tau_2)v_{1,zz}, \tag{4.73}$$

$$\rho v_{3,t} = -\tilde{p}_{,z} - K_1^a u_{,xxxx} + (B_1 u_{,xx} + B_0 u_{,zz}) + B_1\theta_{,x} + \frac{1}{2}(\alpha_4 + \tau_2)v_{3,xx} + \frac{1}{2}(\alpha_4 + 2\tau_1 + 3\tau_2)v_{3,zz}, \tag{4.74}$$

$$K_1^n\theta_{,xx} = B_1(\theta + u_{,x}) + (\alpha_3 - \alpha_2)\theta_{,t} - (\frac{1}{2}\gamma_2 + \kappa_1)(v_{1,z} + v_{3,x}), \tag{4.75}$$

$$v_3 - u_{,t} = \lambda_p[K_1^a u_{xxxx} - B_1(\theta_{,x} + u_{,xx}) - B_0 u_{,zz}], \tag{4.76}$$

for which we have the solution (4.61). Therefore, the corresponding matrix system is

$$\begin{pmatrix} 0 & 0 & 0 & q_x & q_z \\ iq_x & 0 & 0 & \rho\omega + X & 0 \\ iq_z & -iB_1q_x & Q & 0 & \rho\omega + Z \\ 0 & S + \gamma_1\omega & iB_1q_x & i\frac{1}{2}(\gamma_2 + 2\kappa_1)q_z & i\frac{1}{2}(\gamma_2 + 2\kappa_1)q_x \\ 0 & i\lambda_p B_1 q_x & -\omega - \lambda_p Q & 0 & 1 \end{pmatrix} \begin{pmatrix} p_0 \\ \theta_0 \\ u_0 \\ v_{10} \\ v_{30} \end{pmatrix} = \begin{pmatrix} 0 \\ 0 \\ 0 \\ 0 \\ 0 \end{pmatrix}. \tag{4.77}$$

For non-zero solutions, the determinant of the square matrix on the left-hand side of (4.77) must equal zero. This condition is given by the following cubic equation for ω:

$$A_0\omega^3 + A_1\omega^2 + A_2\omega + A_3 = 0, \tag{4.78}$$

where,

$$A_0 = \rho(q_x^2 + q_z^2)\gamma_1,$$

$$A_1 = \gamma_1 T + \rho(q_x^2 + q_z^2)(S + \lambda_p\gamma_1 Q),$$

$$A_2 = \gamma_1 q_x^2 Q + (S + \lambda_p\gamma_1 Q)T + \rho\lambda_p(q_x^2 + q_z^2)R + \frac{1}{2}(q_z^2 - q_x^2)(\gamma_2 + 2\kappa_1)B_1 q_x^2,$$

$$A_3 = (q_x^2 + \lambda_p T)R.$$

We can see clearly that the coefficients A_0, A_1 and A_3 are always positive. For stability ($\Re(\omega) < 0$), using Routh-Hurwitz stability criterion [56], we should have the requirement

$$\Delta_\kappa = A_1 A_2 - A_0 A_3 > 0. \tag{4.79}$$

Now we can write

$$\Delta_\kappa = a\left(\kappa_1 + \frac{1}{2}\gamma_2\right) + b, \tag{4.80}$$

where

$$a = B_1 q_x^2 (q_z^2 - q_x^2)\Big[\gamma_1 T + \rho(q_x^2 + q_z^2)(S + \gamma_1\lambda_p Q)\Big], \tag{4.81}$$

$$\begin{aligned} b = {} & \rho\left(q_x^2 + q_z^2\right)\Big[\gamma_1\left(B_1^2 q_x^4 + \gamma_1\lambda_p Q^2\left(q_x^2 + \lambda_p T\right)\right) + \lambda_p\rho R\left(q_x^2 + q_z^2\right)(S + \gamma_1\lambda_p Q) \\ & + ST\left(S + 2\gamma_1\lambda_p Q\right)\Big] + \gamma_1 T\Big[ST + \gamma_1 Q\left(q_x^2 + \lambda_p T\right)\Big]. \end{aligned} \tag{4.82}$$

We can see from the equations (4.80), (4.81) and (4.82) that there are three cases.

Case 1: $a = 0$ if $q_x = q_z$. Then, $\Delta_k = b$. It is clear that b is always positive. Therefore, $\Delta_k > 0$.

To study other cases, we rewrite the equation (4.80) in the form

$$\Delta_\kappa = a\Big[\kappa_1 + \frac{1}{2}\gamma_2 + \frac{b}{a}\Big], \tag{4.83}$$

and we define, for convenience, $F(\kappa_1, q_x) = \kappa_1 + \kappa_1^c$, where $\kappa_1^c = \dfrac{1}{2}\gamma_2 + \dfrac{b}{a}$.

Case 2: $a > 0$ if $q_x < q_z$. Therefore, $\Delta_k > 0$ if $\kappa_1 + \kappa_1^c > 0$.

Case 3: $a < 0$ if $q_x > q_z$. Therefore, $\Delta_k > 0$ if $\kappa_1 + \kappa_1^c < 0$.

In conclusion, $\Delta_k > 0$ for all wave numbers q_x and q_z when $q_x = q_z$ and for those when $q_x < q_z$ where $\kappa_1 + \kappa_1^c > 0$ or for those when $q_x > q_z$ where $\kappa_1 + \kappa_1^c < 0$. Therefore the initial planar alignment of SmA is linearly asymptotically stable to small perturbations; otherwise, unstable. The stability criteria in the three cases

above are evident where the shaded regions represent instability. We remark that the stability conditions above are novel and give precise and clear conditions for discriminating between stable and unstable regimes for material parameters. It is perhaps surprisingly clear given the rather complex mix of material parameters and are simple criteria to deploy. We now explore this in Figures 4.2-4.5 below, which use the typical data for the material parameters listed in Table 4.1.

Note that the values of Δ_κ are large because of using either small or large numerical values, see Figure 4.2; for example, if $B_1 \sim 10^7\,\mathrm{Nm}^{-2}$, $q_x \sim 10^{-5}\,\mathrm{m}^{-1}$, $\alpha_4 \sim 10^{-1}$Pa s and $\rho \sim 10^3\,\mathrm{kg\ m}^{-3}$ then $\Delta_\kappa \sim 10^{46}$.

d	10^{-4}m
q_z	31415.9 m^{-1}
K_1^a	5×10^{-12} N
K_1^n	5×10^{-12} N
B_0	8.95×10^7 N m^{-2}
B_1	4×10^7 N m^{-2}
λ_p	10^{-16} m^2 Pa^{-1} s^{-1}
α_2	-0.0812 Pa s
α_3	-0.0036 Pa s
α_4	0.0652 Pa s
$\gamma_1 = \alpha_3 - \alpha_2$	0.0776 Pa s
τ_1	0.0652 Pa s
τ_2	0.0652 Pa s
ρ	1000 kg m^{-3}
ϵ_0	8.854×10^{-12} F m^{-1}
ϵ_a	0.7

Table 4.1: The material parameters used to obtain the results displayed in Figures 4.2-4.5 are given by ([78], p. 330) and [81]. Note: ϵ_a is a dimensionless parameter whose magnitude is a measure of the propensity for the alignment of the director (either parallel or perpendicular, according to whether its sign is accordingly positive or negative, respectively).

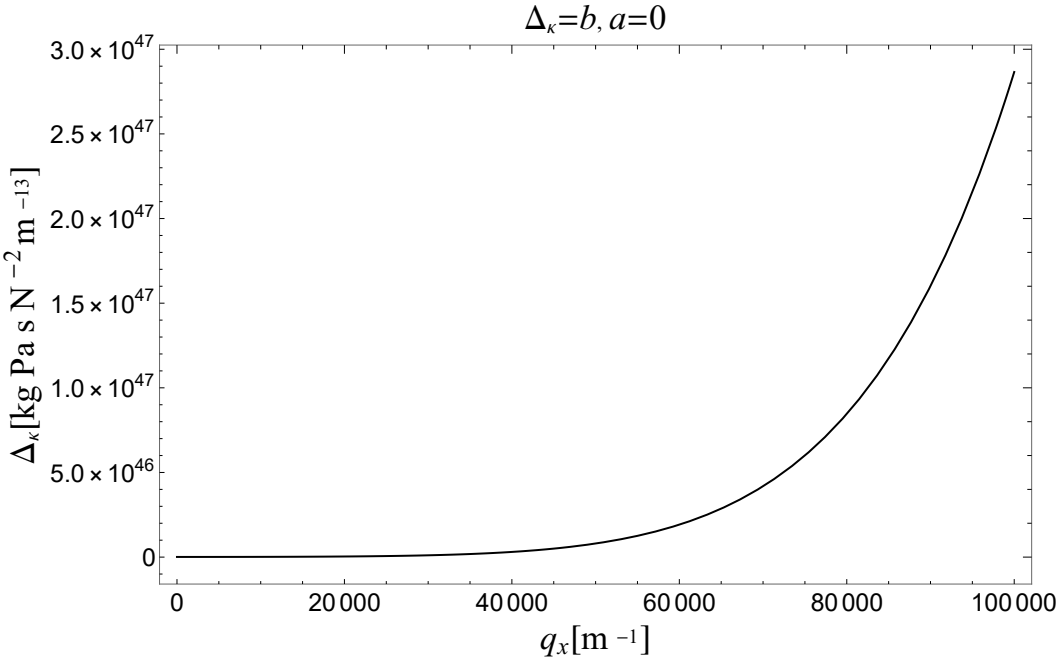

Figure 4.2: Graph for $\Delta_k = b$ as a function of the wave number q_x for the stability and instability of the initial planar alignment of SmA for the material parameters in Table (4.1). The large numerical values for Δ_κ are due to the combination of large and small numerical values that are inserted into its definition. See the thesis text for details.

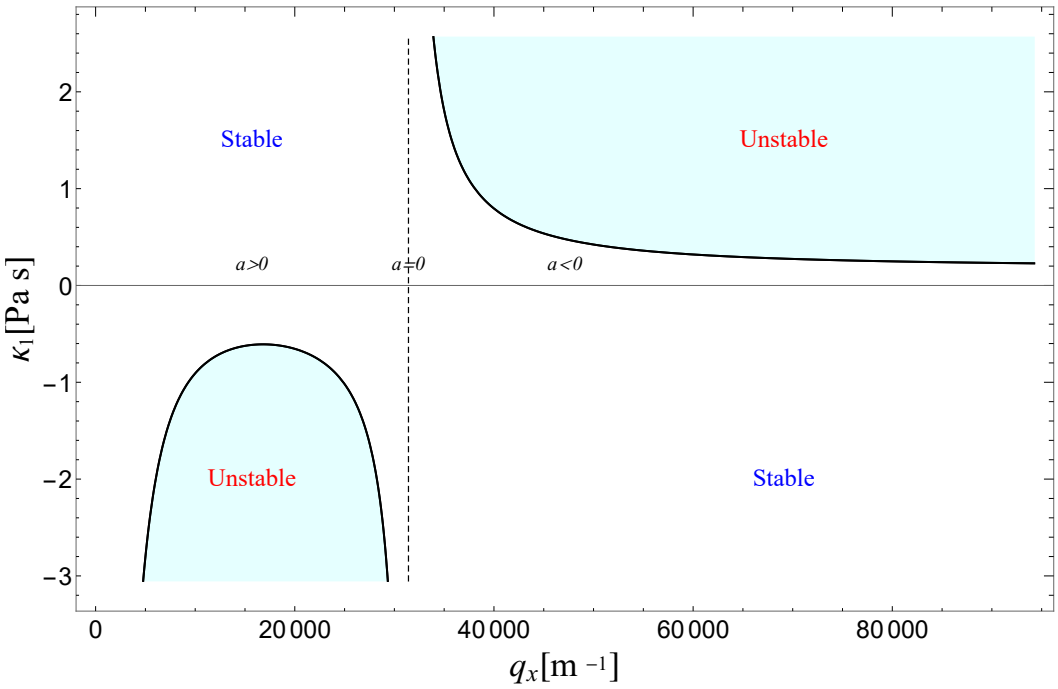

Figure 4.3: Graph for $\kappa_1 = -\kappa_1^c(q_x)$ (when $a \neq 0$) for the stability and instability of the initial planar alignment of SmA for the material parameters in Table (4.1). The stability criteria in case 2 and case 3 above are evident where the shaded regions represent instability.

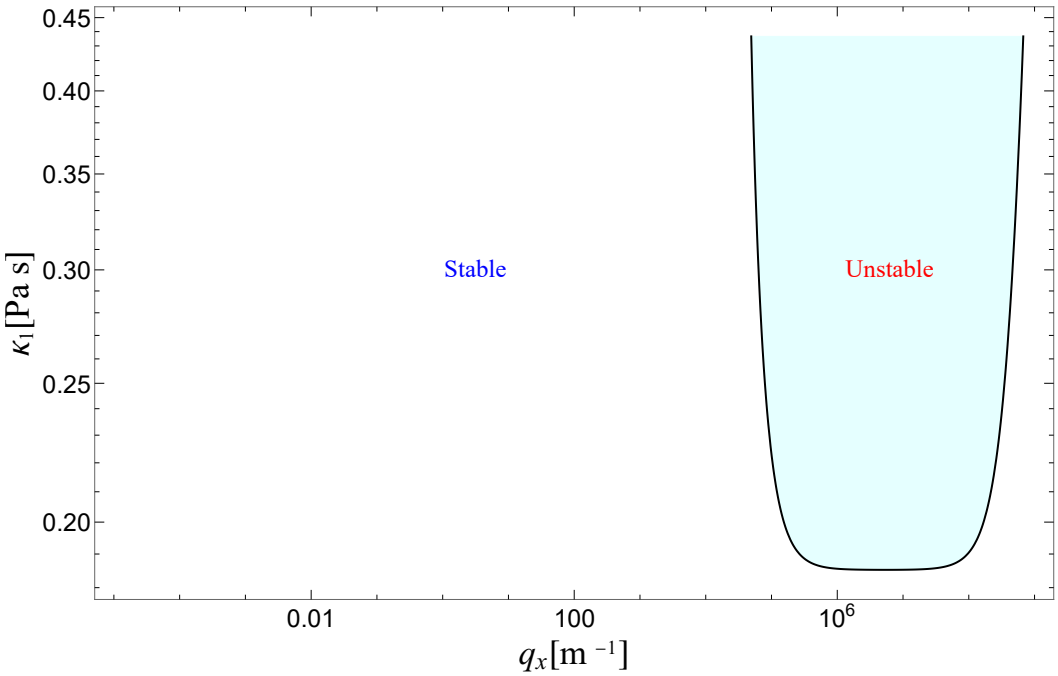

Figure 4.4: Graph for $\kappa_1 = -\kappa_1^c(q_x)$ plotted on a log-log scale for the stability and instability of the initial planar alignment of SmA; this shows that for high wave numbers, the system tends to stability.

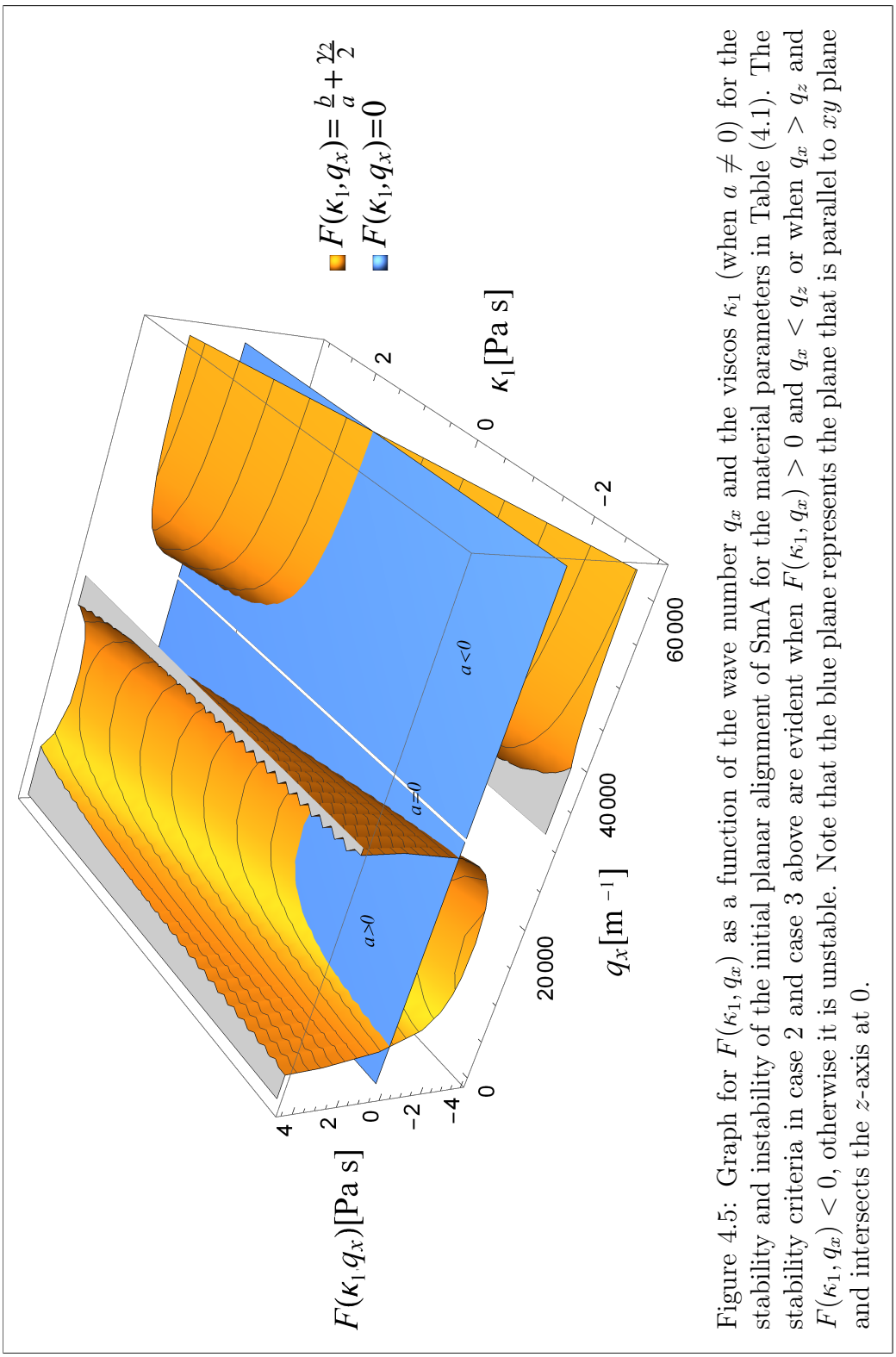

Figure 4.5: Graph for $F(\kappa_1, q_x)$ as a function of the wave number q_x and the viscos κ_1 (when $a \neq 0$) for the stability and instability of the initial planar alignment of SmA for the material parameters in Table (4.1). The stability criteria in case 2 and case 3 above are evident when $F(\kappa_1, q_x) > 0$ and $q_x < q_z$ or when $q_x > q_z$ and $F(\kappa_1, q_x) < 0$, otherwise it is unstable. Note that the blue plane represents the plane that is parallel to xy plane and intersects the z-axis at 0.

These stable regions show that for certain regions of the wave disturbance, we have stability but only for certain ranges of relatively small numbers as small magnitudes of κ_1. If we imagine κ_1 being very close to 0, then we have stability, see Figure 4.3. Stewart and other collaborators have unpublished results that have shown that κ_1 is a destabilising viscosity, especially in examples. We would expect restrictions on κ_1 that can be positive or negative as a viscosity coefficient, but the combinations it enters must be linked to real effective viscosity parameters that are positive (cf. equation (6.247), [78]). This graph explains the situation quite generally yet precisely. It reveals the potential stability or instability that can arise as the magnitude of κ_1 grows very large (we do not know the apriori sign of κ_1). As it grows too in magnitude, we are going to have increasing regimes of instability and that is what previous results by Stewart et al. were pointing towards, but this is the first evidence of it in a more general case. So, there is a narrow band of small κ_1 where there is stability for a wide range of realistic wave number disturbances. But if κ_1 is too big, we will hit regions of instability for various wave numbers. This confirms the conjecture from other works [4–6, 77, 81]. These are important graphs because they tell us about stability and influence of κ_1 motivated by the works of Fiona and others [4–6, 75, 77, 81] in the field. Also, Figure 4.4 shows that for small values of κ_1 there is definitely more chance of it being stable. The behaviour in Figure 4.4 is perhaps physically meaningful: at high wave numbers, the perturbation decay exponentially rapidly, and as the wave number decreases, the opportunities for instability increase. As mentioned above, identifying stability and instability regimes is important in multiple and varied applications. In Figure 4.5; we are looking at the cut across the critical plane (blue), and we can see how the influences are changing as $F(\kappa_1, q_x)$ (except that plane) relative to that plane. We can see the surfaces shift across the white line (when $a = 0$) effectively. This graph can be useful for doing other analyses in the

future where the instabilities may occur in a non-linear analysis and these are good starting points for a non-linear analysis in the future. This is because it forms a basis to build upon the instability when looking at a non-linear analysis. So, we do a linear analysis first, and then we compare and look at non-linear analysis. This is used for the future as a basis to build upon for non-linear analysis because it gives information about the way these curves could behave around the critical regions that we've identified. This gives us an idea of a non-linear analysis and of where to begin.

4.3 Conclusions and comments

The presumed identical time and space dependencies in the perturbations, in this chapter, are common practice in an elementary first order approach to stability when small perturbations are modelled as being applied to a physical system. This assumption is sufficient to derive conditions and requirements that mathematically guarantee stability. How well this reflects on real physical systems can only be determined by comparison with actual experiments, again a common feature, and possible limitation, of this modelling approach. More sophisticated differing dependencies could be introduced and analysed, but this is beyond the remit of a first investigation; it is possible to explore this, but the scope is beyond this present thesis, although it is worthy of a future investigation. In Section 4.2, we have used the continuum theory for SmA liquid crystals by using the classical balance laws of continuum theory mechanics when the director $\mathbf{n}$ and the layer normal $\mathbf{a}$ are separated and the effect of permeation is considered. The dynamic equations has been summarised in Subsection 4.2.1. In Subsection 4.2.2, we found that the system of equations (4.40) is linearly asymptotically stable. When $\widetilde{g}_i$ is included, the system of equations (4.53) also is linearly asymptotically stable. In

Subsection 4.2.3, we included flow and found that the system of equations (4.62) is linearly asymptotically stable. In Subsection 4.2.4, we found that the system in (4.77) is linearly asymptotically stable in three cases; when $q_x = q_z$ or for those when $q_x < q_z$ where $\kappa_1 + \kappa_1^c > 0$ or for those when $q_x > q_z$ where $\kappa_1 + \kappa_1^c < 0$; otherwise, unstable. These cases are illustrated in Figures 4.2-4.5.

Chapter 5

Dynamic theory for SmA liquid crystals and electric field included

5.1 Introduction

Here we consider and explore further the problem discussed by Stewart [79] to study the stability of planar alignments of a sample of SmA when an electric field is applied. The dynamic continuum theory for SmA is used when an electric field **E** is applied parallel to the smectic layers. Furthermore, when the electric field is applied parallel to smectic layers, the magnitude of **E** is expected to be increased, and a critical threshold will occur when the director attempts to be aligned to the electric field.

In Section 5.2, we discuss the cases when an electric field is included to study stability and instability. In Subsection 5.2.1, flow is ignored to study the simplest case. The minimum values for the previous problem in Subsection 5.2.1 are also considered in Subsection 5.2.2. Then we extend this problem by including director

dynamics via the $\widetilde{g}_i$ term. In Subsection 5.2.3, we consider the case when flow is included. Response times will also be discussed for stability and instability. In Subsection 5.2.4, we extend the problem in Subsection 5.2.3 by including the term $\widetilde{g}_i$.

5.2 An electric field included

Model

The energy density is given by the following form [77, 79] when an electric field is included:

$$w_A = \frac{1}{2}K_1^n(\nabla\cdot\boldsymbol{n})^2 + \frac{1}{2}K_1^a(\nabla\cdot\boldsymbol{a})^2 + \frac{1}{2}B_0\Big(|\nabla\Phi|+\boldsymbol{n}\cdot\boldsymbol{a}-2\Big)^2 + \frac{1}{2}B_1\Big(1-(\boldsymbol{n}\cdot\boldsymbol{a})^2\Big) - \frac{1}{2}\epsilon_0\epsilon_a(\boldsymbol{n}\cdot\mathbf{E})^2. \tag{5.1}$$

5.2.1 No flow included

In this case, we ignore flow to simplify the problem and illustrate the stability of planar alignment of SmA. We apply an electric field $\mathbf{E}$ (in the x-direction) which is given in the form

$$\mathbf{E} = (E, 0, 0), \qquad E = |\mathbf{E}|\,. \tag{5.2}$$

Substituting (4.5), (4.6) and (5.2) into (4.18) and (4.11) into (4.18) and following the same procedure in the previous chapter, we get the matrix system in θ_0 and u_0

$$\begin{pmatrix} S-\epsilon_0\epsilon_a E^2 & B_1\boldsymbol{i}q_x \\ -\lambda_p\boldsymbol{i}q_xB_1 & \omega+\lambda_pQ \end{pmatrix}\begin{pmatrix}\theta_0\\ u_0\end{pmatrix} = \begin{pmatrix}0\\0\end{pmatrix}. \tag{5.3}$$

For non-zero solutions, the determinant of the square matrix on the left-hand side of (5.3) must equal zero. This condition is given by the following linear equation

in ω:

$$a\omega + b = 0, \tag{5.4}$$

where

$$a = S - \epsilon_0 \epsilon_a E^2, \tag{5.5}$$

$$b = \lambda_p (R - \epsilon_0 \epsilon_a Q E^2), \tag{5.6}$$

and S, Q and R are defined in the previous chapter in equations (4.41), (4.42) and (4.44) respectively. Note that for stability, we simply require the real part of ω to be negative, i.e., $\Re(-b/a) < 0$. We have two cases,

Case 1: $\epsilon_a < 0$

In this case, we can see clearly that the coefficients a and b are both positive, so the root of the equation (5.4) must be negative. Therefore, $\omega < 0$ for all wave numbers q_x and q_z. Thus, the initial planar alignment of SmA is linearly asymptotically stable to small perturbations.

Case 2: $\epsilon_a > 0$

We can see that

$a < 0$ if

$$E > \sqrt{\frac{S}{\epsilon_0 \epsilon_a}} \equiv E_a, \tag{5.7}$$

and $a > 0$ if

$$E < E_a. \tag{5.8}$$

Also, $b < 0$ if

$$E > \sqrt{E_a^2 - \frac{B_1^2 q_x^2}{\epsilon_0 \epsilon_a Q}} \equiv E_b, \tag{5.9}$$

and

$b > 0$ if

$$E < E_b. \tag{5.10}$$

It is clear that $E_a > E_b$. Thus, $a < 0$ and $b < 0$ if $E > E_a$. Also, $a > 0$ and $b > 0$ if $E < E_b$. Consequently, $\omega < 0$ if $E > E_a$ or $E < E_b$ for all wave numbers q_x and q_z. Therefore, the initial planar alignment of SmA is linearly asymptotically stable to small perturbations; otherwise, it is unstable, see Figures 5.1 and 5.2. Again, these figures use the data in Table 4.1.

We state that, usually, the voltages required for effects in liquid crystal are of the order of 1 to 100 volts; however, samples are very thin (around 5 to 10 microns) and so megavolts per meter are required for the electric field.

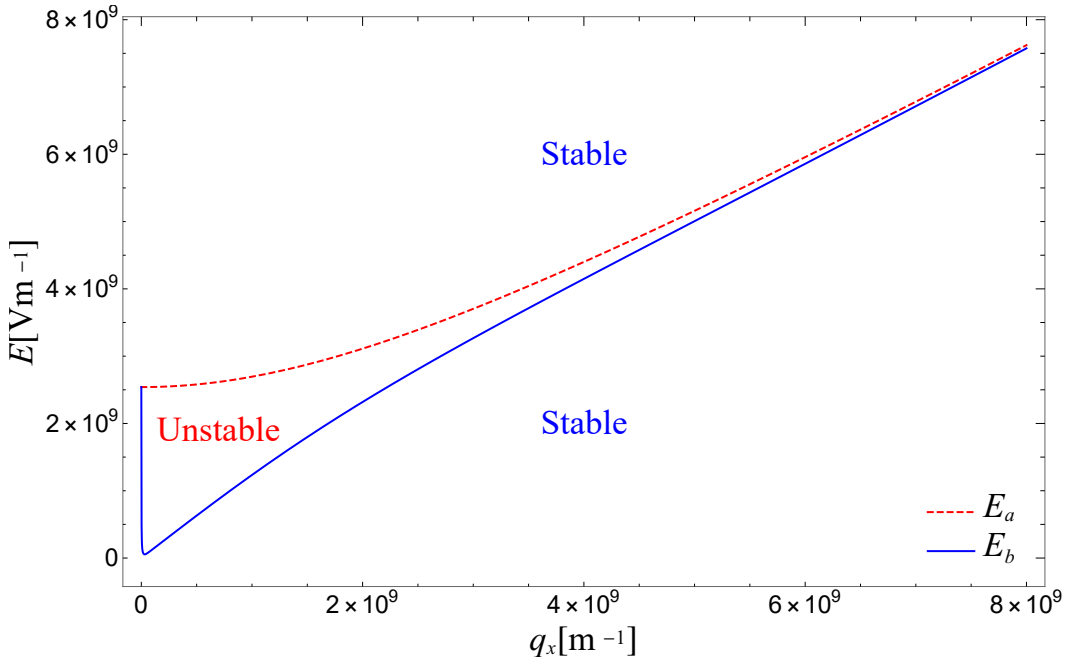

Figure 5.1: This graph shows the critical electric fields strength E_a and E_b upon the wave number q_x for the stability of the initial planar alignment of SmA. It is stable when $E > E_a$ or $E < E_b$; otherwise, it is unstable.

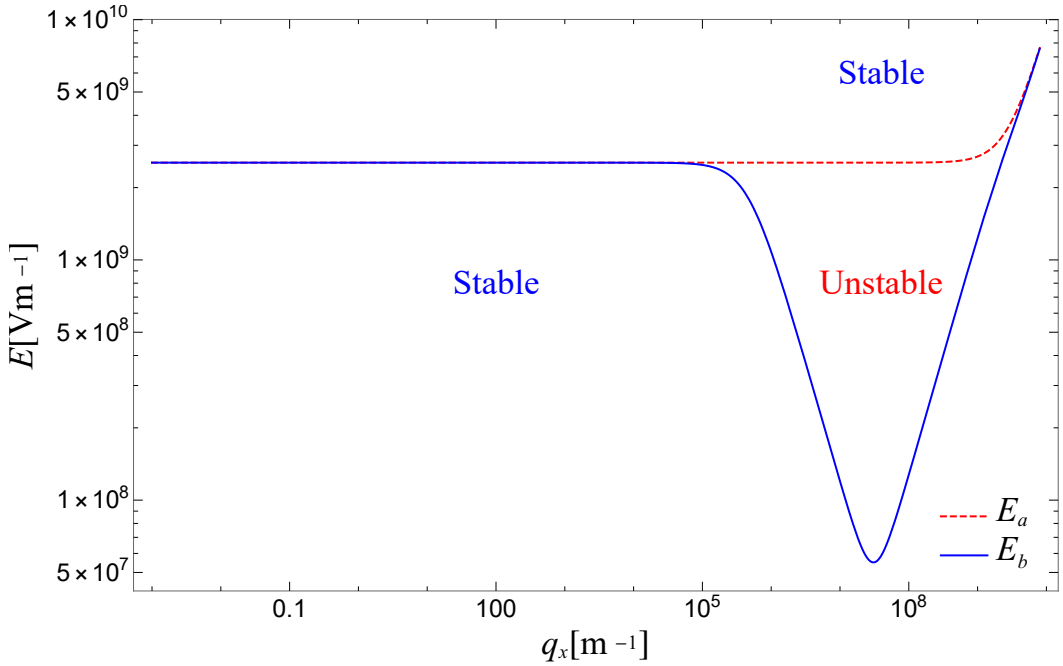

Figure 5.2: This graph shows the critical electric fields strength E_a and E_b upon the wave number q_x for the stability and instability of the initial planar alignment of SmA plotted on a log-log scale.

5.2.2 Minimum values

For E_a,

$$E_a^2 = \frac{B_1 + K_1^n q_x^2}{\epsilon_0 \epsilon_a}. \tag{5.11}$$

It is clear that there is only one critical value for E_a. We can see that E_a is increasing for positive values $q_x > 0$; therefore, at $q_x = 0$, we have the minimum value.

For E_b,

$$E_b^2 = E_a^2 - \frac{B_1^2 q_x^2}{\epsilon_0 \epsilon_a \left(B_1 q_x^2 + B_0 q_z^2 + K_1^a q_x^4\right)}. \tag{5.12}$$

Critical values are obtained by minimising with respect to q_x when q_z is given in Table 4.1 as $\frac{\pi}{d}$.

$$\frac{d}{dq_x}(E_b^2) = \frac{2q_x F(q_x)}{\epsilon_0 \epsilon_a \left(K_1^a q_x^4 + B_1 q_x^2 + B_0 q_z^2\right)^2},$$

therefore,

$$E_b^{'} = \frac{1}{E_b} \frac{q_x F(q_x)}{\epsilon_0 \epsilon_a \left(K_1^a q_x^4 + B_1 q_x^2 + B_0 q_z^2\right)^2},$$

where,

$$\begin{aligned} F(q_x) = &\left(K_1^a\right)^2 K_1^n q_x^8 + 2B_1 K_1^a K_1^n q_x^6 + \left(2B_0 K_1^a K_1^n q_z^2 + B_1^2 \left(K_1^a + K_1^n\right)\right) q_x^4 \\ &+ 2B_0 B_1 K_1^n q_z^2 q_x^2 + B_0 q_z^2 C^*, \end{aligned} \tag{5.13}$$

and

$$C^* = B_0 K_1^n q_z^2 - B_1^2. \tag{5.14}$$

Note that $E_b \neq 0$. Also for $q_x \geq 0$, $E_b^{'} = 0$ if $q_x = 0$ or $F(q_x) = 0$.

It is clear that $F(q_x)$ is increasing for $q_x > 0$. We can discuss two cases:

Case 1: $C^* > 0 \Rightarrow F(q_x) \neq 0$ for $q_x > 0$. Therefore, we have only one critical value, $q_x = 0$ which means that $E_b(0)$ is the minimum value for E_b.

Case 2: If $C^* < 0$, there is a unique positive value say, q_x^c where $F(q_x^c) = 0$. Therefore, $F(q_x) < 0$ for $0 < q_x < q_x^c \Rightarrow E_b^{'} < 0$ for $0 < q_x < q_x^c \Rightarrow E_b$ is decreasing for $0 < q_x < q_x^c$ and $F(q_x) > 0$ for $q_x > q_x^c \Rightarrow E_b^{'} > 0$ for $q_x > q_x^c \Rightarrow E_b$ is increasing for $q_x > q_x^c$. Therefore, $E_b(q_x^c)$ is the minimum value.

Director dynamics included via the $\tilde{g}_i$ term

If we include $\tilde{g}_i$ in the previous problem, we will get the following matrix system in θ_0 and u_0

$$\begin{pmatrix} S - \epsilon_0\epsilon_a E^2 + \gamma_1\omega & B_1 i q_x \\ -\lambda_p i q_x B_1 & \omega + \lambda_p Q \end{pmatrix} \begin{pmatrix} \theta_0 \\ u_0 \end{pmatrix} = \begin{pmatrix} 0 \\ 0 \end{pmatrix}. \tag{5.15}$$

For non-zero solutions, the determinant of the square matrix on the left-hand side of (5.15) must equal zero. This condition is given by the following quadratic equation for ω:

$$A_1\omega^2 + A_2\omega + A_3 = 0, \tag{5.16}$$

where,

$$\begin{aligned} A_1 &= \gamma_1, \\ A_2 &= (S + \gamma_1\lambda_p Q - \epsilon_0\epsilon_a E^2), \\ A_3 &= \lambda_p(R - \epsilon_0\epsilon_a Q E^2). \end{aligned} \tag{5.17}$$

Now we can discuss two cases:

Case 1: $\epsilon_a < 0$

In this case, we can see clearly that the coefficients A_1, A_2 and A_3 are positive, using Routh-Hurwitz stability criterion [56], the roots of the equation (5.16) must satisfy the following condition

$$\Re(\omega) < 0, \tag{5.18}$$

for all wave numbers q_x and q_z. Therefore, the initial planar alignment of SmA is linearly asymptotically stable to small perturbations.

Case 2: $\epsilon_a > 0$

It is clear that A_1 is always positive and we can see that $A_2 > 0$ if

$$E < \sqrt{\frac{S + \lambda_p \gamma_1 Q}{\epsilon_0 \epsilon_a}} \equiv E^c_{A_2},$$

and $A_3 > 0$ if

$$E < \sqrt{(E^c_{A_2})^2 - \frac{B_1^2 q_x^2 + \lambda_p \gamma_1 Q^2}{Q \epsilon_0 \epsilon_a}} \equiv E^c_{A_3}.$$

However, $E^c_{A_2} > E^c_{A_3}$, then, A_2 and A_3 are both positive if

$$E < E^c_{A_3}. \tag{5.19}$$

Therefore, using Routh-Hurwitz stability criterion [56], the roots of the equation (5.16) must satisfy the condition

$$\Re(\omega) < 0, \tag{5.20}$$

for all wave numbers q_x and q_z and therefore the initial planar alignment of SmA is linearly asymptotically stable to small perturbations; otherwise, unstable. See Figures 5.3 and 5.4. These figures use the data in Table 4.1.

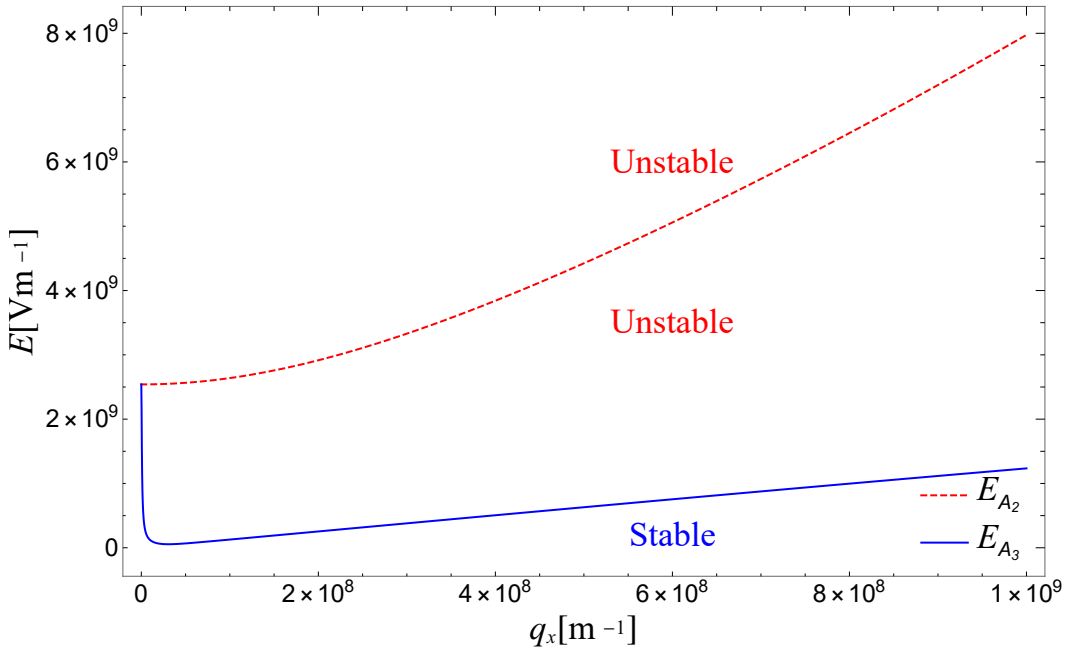

Figure 5.3: This graph shows the critical electric field strengths E_{A_2} and E_{A_3} upon the wave number q_x for the stability and instability of the initial planar alignment of SmA. It is stable when $E < E_{A_3}$; otherwise, it is unstable.

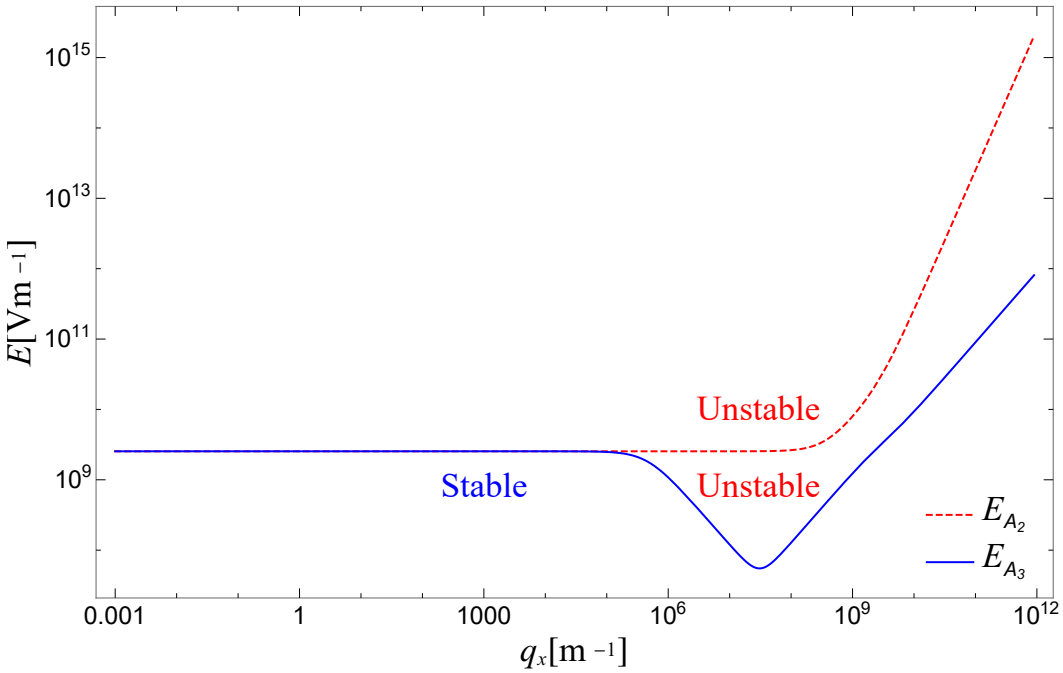

Figure 5.4: This graph shows the critical electric field strengths E_{A_2} and E_{A_3} upon the wave number q_x for the stability and instability of the initial planar alignment of SmA plotted on a log-log scale.

5.2.3 Flow included

Now, in this section, we extend the problem in the previous section by including flow. Also, $\tilde{g}_i$ is ignored for the present. Therefore, the dynamic equations in (4.7)-(4.13) are given explicitly to first order as

$$v_{1,x} + v_{3,z} = 0, \tag{5.21}$$

$$\rho v_{1,t} = -\tilde{p}_{,x} + \frac{1}{2}(\alpha_4 - \tau_2)v_{1,xx} + \frac{1}{2}(\alpha_4 + \tau_2)v_{1,zz}, \tag{5.22}$$

$$\rho v_{3,t} = -\tilde{p}_{,z} - K_1^a u_{,xxxx} + (B_1 u_{,xx} + B_0 u_{,zz}) + B_1\theta_{,x} + \frac{1}{2}(\alpha_4 + \tau_2)v_{3,xx} + \frac{1}{2}(\alpha_4 + 2\tau_1 + 3\tau_2)v_{3,zz}, \tag{5.23}$$

$$K_1^n\theta_{,xx} = B_1(\theta + u_{,x}) - \epsilon_0\epsilon_a E^2\theta, \tag{5.24}$$

$$v_3 - u_{,t} = \lambda_p\Big[K_1^a u_{xxxx} - B_1(\theta_{,x} + u_{,xx}) - B_0 u_{,zz}\Big], \tag{5.25}$$

where the solution of this system is given in (4.61). Inserting (4.61) into (5.21)-(5.25) we obtain the matrix system

$$\begin{pmatrix} 0 & 0 & 0 & q_x & q_z \\ iq_x & 0 & 0 & X & 0 \\ iq_z & -iB_1q_x & Q & 0 & Z \\ 0 & S - \epsilon_0\epsilon_a E^2 & iB_1q_x & 0 & 0 \\ 0 & i\lambda_p B_1 q_x & -\omega - \lambda_p Q & 0 & 1 \end{pmatrix} \begin{pmatrix} p_0 \\ \theta_0 \\ u_0 \\ v_{10} \\ v_{30} \end{pmatrix} = \begin{pmatrix} 0 \\ 0 \\ 0 \\ 0 \\ 0 \end{pmatrix}, \tag{5.26}$$

where S, Q, R, X and Z are defined in the previous chapter in equations (4.41), (4.42), (4.44), (4.64) and (4.65), respectively.

For non-zero solutions, the determinant of the square matrix on the left-hand side of (5.26) must equal zero. This condition is given by the following quadratic equation for ω:

$$c_1\omega^2 + c_2\omega + c_3 = 0, \tag{5.27}$$

where,

$$c_1 = \rho\left(q_x^2 + q_z^2\right)\left(S - \epsilon_0\epsilon_a E^2\right), \tag{5.28}$$

$$c_2 = \Big[T + \lambda_p\rho Q(q_x^2 + q_z^2)\Big]\Big(S - \epsilon_0\epsilon_a E^2\Big) - \lambda_p\rho B_1^2 q_x^2(q_x^2 + q_z^2), \tag{5.29}$$

$$c_3 = \Big[R - \epsilon_0\epsilon_a E^2)\Big]\Big[q_x^2 + \lambda_p T\Big]. \tag{5.30}$$

Now we can see that there are two cases.

Case 1: $\epsilon_a < 0$

In this case, we can see clearly that the coefficients c_1, c_2 and c_3 are positive, so, the roots of the equation (5.27) must satisfy the following condition

$$\Re(\omega) < 0, \tag{5.31}$$

for all wave numbers q_x and q_z. Therefore, the initial planar alignment of SmA is linearly asymptotically stable to small perturbations.

Case 2: $\epsilon_a > 0$

We can rewrite equations (5.28), (5.29) and (5.30) in the forms

$$c_1 = \rho\epsilon_0\epsilon_a\left(q_x^2 + q_z^2\right)\left(E_{c_1}^2 - E^2\right), \tag{5.32}$$

$$c_2 = \epsilon_0\epsilon_a\Big[T + \lambda_p\rho Q(q_x^2 + q_z^2)\Big]\left(E_{c_1}^2 - E^2\right) - \lambda_p\rho B_1^2 q_x^2(q_x^2 + q_z^2), \tag{5.33}$$

$$c_3 = \Big[\epsilon_0\epsilon_a Q(E_{c_1}^2 - E^2) - B_1^2 q_x^2\Big]\Big[q_x^2 + \lambda_p T\Big], \tag{5.34}$$

where $E_{c_1} = \sqrt{\frac{S}{\epsilon_0\epsilon_a}}$. Now, we can see that $c_1 > 0 \;\; if \;\; E < E_{c_1}$, and $c_1 < 0 \;\; if \;\; E > E_{c_1}$,

and $c_2 > 0 \;\; if \;\; E < \sqrt{E_{c_1}^2 - \dfrac{\lambda_p\rho B_1^2 q_x^2(q_x^2 + q_z^2)}{\epsilon_0\epsilon_a[T + \lambda_p\rho Q(q_x^2 + q_z^2)]}} \equiv E_{c_2}$, and $c_2 < 0 \; if \; E > E_{c_2}$.

also,

$c_3 > 0 \;\; if \;\; E < \sqrt{E_{c_1}^2 - \dfrac{B_1^2 q_x^2}{\epsilon_0 \epsilon_a Q}} \equiv E_{c_3}$ and $c_3 < 0 \;\; if \;\; E > E_{c_3}$,

However, we can write $E_{c_3} = \sqrt{E_{c_2}^2 - \dfrac{B_1^2 q_x^2 T}{\epsilon_0 \epsilon_a Q \left[T + \lambda_p \rho Q (q_x^2 + q_z^2)\right]}}$. Therefore, it is clear that

$$E_{c_3} < E_{c_2} < E_{c_1}. \tag{5.35}$$

5.2.3.1 Stability

Using the Routh-Hurwitz stability criterion to study the stability, we can summarise the signs of the coefficients of the equation (5.27) in the table below in Figure 5.6. We also plot graphs of E_{c_1}, E_{c_2} and E_{c_3} to indicate stability and instability of the initial planar alignment of SmA, see Figures 5.6 and 5.7. These figures use the data in Table 4.1.

	0	E_{c_3}	E_{c_2}	E_{c_1}
c_1	⊕	⊕	⊕	⊖
c_2	⊕	⊕	⊖	⊖
c_3	⊕	⊖	⊖	⊖
Stability	Stable	Unstable	Unstable	Stable

Figure 5.5: This is a summary of the signs of the coefficients of the equation (5.27). We can see clearly that the initial planar alignment of SmA is stable when $0 < E < E_{c_3}$ or $E > E_{c_1}$; otherwise, it is unstable.

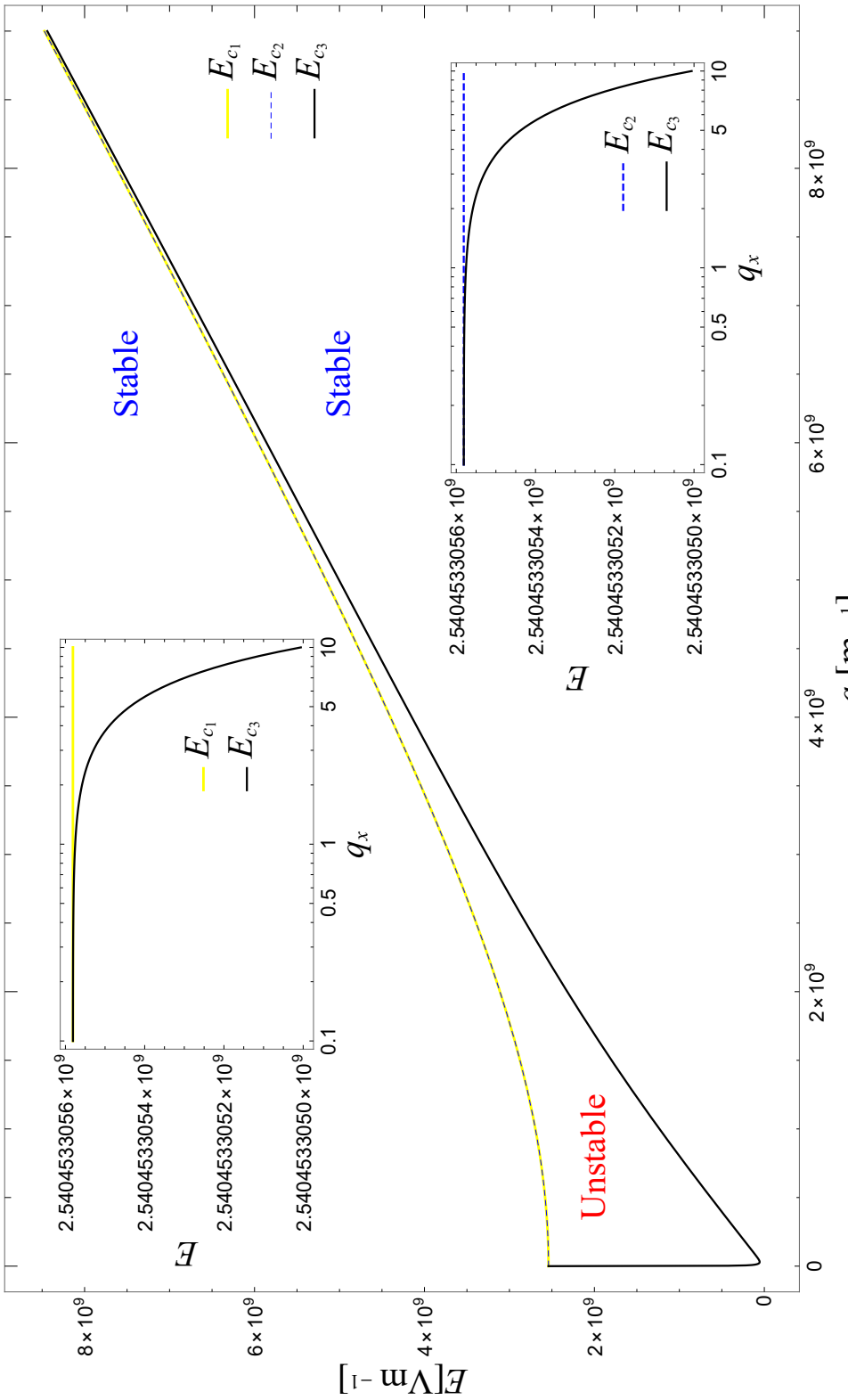

Figure 5.6: This graph shows the critical electric field strengths E_{c_1}, E_{c_2} and E_{c_3} upon the wave number q_x for the stability and instability of the initial planar alignment of SmA. The upper inserted graph shows the behaviour of the indicated smaller region for E_{c_1} and E_{c_3} and the lower inserted graph that of the same region for E_{c_2} and E_{c_3}. The curves for E_{c1} and E_{c2} are indistinguishable at this scale in this Figure. Nevertheless, the distinction between these related curves can be seen explicitly in Figure 5.7.

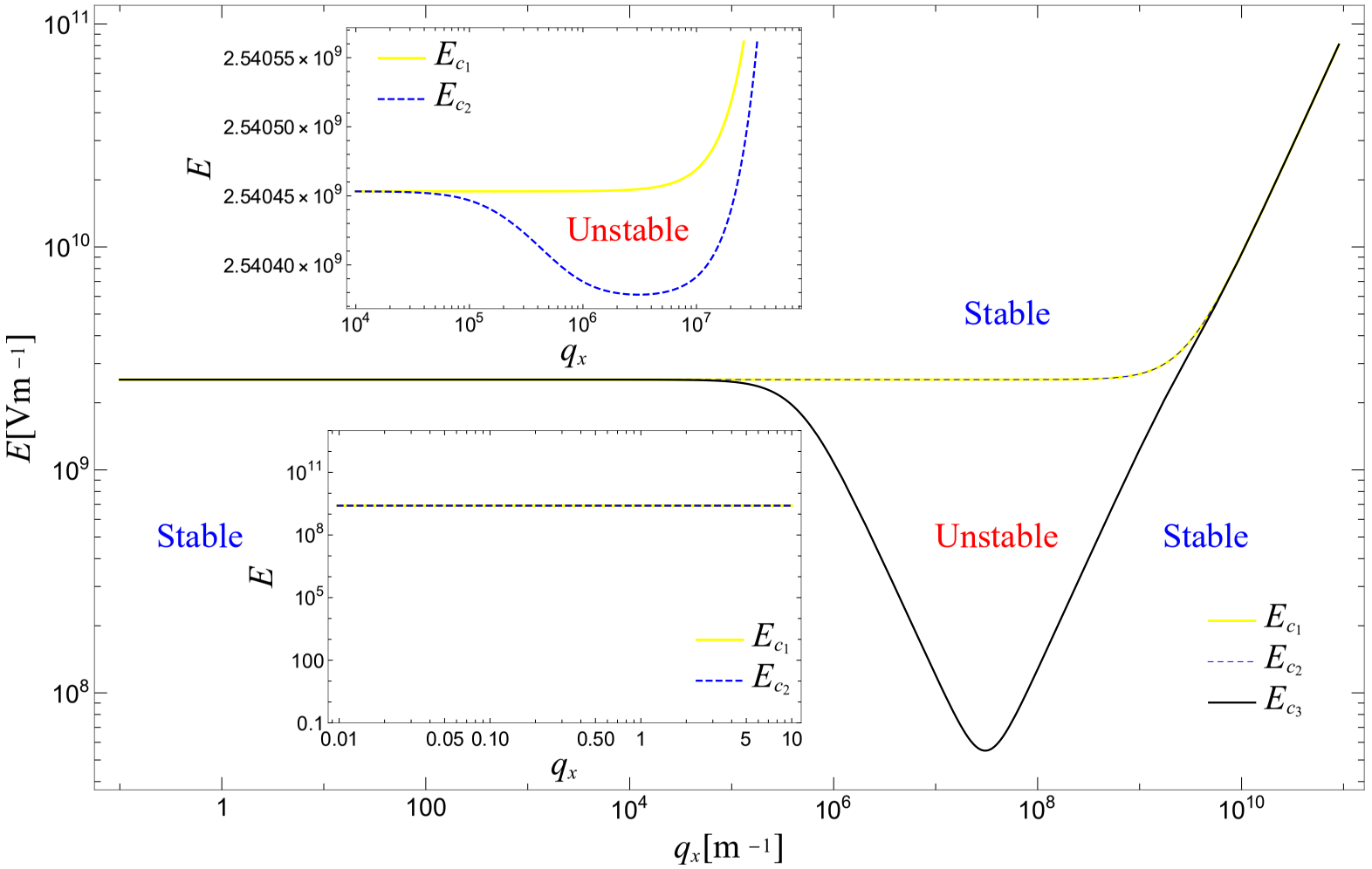

Figure 5.7: This graph shows the critical electric field strengths E_{c_1}, E_{c_2} and E_{c_3} upon the wave number q_x for the stability and instability of the initial planar alignment of SmA plotted on a log-log scale. We can clearly see that the curves for E_{c1} and E_{c2} are indistinguishable in some ranges (when q_x is small or very large).

Response times

Now we look for the response times for the cases that are shown in Figure 5.5 by plotting the eigenvalues, ω of the equation (5.27) and the corresponding response time, τ, see Figures 5.8-5.15. Note that the response time is defined as $|\omega|^{-1}$. This is a standard indicative measure of the time it takes for the physical system to respond to a perturbation.

Stability Regions

We can clearly see from graphs 5.1-5.7; where an electric field is included, that there is always induced instability. Also, we can see that the instability regions are greater than stability regions in some cases, especially when the dynamic term $\tilde{g}_i$ is included, but they are smaller in other cases for the linear case. This means that there is an opportunity to have instability in the non-linear case, which can be investigated in future work.

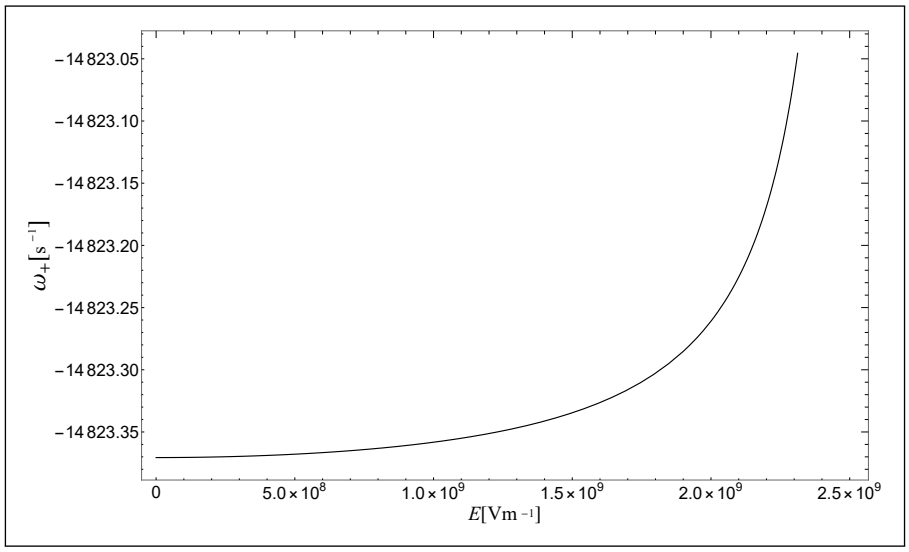

(a) First solution, ω_+ graph.

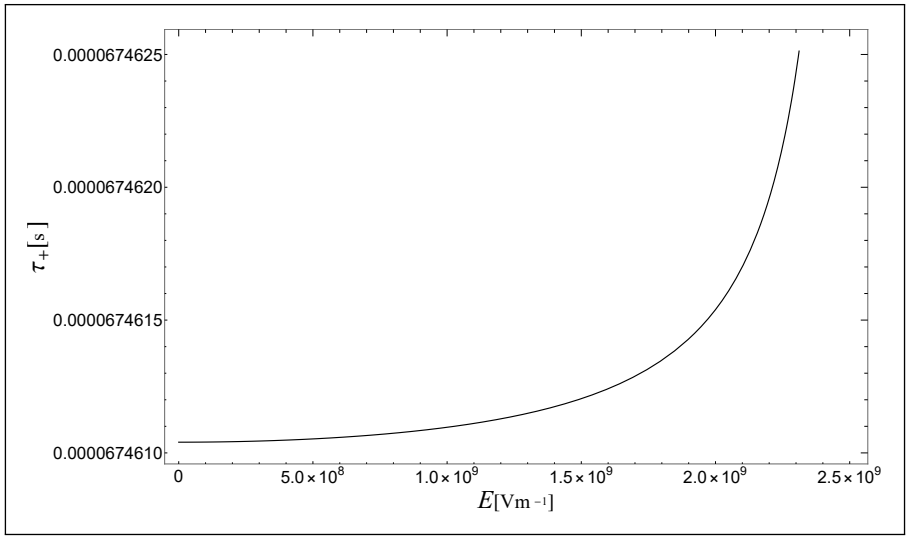

(b) First solution, τ_+ graph.

Figure 5.8: These graphs show the eigenvalue ω_+ of the equation (5.27) and the consequent decay times that depend on the electric field E for stability when $0 < E < E_{c_3}$ for the initial planar alignment of SmA. Graph 5.8b displays the response time. It is clear that the response time (i.e., the mode with the slowest decay rate) is given by $|\omega^+|^{-1}$.

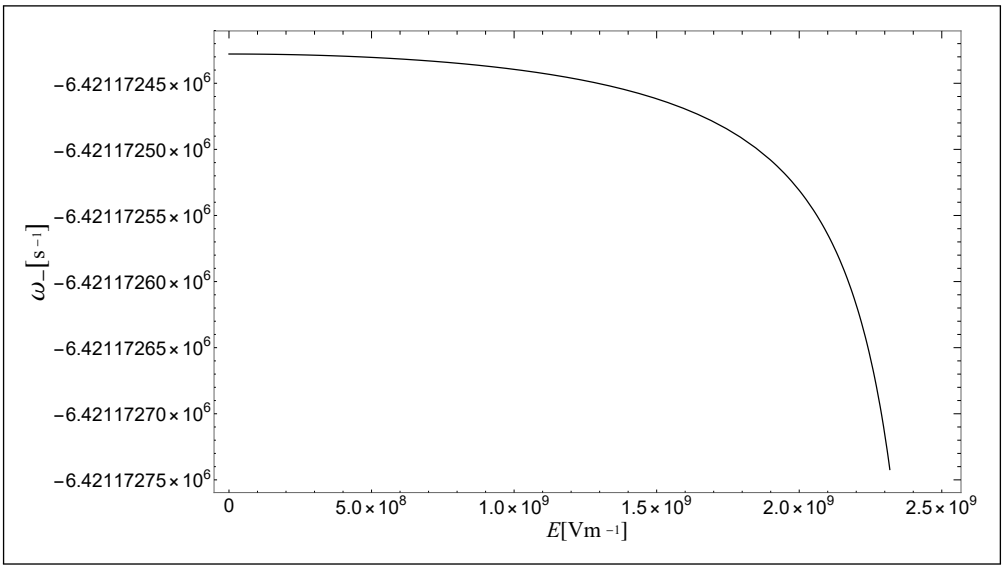

(a) Second solution, ω_- graph.

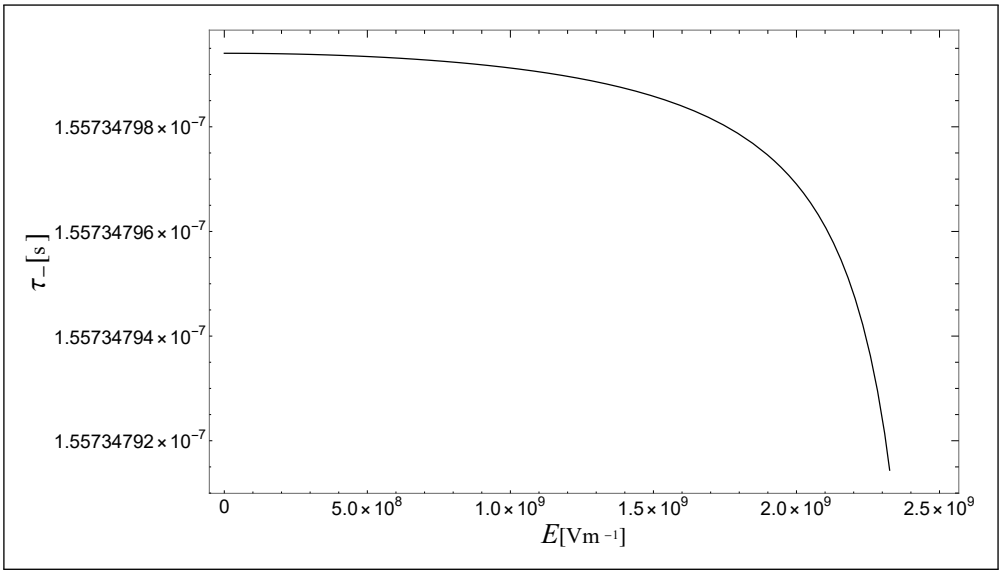

(b) Second solution, τ_- graph.

Figure 5.9: These graphs show the eigenvalue ω_- of the equation (5.27) and the consequent decay times that depend on the electric field E for stability when $0 < E < E_{c_3}$ for the initial planar alignment of SmA.

We can see from the graphs above that graph (5.8b) displays the response time. It is clear that the response time (i.e., the mode with the slowest decay rate) is given by $|\omega^+|^{-1}$. For demonstration purposes, we selected $q_x = 1000$ to investigate the consequences of the results in Figures 5.8-5.15. These figures use the data in Table 4.1.

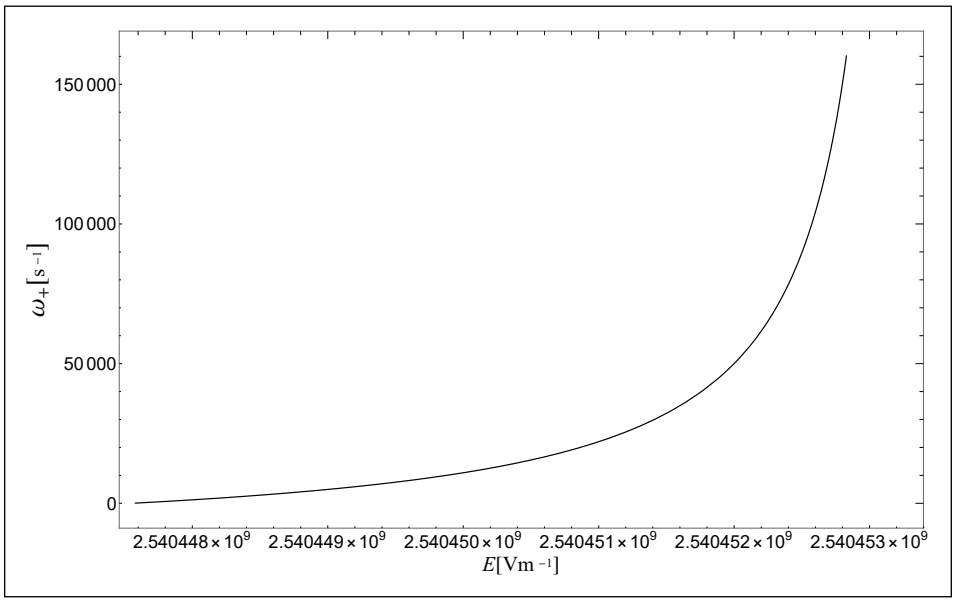

(a) First solution, ω_+ graph.

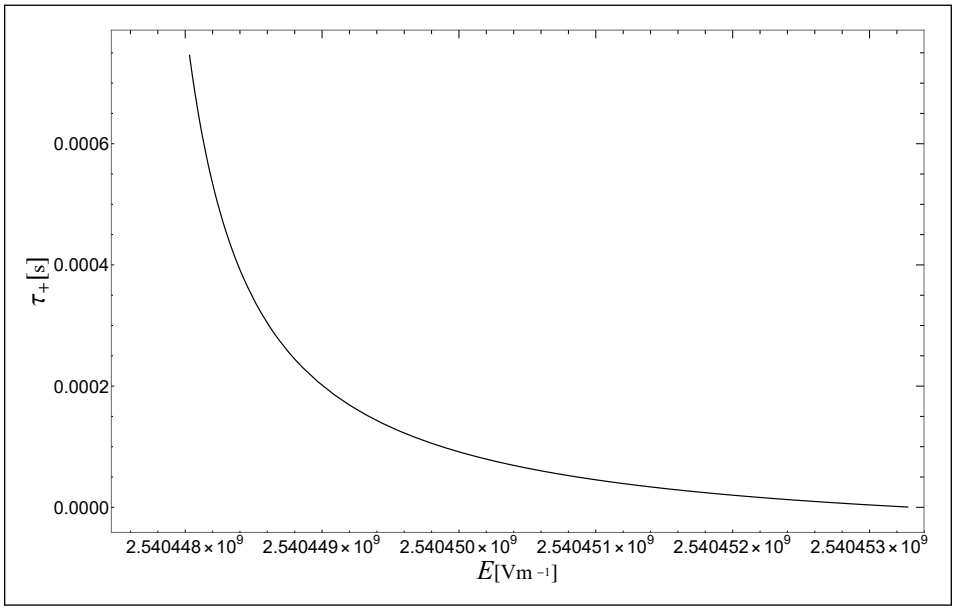

(b) First solution, τ_+ graph.

Figure 5.10: These graphs show the eigenvalue ω_+ of the equation (5.27) and the consequent decay times that depend on the electric field E for instability when $E_{c_3} < E < E_{c_2}$ for the initial planar alignment of SmA. Graph 5.10b displays the response time.

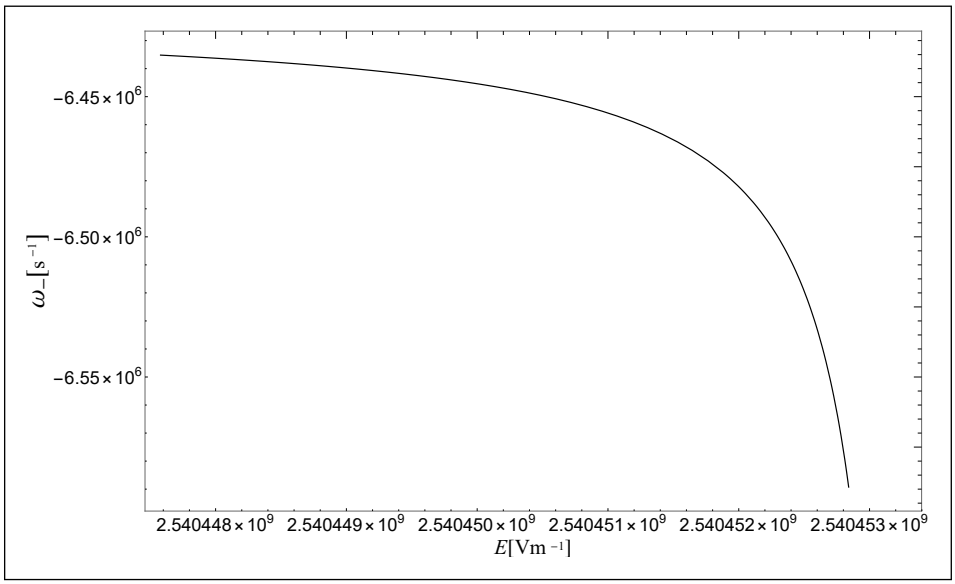

(a) Second solution, ω_{-} graph.

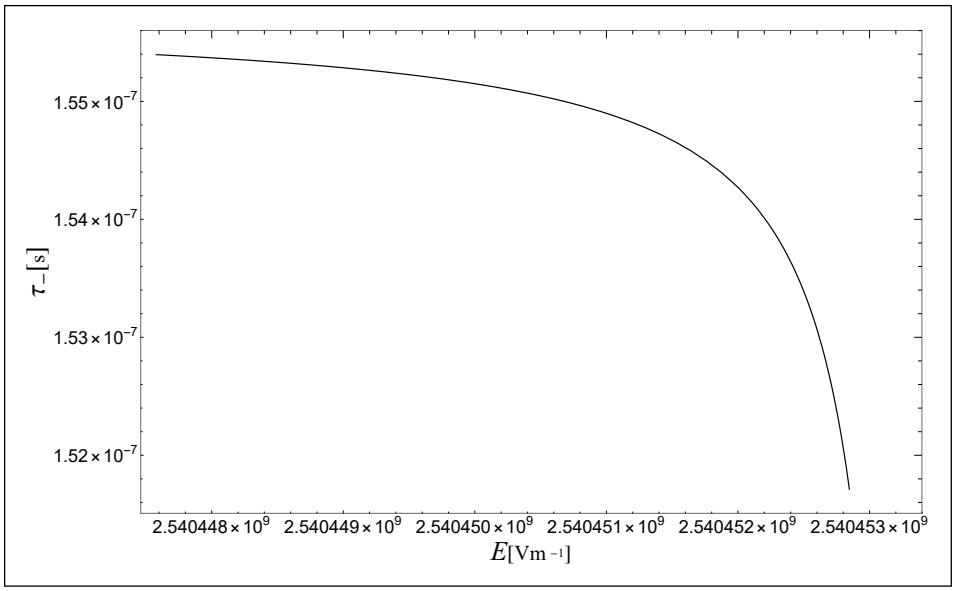

(b) Second solution, τ_{-} graph.

Figure 5.11: These graphs show the eigenvalue ω_{-} of the equation (5.27) and the consequent decay times that depend on the electric field E for instability when $E_{c_3} < E < E_{c_2}$ for the initial planar alignment of SmA.

Note that the response time in this case for the onset of instability is given in graph 5.10b. Notice that typical response times for stability in Figure 5.8 are faster than those for instability in Figure 5.10.

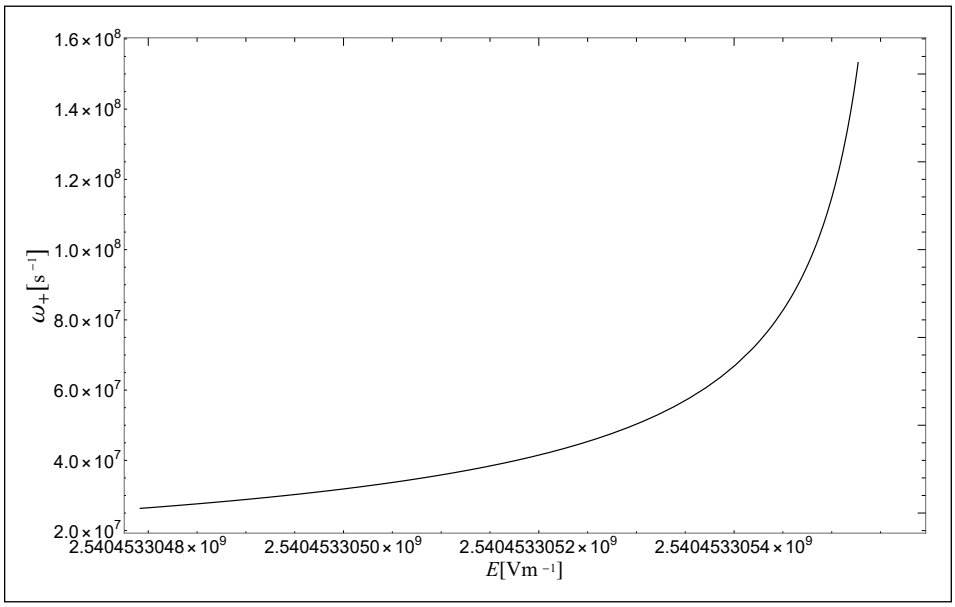

(a) First solution, ω_+ graph.

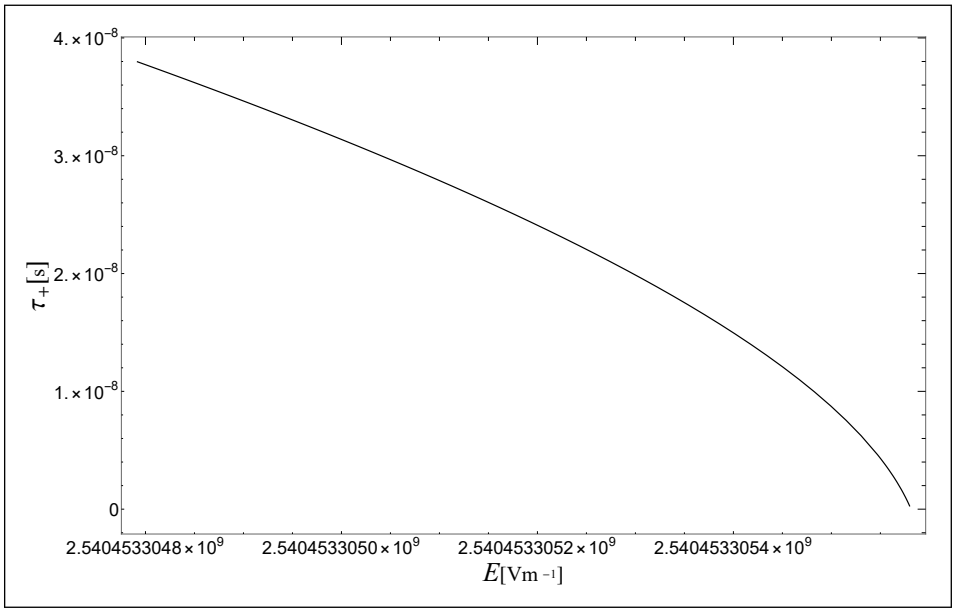

(b) First solution, τ_+ graph.

Figure 5.12: These graphs show the eigenvalue ω_+ of the equation (5.27) and the consequent decay times that depend on the electric field E for instability when $E_{c_2} < E < E_{c_1}$ for the initial planar alignment of SmA.

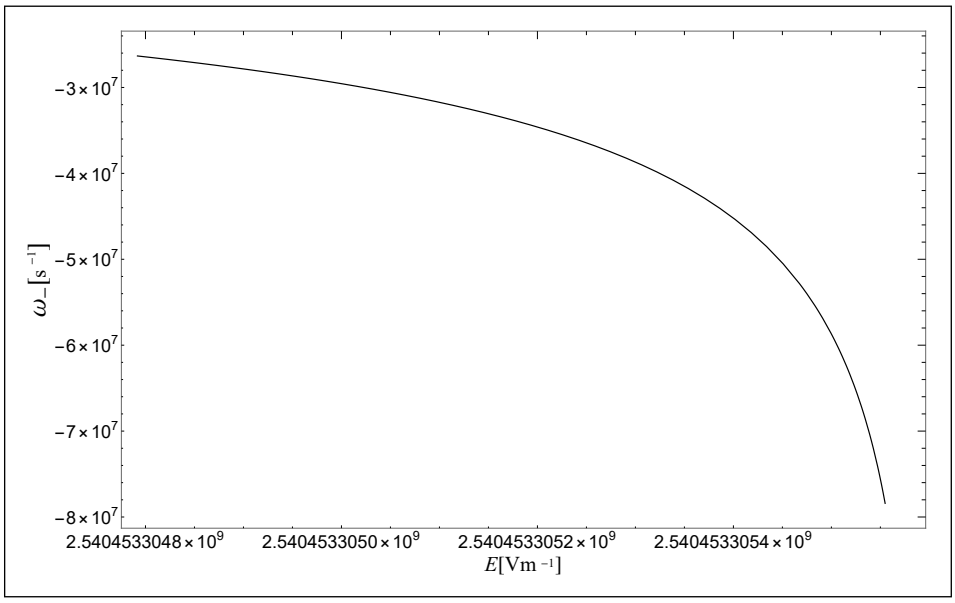

(a) Second solution, ω_{-} graph.

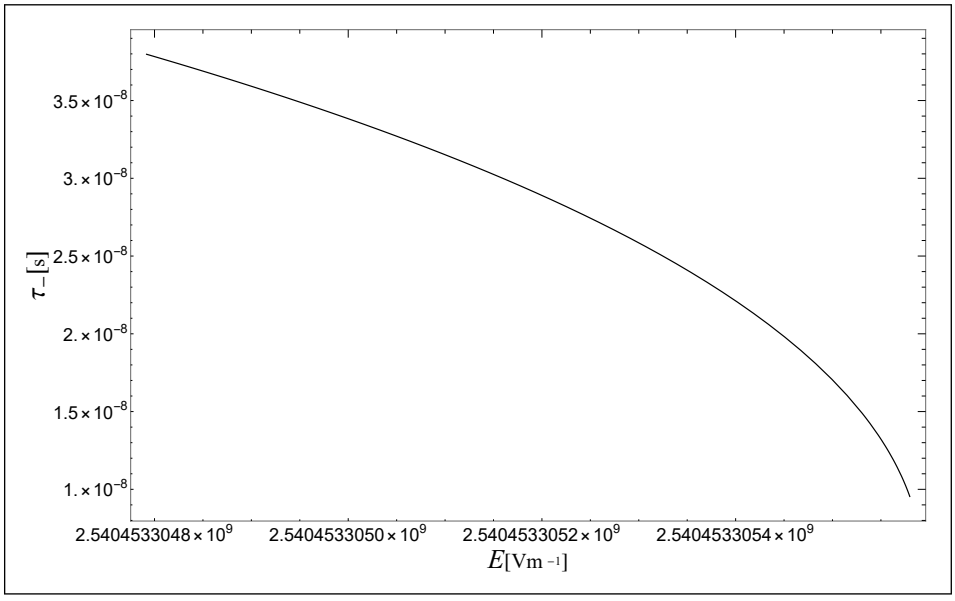

(b) Second solution, τ_{-} graph.

Figure 5.13: These graphs show the eigenvalue ω_{-} of the equation (5.27) and the consequent decay times that depend on the electric field E for instability when $E_{c_2} < E < E_{c_1}$ for the initial planar alignment of SmA. Graph 5.13b displays the response time.

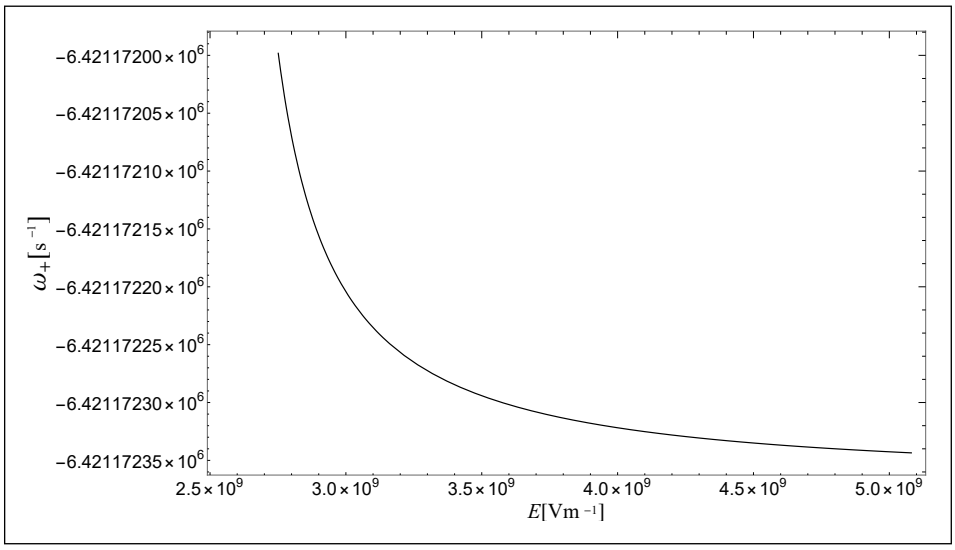

(a) First solution, ω_+ graph.

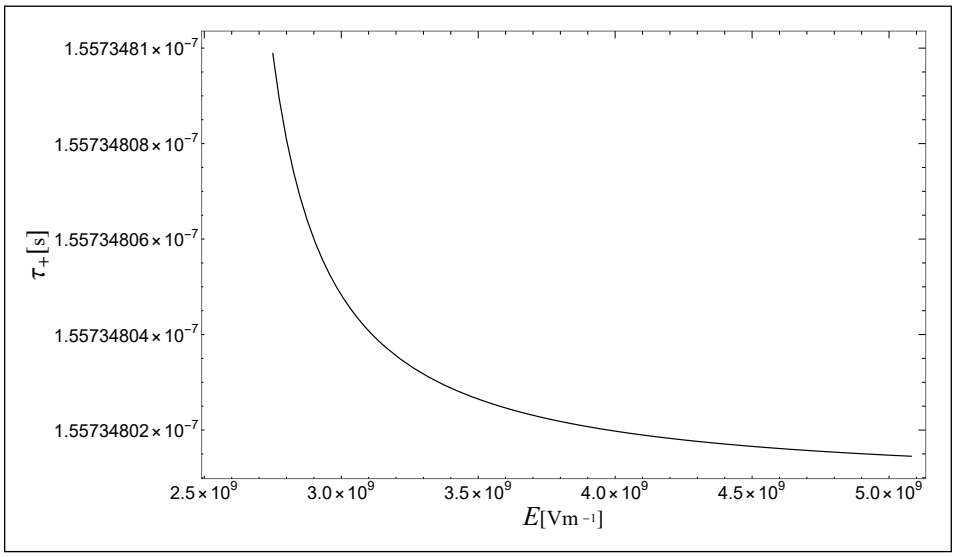

(b) First solution, τ_+ graph.

Figure 5.14: These graphs show the eigenvalue ω_+ of the equation (5.27) and the consequent decay times that depend on the field E for stability when $E > E_{c_1}$ for the initial planar alignment of SmA.

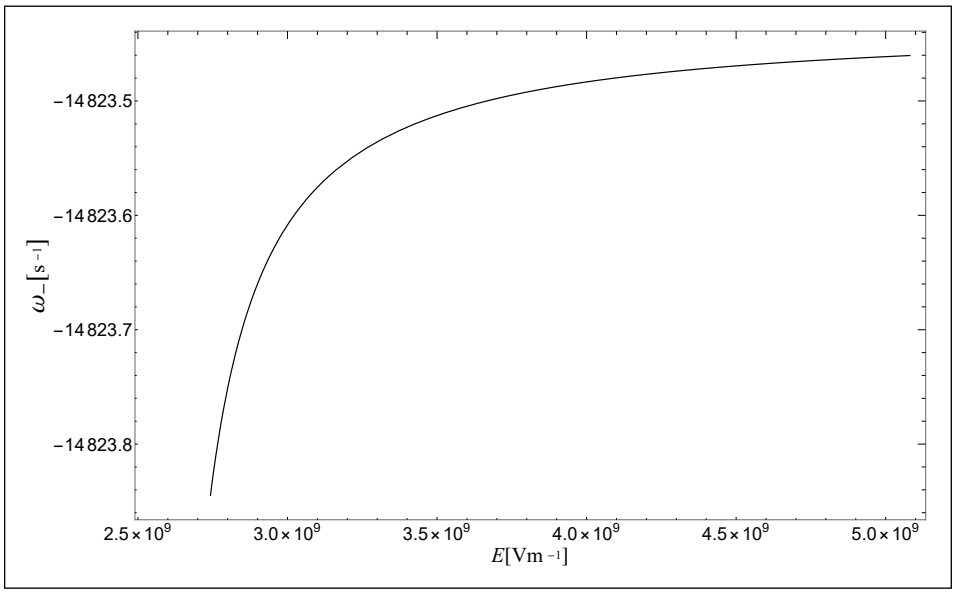

(a) Second solution, ω_{-} graph.

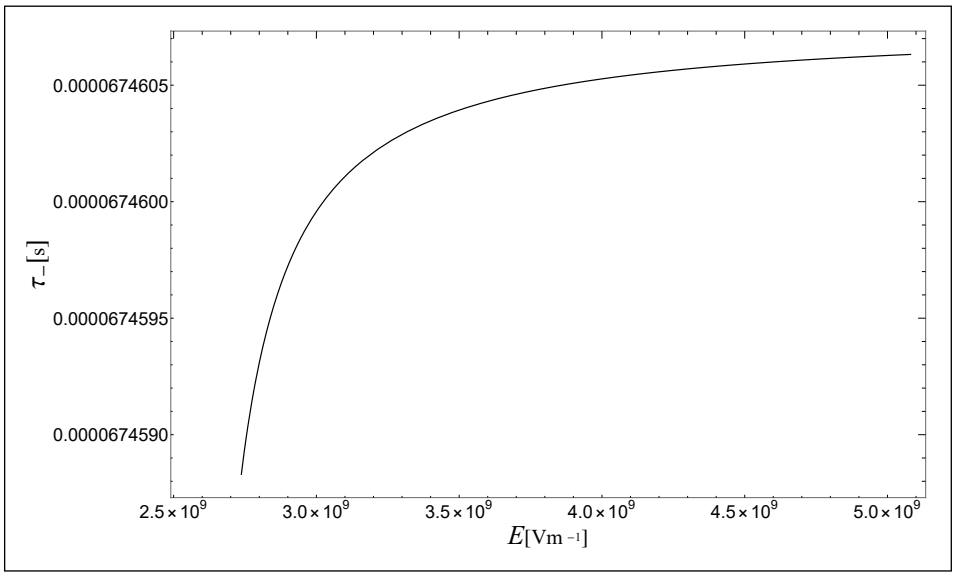

(b) Second solution, τ_{-} graph.

Figure 5.15: These graphs show the eigenvalue ω_{-} of the equation (5.27) and the consequent decay times that depend on the field E for stability when $E > E_{c_1}$ for the initial planar alignment of SmA. Graph 5.15b displays the response time.

Remarks. The instability response times in 5.13 are much faster than those for stability in Figures 5.8, and those for instability in Figures 5.10, and those for stability in Figures 5.15. This is based on a linearised set of model equations. However, the existence of instability criteria from the linear analysis may indicate that a more intricate non-linear analysis could explore and reveal more potential restriction bounds on stability criteria.

These theoretical investigations reveal predicted response times for the behaviour of a general SmA material. These nanosecond response times for SmA liquid crystals (see Figures 5.13) match recently identified experimental response times published and patented in 2016 [8]. The γ_1 dependence influences the boundaries of the stability regions. This is purely driven by the dynamics induced by the director motion by neglecting flow. In the next subsection, we explore the impact of flow upon the system.

Nematics generally respond in ms and smectics can respond in μs. It has been reported that some smectics respond in ns [78].

5.2.4 Flow, $\tilde{g}_i$ and electric field included

Here, we extend Stewart's problem in [79], which includes flow. We also include the term $\tilde{g}_i$. Substituting the results in (4.35) and (4.52), the dynamic equations (4.7) to (4.13) are given explicitly to first order as

$$v_{1,x} + v_{3,z} = 0, \tag{5.36}$$

$$\rho v_{1,t} = -\tilde{p}_{,x} + \frac{1}{2}(\alpha_4 - \tau_2)v_{1,xx} + \frac{1}{2}(\alpha_4 + \tau_2)v_{1,zz}, \tag{5.37}$$

$$\begin{aligned}\rho v_{3,t} = &-\tilde{p}_{,z} - K_1^a u_{,xxxx} + (B_1 u_{,xx} + B_0 u_{,zz}) + B_1\theta_{,x} + \frac{1}{2}(\alpha_4 + \tau_2)v_{3,xx} \\ &+ \frac{1}{2}(\alpha_4 + 2\tau_1 + 3\tau_2)v_{3,zz},\end{aligned} \tag{5.38}$$

$$K_1^n\theta_{,xx} = B_1(\theta + u_{,x}) + (\alpha_3 - \alpha_2)\theta_{,t} - \epsilon_0\epsilon_a E^2\theta, \tag{5.39}$$

$$v_3 - u_{,t} = \lambda_p\Big[K_1^a u_{xxxx} - B_1(\theta_{,x} + u_{,xx}) - B_0 u_{,zz}\Big], \tag{5.40}$$

where the solution of this system of equations is given in (4.61). Inserting (4.61) into (5.36)-(5.40), we then obtain the corresponding matrix system

$$\begin{pmatrix} 0 & 0 & 0 & q_x & q_z \\ iq_x & 0 & 0 & \rho\omega + X & 0 \\ iq_z & -iB_1q_x & Q & 0 & \rho\omega + Z \\ 0 & S + \gamma_1\omega - \epsilon_0\epsilon_a E^2\theta & iB_1q_x & 0 & 0 \\ 0 & i\lambda_p B_1 q_x & -\omega - \lambda_p Q & 0 & 1 \end{pmatrix} \begin{pmatrix} p_0 \\ \theta_0 \\ u_0 \\ v_{10} \\ v_{30} \end{pmatrix} = \begin{pmatrix} 0 \\ 0 \\ 0 \\ 0 \\ 0 \end{pmatrix}, \tag{5.41}$$

where S, Q, R, X and Z are defined in the previous chapter in equations (4.41), (4.42), (4.44), (4.64) and (4.65), respectively. For non-zero solutions, the determinant of the square matrix on the left-hand side of (5.41) must equal zero. This condition is given by the following cubic equation for ω:

$$a_0\omega^3 + a_1\omega^2 + a_2\omega + a_3 = 0, \tag{5.42}$$

where,

$$a_0 = \rho\gamma_1(q_x^2 + q_z^2),$$

$$a_1 = \rho(S - \epsilon_0\epsilon_a E^2)(q_x^2 + q_z^2) + \gamma_1\Big(T + \rho\lambda_p Q(q_x^2 + q_z^2)\Big),$$

$$a_2 = \left(S - \epsilon_0\epsilon_a E^2\right)\left(T + \rho\lambda_p Q\left(q_x^2 + q_z^2\right)\right) + \gamma_1 Q(q_x^2 + \lambda_p T) - \rho\lambda_p(q_x^2 + q_z^2)B_1^2 q_x^2,$$

$$a_3 = (R - \epsilon_0\epsilon_a Q E^2)(q_x^2 + \lambda_p T).$$

For stability ($\Re(\omega) < 0$), it is clear that a_0 is always positive; using Routh-Hurwitz stability criterion [56], the coefficients of equation (5.42) must satisfy the following conditions

$$a_1 > 0, \tag{5.43}$$

$$a_3 > 0, \tag{5.44}$$

$$a_1 a_2 - a_0 a_3 > 0. \tag{5.45}$$

Let $F(E) = a_1 a_2 - a_0 a_3$. We can rewrite $F(E)$ in the following form

$$F(E) = AE^4 - BE^2 + C, \tag{5.46}$$

where

$$A = \rho\epsilon_0^2\epsilon_a^2(q_x^2+q_z^2)\left[T + \rho\lambda_p(q_x^2+q_z^2)Q\right], \tag{5.47}$$

$$B = \epsilon_0\epsilon_a\Bigg[2\rho(q_x^2+q_z^2)\left(R + B_1^2 q_x^2\right)\frac{T}{Q} + \lambda_p\rho^2(2R + B_1^2 q_x^2)(q_x^2+q_z^2)^2 + \gamma_1\Big(T + \lambda_p\rho Q(q_x^2+q_z^2)\Big)^2\Bigg], \tag{5.48}$$

$$C = k_0Q^2 + k_1Q + k_2 + k_3Q^{-1} + k_4Q^{-2}, \tag{5.49}$$

and

$$\begin{pmatrix} k_4 \\ k_3 \\ k_2 \\ k_1 \\ k_0 \end{pmatrix} = \begin{pmatrix} \rho T(R + B_1^2 q_x^2)^2(q_x^2+q_z^2) \\ (R + B_1^2 q_x^2)\left(\lambda_p\rho^2 R(q_x^2+q_z^2)^2 + \gamma_1 T^2\right) \\ \rho\gamma_1(q_x^2+q_z^2)\left(2\lambda_p RT + B_1^2(q_x^4 + 2\lambda_p T q_x^2)\right) \\ \gamma_1\left(\lambda_p^2\rho^2 R(q_x^2+q_z^2)^2 + \gamma_1 T(q_x^2 + \lambda_p T)\right) \\ \rho\gamma_1^2\lambda_p(q_x^2+q_z^2)(q_x^2+\lambda_p T) \end{pmatrix}. \tag{5.50}$$

It is clear that all coefficients a_0, A, B and C are always positive. Now, there are two cases:

Case 1: If $\epsilon_a < 0$, then a_1, a_3 and $F(E)$ are always positive. Therefore, the initial planar alignment of SmA is linearly asymptotically stable to small perturbations.

Case 2: If $\epsilon_a > 0$, it is straightforward to prove that

$$a_1 > 0 \quad \text{if} \quad E < \sqrt{\frac{\gamma_1 T + \rho(q_x^2+q_z^2)(S + \lambda_p\gamma_1 Q)}{\rho\epsilon_0\epsilon_a(q_x^2+q_z^2)}} \equiv E_1^c, \tag{5.51}$$

and

$$a_3 > 0 \quad \text{if} \quad E < \sqrt{\frac{R}{\epsilon_0\epsilon_a Q}} \equiv E_3^c. \tag{5.52}$$

Moreover, it is easy to verify that $E_3^c < E_1^c$. In the function $F(E)$, we have two cases:

Firstly, when $B^2 - 4AC < 0$, then $F(E)$ is always positive. Thus, the system (5.41) is linearly asymptotically stable if the two conditions (5.51) and (5.52) are satisfied.

Secondly, when $B^2 - 4AC > 0$, there are two positive roots say, E_- and E_+ where $E_- < E_+$. Let $F(q, \beta, E) = AE^4 - BE^2 + C$, where

$$q_x = q\cos\beta, \quad q_z = q\sin\beta.$$

We note here that this mathematical expression has physical units, but its physical values are not directly of interest to the measures of the values in reality. It is a mathematical expression that identifies stability; the units are stated in Figures 5.17, 5.19, 5.21 and 5.23 for reference, as this explains its high numerical values for the material parameters we use. In order to generalise the stability results further, unlike the work in the previous Chapters 3, 4 and 5, we do not fix on a first mode analysis and do not presume a fixed sample depth d where $q_z = \pi/d$; introducing the more general form of q_z in the above ansatz will allow us to explore more deeply the stability criteria that will arise.

Take note that q_x and q_z are related through the relation $q^2 = q_x^2 + q_z^2$. We remark that the wavenumber q is controlled by the experimentalist as it is the amplitude of the physically applied perturbation. Also, the direction of travel of the wave is determined by β, again controlled by the experimentalist. The combinations of varying q and β allow the experimentalist to obtain data on critical directions and amplitudes of the perturbations that induce instability and stability, and these results can be collated and compared to the theoretical results derived here. It follows that these results can, in principle, be used for guiding experimentalists in applications and also allow an analysis of the data obtained that will reveal the

critical dependencies on crucial material parameters, which will only become evident after experimental data has been collected and compared with the presented theoretical results.

It then follows that $F(q, \beta, E) = 0$ for $E \geq 0$ if

$$E_{\pm}(q, \beta) = \sqrt{\frac{B \pm \sqrt{B^2 - 4AC}}{2A}}. \tag{5.53}$$

Note that $E_- < E_+$. Therefore, $F(E) > 0$ if $0 \leq E < E_-$ and $E > E_+$. Moreover, it is easy to prove that $E_3^c < E_- < E_+$. So, all conditions (5.43) to (5.45) can be reduced to one condition, which is

$$E < E_3^c. \tag{5.54}$$

Therefore, the initial planar alignment of SmA is linearly asymptotically stable to small perturbations when the condition (5.54) is satisfied. Otherwise, it is unstable: there exists a finite sensitive regime, $E > E_3^c$, where instabilities can occur. This system is sensitive only for $\epsilon_a > 0$, where stability is determined by the material parameters and the magnitude of the electric field. At $\beta = \frac{\pi}{2}$, the system (5.41) is linearly asymptotically stable when $E < \sqrt{\frac{B_1}{\epsilon_0 \epsilon_a}}$; otherwise, unstable. Also, we can see that the curves E_- and E_+ tend to reach the constant value $\sqrt{\frac{B_1}{\epsilon_0 \epsilon_a}}$ when q goes to 0. This value is equal to the value on the critical curve E_3^c at $q = 0$, see Figure 5.22. For more investigation, we will look at the different values of β to see the behaviour of stability and instability, see Figures 5.16-5.23 below. For demonstration purposes, we selected $q = 10^7$ to investigate the consequences of the results in Figures 5.17, 5.19,5.21 and 5.23.

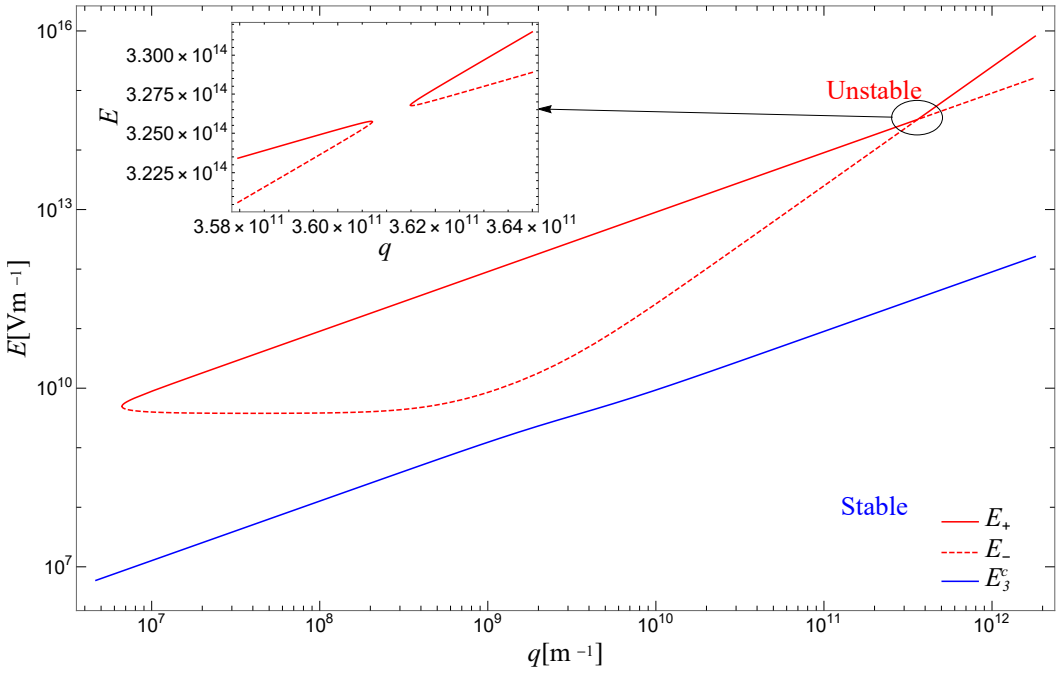

Figure 5.16: This shows the graphs of the values E_-, E_+ and the condition E_3^c for discriminating between stability and instability when $\beta = 0$ as a function of the wave number q. The system (5.41) is linearly asymptotically stable when $E < E_3^c$; otherwise, unstable.

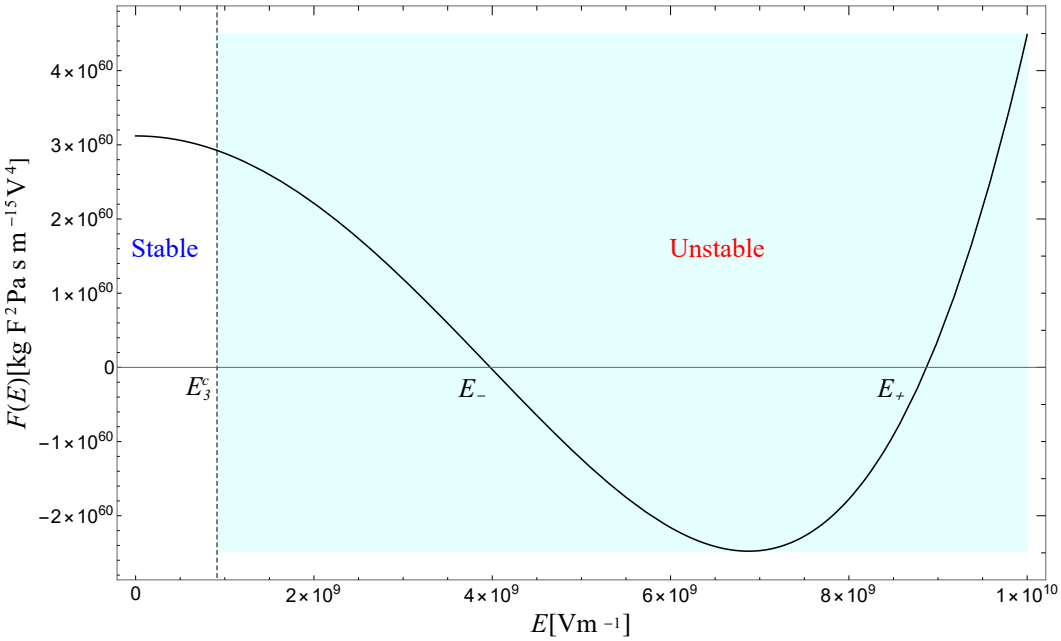

Figure 5.17: This shows the graph of the function $F(E) = AE^4 - BE^2 + C$ where $B^2 - 4AC > 0$ and $\beta = 0$. This graph illustrates that the system (5.41) is asymptotically linearly stable if $E < E_3^c$; otherwise, unstable.

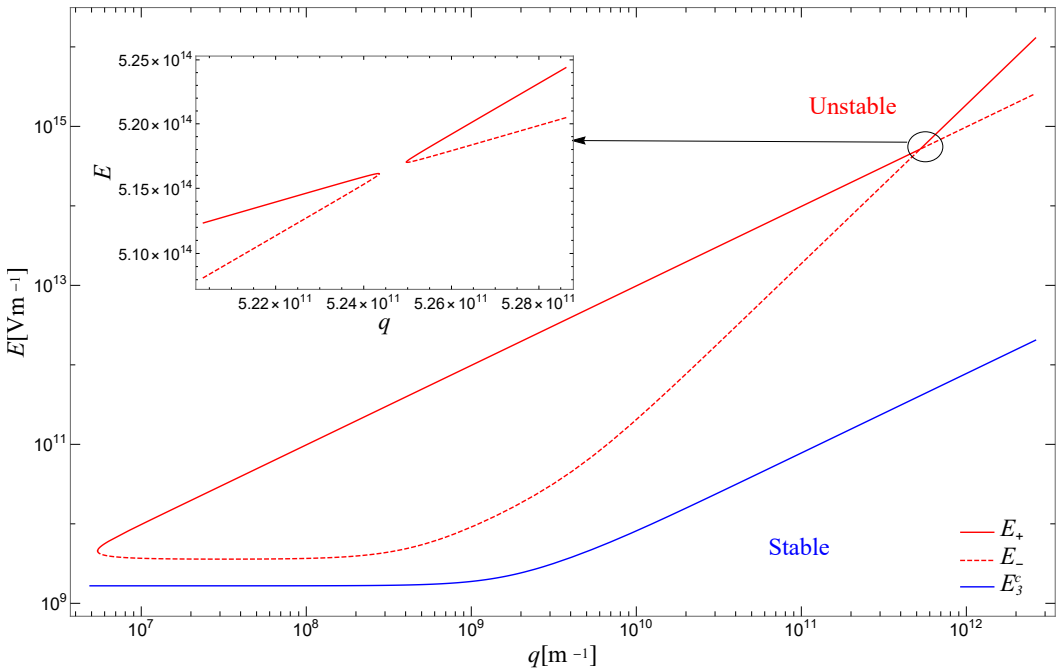

Figure 5.18: This shows the graphs of the values E_-, E_+ and the condition E_3^c for discriminating between stability and instability when $\beta = \frac{\pi}{6}$ as a function of the wave number q. The system (5.41) is linearly asymptotically stable when $E < E_3^c$; otherwise, unstable.

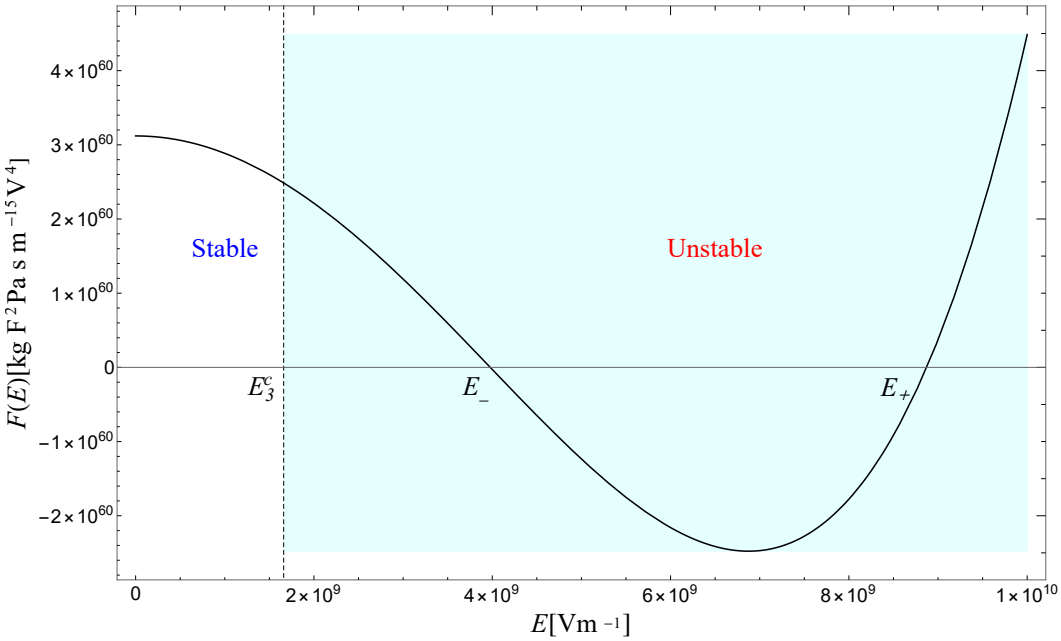

Figure 5.19: This shows the graph of the function $F(E) = AE^4 - BE^2 + C$ where $B^2 - 4AC > 0$ and $\beta = \frac{\pi}{6}$. This graph illustrates that the system (5.41) is linearly asymptotically stable if $E < E_3^c$; otherwise, unstable.

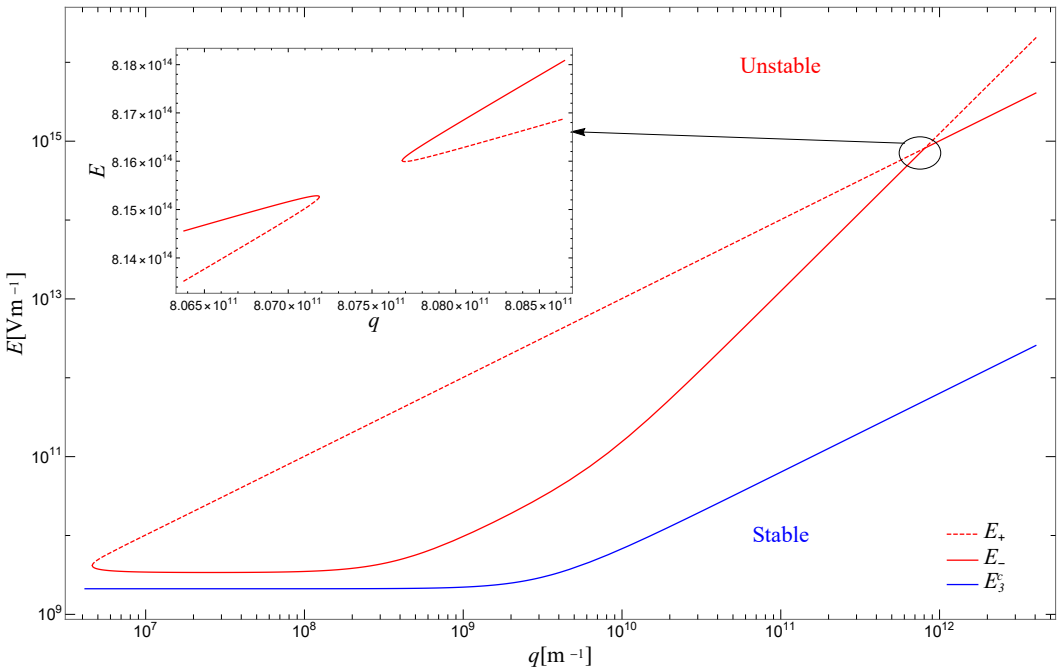

Figure 5.20: This shows the graphs of the values E_-, E_+ and the condition E_3^c for discriminating between stability and instability when $\beta = \frac{\pi}{4}$ as a function of the wave number q. The system (5.41) is linearly asymptotically stable when $E < E_3^c$; otherwise, unstable.

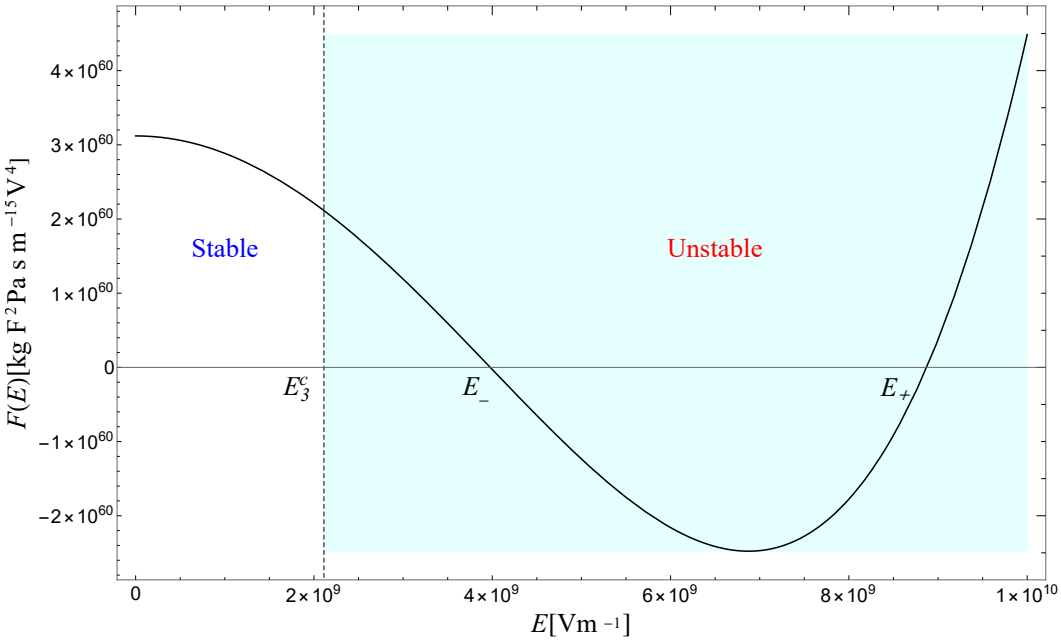

Figure 5.21: This shows the graph of the function $F(E) = AE^4 - BE^2 + C$ where $B^2 - 4AC > 0$ and $\beta = \frac{\pi}{4}$. This graph illustrates that the system (5.41) is linearly asymptotically stable if $E < E_3^c$; otherwise, unstable.

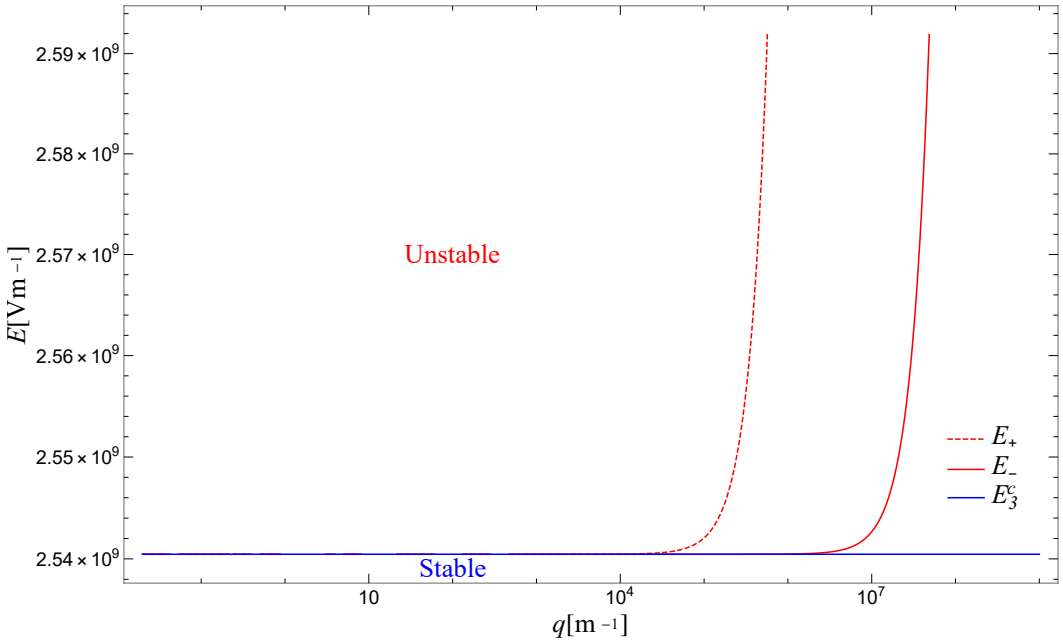

Figure 5.22: This shows the graphs of the values E_-, E_+ and the condition E_3^c for discriminating between stability and instability when $\beta = \frac{\pi}{2}$ as a function of the wave number q. The system (5.41) is linearly asymptotically stable when $E < E_3^c$; otherwise, unstable.

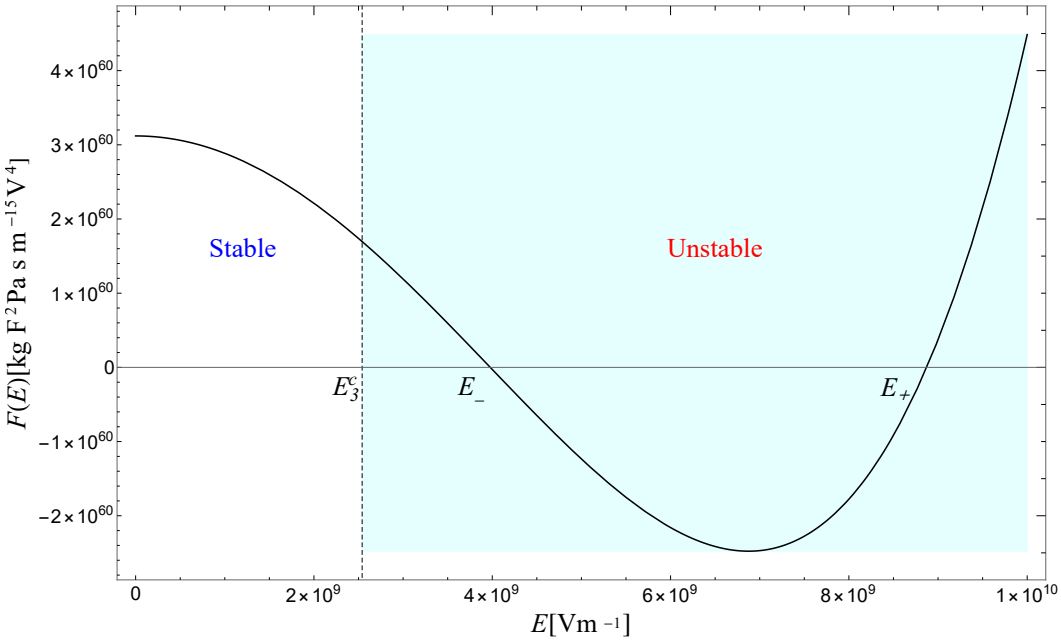

Figure 5.23: This shows the graph of the function $F(E) = AE^4 - BE^2 + C$ where $B^2 - 4AC > 0$ and $\beta = \frac{\pi}{2}$. This graph illustrates that the system (5.41) is linearly asymptotically stable if $E < E_3^c$; otherwise, unstable.

From the graphs in Figures 5.16, 5.18, 5.20 and 5.22, we can see that the system is unstable in some areas for the linear case. Therefore, it is worthwhile to look for instability in the non-linear case. This needs more advanced work, which is beyond the scope of this thesis. Notice from the graphs in Figures 5.17, 5.19, 5.21 and 5.23 that the E_3^c criterion curve changes form as β changes. Nevertheless, regions of stability and instability are clearly distinguished between two separated

regions.

In conclusion, we can see that applying an electric field to a sample of SmA liquid crystal can lead to a linear instability for the initial planar alignment of SmA when $\epsilon_a > 0$. When the term $\tilde{g}_i$ is included, we have linear stability when the electric field magnitude is less than a critical value. The graphs above display new qualitative results and an instability criteria. The regions of stability and instability are intricate and have been investigated in detail.

5.3 Conclusions and comments

In Subsection 5.2.1, we discussed two cases. When $\epsilon_a < 0$, we found that the system of equations (5.3) is always linearly asymptotically stable, while when $\epsilon_a > 0$, we can have regimes of stability or instability, see Figures 5.1 and 5.2. Minimum values are also discussed in Subsection 5.2.2. When we included the term $\widetilde{g}_i$, we still have only stability when $\epsilon_a < 0$, and have possible instances of stability or instability when $\epsilon_a > 0$, see Figures 5.3 and 5.4. In Subsection 5.2.3, we included an electric field and flow. We found that the system of equations (5.26) is always linearly asymptotically stable when $\epsilon_a < 0$. We also found that when $\epsilon_a > 0$, there are three critical curves, E_{c_1}, E_{c_2} and E_{c_3}, where we can see that the system of equations (5.26) is linearly asymptotically stable when $0 < E < E_{c_3}$ or $E > E_{c_1}$; otherwise, unstable, see Figures 5.5-5.7. We also discussed response times for the cases in this Subsection. We found that the instability response times when $E_{c_2} < E < E_{c1}$ are much faster than those in other cases, see Figures 5.8-5.15. In Subsection 5.2.4, we sought the stability and instability when we incorporate flow, $\tilde{g}_i$ and an electric field. We then found that the system of equations (5.41) is always linearly asymptotically stable when $\epsilon_a < 0$. On the other hand, when $\epsilon_a > 0$, we found that the system (5.41) is linearly asymptotically stable when

$E < E_3^c$ and unstable when $E > E_3^c$; see Figures 5.16-5.23.

Chapter 6

Dynamic continuum theory of biaxial nematic liquid crystals

6.1 Introduction

A biaxial nematic is a spatially homogeneous liquid crystal with three distinct optical axes. This is to be contrasted to a simple nematic, which has a single preferred axis, around which the system is rotationally symmetric. We will apply the continuum equations for the dynamics of an incompressible biaxial nematic liquid crystal [50, 51, 80]; the necessary derivations and calculations required to establish these equations are sophisticated and extensive and are beyond the scope of this thesis. Nevertheless, the Reader is therefore urged to consult these definitive texts and review articles for more details if required. We deploy this biaxial theory and its equations to look at stability and instability.

The biaxial alignment phase can be modelled via a regular rectangular plate with sides of lengths a, b and c with $a > b > c$. Although the average molecular shape

may be changed, it can be made up of plate-like, lozenge-like, cross-shaped, bone-shaped and boomerang-shaped molecules [53,54,80,89]. Here, the three orthogonal unit vectors $\mathbf{n}, \mathbf{m}$ and $\mathbf{l}$ are used to describe the orientation of this plate. These vectors generally depend on the spatial variable $\mathbf{x}$ and time t; see Figure 6.1 below. The vectors $\mathbf{n}$ and $\mathbf{m}$ are called the major and minor directors, respectively. The biaxial alignment is described by the orientation of the major and minor directors. The two vectors $\mathbf{n}, \mathbf{m}$ and $\mathbf{l}$ are related by the relation $\mathbf{l} = \mathbf{n} \times \mathbf{m}$. Moreover, the major director $\mathbf{n}$ and the minor director $\mathbf{m}$ are constrained by the following equations $\mathbf{n} \cdot \mathbf{n} = 1$, $\mathbf{m} \cdot \mathbf{m} = 1$, $\mathbf{n} \cdot \mathbf{m} = 0$ [80].

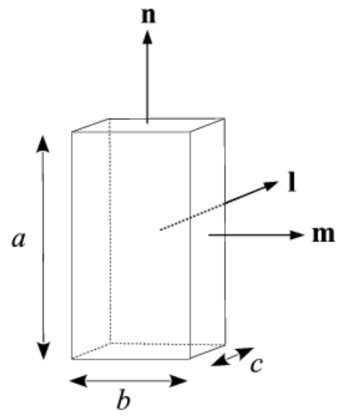

Figure 6.1: This diagram describes the biaxial phase via a biaxial plate. $\mathbf{n}$ represents the major director while $\mathbf{m}$ represents the minor director. a, b and c represent the dimensions of the biaxial plate that represents the constituent local molecular structure, where $a > b > c$ [80].

In this section, we use the biaxial nematic liquid crystal dynamic equations and apply the established balance laws. In Section 6.2, we look at oscillatory shear flow of biaxial nematic liquid crystal. In Section 6.2.1, oscillatory shear flow solutions will be obtained. Then we add a perturbation to these solutions. In Section 6.3, we look at stability and instability. In Subsection 6.3.1, we study the linear stability

of nematic liquid crystals, which guides us to study the linear stability of biaxial nematics in Subsection 6.3.2. In Section 6.4, an exploration of the dissipation function is considered.

The biaxial nematic dynamic equations

To apply the dynamic theory to the biaxial nematic liquid crystals, we return to the general balance laws for linear and angular momentum at the equations (2.15)-(2.25). It has been shown [52] that the local angular velocity of the liquid crystal material element $\mathbf{w}$ is then the local angular velocity of both the major and minor directors and [50, 51, 80] (cf. [14] for the method to find $\mathbf{w}$)

$$\dot{\mathbf{n}} = \mathbf{w} \times \mathbf{n}, \quad \dot{\mathbf{m}} = \mathbf{w} \times \mathbf{m}. \tag{6.1}$$

The rate of strain tensor $\mathbf{A}$ and vorticity tensor $\mathbf{W}$ are given by [80]

$$\mathbf{A} = \frac{1}{2}\left(\nabla\mathbf{v} + (\nabla\mathbf{v})^{\mathrm{T}}\right), \quad \mathbf{W} = \frac{1}{2}\left(\nabla\mathbf{v} - (\nabla\mathbf{v})^{\mathrm{T}}\right). \tag{6.2}$$

The co-rotational time flux vectors of $\mathbf{n}$ and $\mathbf{m}$ defined respectively by

$$\mathbf{N} = \dot{\mathbf{n}} - \mathbf{W}\mathbf{n}, \quad \mathbf{M} = \dot{\mathbf{m}} - \mathbf{W}\mathbf{m}, \tag{6.3}$$

where, because $\mathbf{m} \cdot \mathbf{n} = 0$ and $\mathbf{W}$ is skew-symmetric,

$$\mathbf{M} \cdot \mathbf{n} + \mathbf{N} \cdot \mathbf{m} = 0. \tag{6.4}$$

If we assume that elastic energy density w_{el} is considered with the inclusion of the magnetic or electric field, using the balance laws leads us to conclude the continuum equations for the dynamics of an incompressible biaxial nematic liquid crystal [80]. The major director $\mathbf{n}$ and minor director $\mathbf{m}$ obey the constraints, as noted earlier,

$$\mathbf{n} \cdot \mathbf{n} = 1, \quad \mathbf{m} \cdot \mathbf{m} = 1, \quad \mathbf{n} \cdot \mathbf{m} = 0. \tag{6.5}$$

The conservation of mass gives the classical incompressible flow condition

$$v_{i,i} = 0, \tag{6.6}$$

and the balance of linear momentum equation is given by

$$\rho \dot{v}_i = \rho F_i - (p + w_{el})_{,i} + \tilde{g}^n_j n_{j,i} + \tilde{g}^m_j m_{j,i} + G^n_j n_{j,i} + G^m_j m_{j,i} + \tilde{t}_{ij,j}, \tag{6.7}$$

and the angular momentum equations are given by

$$\left(\frac{\partial w_{el}}{\partial n_{i,j}}\right)_{,j} - \frac{\partial w_{el}}{\partial n_i} + \tilde{g}^n_i + G^n_i = \gamma n_i + \kappa m_i, \tag{6.8}$$

$$\left(\frac{\partial w_{el}}{\partial m_{i,j}}\right)_{,j} - \frac{\partial w_{el}}{\partial m_i} + \tilde{g}^m_i + G^m_i = \tau m_i + \kappa n_i, \tag{6.9}$$

where G^n and G^m are the generalised torques and γ, τ and κ are scalar Lagrange multipliers (for more details on a comparison, see [79, p 266]). These multipliers reflect the constraints that $\mathbf{n}$ and $\mathbf{m}$ are unit vectors and that they are mutually orthogonal. Notice that the number of equations (6.5)-(6.9) are 13 equations in 13 unknowns. These equations represent the dynamic equations of an incompressible biaxial nematic liquid crystal. In the absence of elasticity and external fields, the dynamic equations (6.6)-(6.9) above reduce to the following equations, respectively

$$v_{i,i} = 0, \tag{6.10}$$

$$\rho \dot{v}_i = -p_{,i} + t_{ij,j}, \tag{6.11}$$

$$\tilde{g}^n_i = \kappa m_i + \gamma n_i, \tag{6.12}$$

$$\tilde{g}^m_i = \tau m_i + \kappa n_i. \tag{6.13}$$

The definitions of $\tilde{g}^n_i$ and $\tilde{g}^m_i$ arise from the associated Lagrange multipliers to the three constraints (6.5), and these, in turn, allow their identification in equations (6.15) and (6.16) below through constitutive theory as derived in [57,59], where details can be found on this derivation; we concentrate here on applications of this theory and leave the interested reader to these references if they wish to delve into

the derivations further. Also, the constitutive equations for the viscous stress $\tilde{t}_{ij}$ and the vectors $\tilde{g}_i^n$ and $\tilde{g}_i^m$ are given by [78, 80]

$$\begin{aligned}\tilde{t}_{ij} =&\alpha_1 n_k A_{kp} n_p n_i n_j + \alpha_2 N_i n_j + \alpha_3 N_j n_i + \alpha_4 A_{ij} + \alpha_5 n_j A_{ik} n_k + \alpha_6 n_i A_{jk} n_k \\ &+ \beta_1 m_k A_{kp} m_p m_i m_j + \beta_2 M_i m_j + \beta_3 M_j m_i + \beta_5 m_j A_{ik} m_k + \beta_6 m_i A_{jk} m_k \\ &+ \left(\mu_1 m_i n_j + \mu_2 m_j n_i\right) N_p m_p + \left(\mu_3 m_i n_j + \mu_4 m_j n_i\right) n_k A_{kp} m_p \\ &+ \mu_5 m_k A_{kp} m_p n_i n_j, \end{aligned} \tag{6.14}$$

$$\tilde{g}_i^n = -\left(\gamma_1 N_i + \gamma_2 A_{ij} n_j + \gamma_3 N_j m_j m_i + \gamma_4 n_j A_{jk} m_k m_i\right), \tag{6.15}$$

$$\tilde{g}_i^m = -\left(\lambda_1 M_i + \lambda_2 A_{ij} m_j\right), \tag{6.16}$$

where the α_i, β_i and μ_i are dynamic viscosity coefficients and

$$\begin{aligned}&\gamma_1 = \alpha_3 - \alpha_2, \quad \gamma_2 = \alpha_6 - \alpha_5, \quad \gamma_3 = \mu_2 - \mu_1, \\ &\gamma_4 = \mu_4 - \mu_3, \quad \lambda_1 = \beta_3 - \beta_2, \quad \lambda_2 = \beta_6 - \beta_5.\end{aligned} \tag{6.17}$$

We remark that *apriori* inequalities of the viscosities can be determined in regards to their relative magnitudes and signs (see the list in the review by Stewart [80], equation (7.53)). Of particular interest for modelling are the viscosity combinations and inequalities (that often appear in calculations) defined by:

$$\begin{aligned}\gamma_n &= \alpha_3 - \alpha_2 > 0, \\ \gamma_m &= \beta_3 - \beta_2 > 0, \\ \gamma_{nm} &= \alpha_3 - \alpha_2 + \beta_3 - \beta_2 + \mu_2 - \mu_1 > 0.\end{aligned} \tag{6.18}$$

6.2 Oscillatory shear flow

In this chapter, an analysis will be made of the response of biaxial nematic liquid crystals to an induced oscillatory shear flow. We will follow [78] to study stability and instability and extend our analysis to biaxial nematic liquid crystals. We consider biaxial nematic liquid crystals under oscillatory shear without elas-

tic contributions; this assumption was made for nematics under oscillatory shear in [78] and is a common approximation in early investigations [48, 79]. We seek solutions to the dynamic continuum equations, which are applied to an incompressible biaxial nematic liquid crystals sample for $\mathbf{n}$ and $\mathbf{m}$ in terms of what are, effectively, Euler angles θ and ϕ [80]. A suitable velocity is included to induced oscillatory shear flow. The motivation for looking at oscillatory shear in biaxial liquid crystals is that it is a way to investigate the key material parameters that include flow by looking at the effect of different material parameters on the mathematical stability of biaxial. Key influential material parameters are often identified via critical thresholds or stability/instability thresholds.

6.2.1 Oscillatory shear flow solutions

In this case, the director is strongly anchored parallel to the bounding plates. The lower plate is subject to sinusoidal oscillations parallel to the initial alignment. Also, the effect of the surface and inertia are considered. Moreover, we concentrate on when the impact of the oscillatory flow, induced by the oscillating upper plate, is supposed. As common in vesco-elastic fluids, it is appropriate to look at the general Reynolds number and Ericksen number. The Reynolds number is an important quantity in fluid mechanics. It is defined as the ratio of inertial forces to viscous forces [78, 86].

$$R_e = dv\frac{\rho}{\eta}. \tag{6.19}$$

The Ericksen number is a measure of the ratio of viscous to elastic forces and moments. It is defined by

$$\varepsilon_r = dv\frac{\eta}{K}, \tag{6.20}$$

where d represents a typical length, v a typical velocity, ρ the density, η a representative dynamic viscosity and K a typical elastic constant. The Reynolds number is small in fluid problems [58, 78], whereas the Ericksen number can be large. We now deploy these ideas and observations to the mathematical modelling.

Now, we consider solutions of the form

$$\mathbf{v} = (\kappa_0(t)z, 0, 0), \quad \kappa_0(t) = a\frac{\omega}{d}\cos(\omega t), \tag{6.21}$$

$$\mathbf{n} = (\cos\theta(t), 0, \sin\theta(t)), \quad \mathbf{m} = (-\sin\theta, 0, \cos\theta(t)). \tag{6.22}$$

We can see that

$$\dot{\mathbf{v}} = \left(\frac{\partial v}{\partial t}, 0, 0\right) = -\left(a\omega^2\frac{z}{d}\sin(\omega t), 0, 0\right), \tag{6.23}$$

Now, substituting (6.21) into (6.2), then

$$\mathbf{A} = \frac{1}{2}\left(\nabla\mathbf{v} + (\nabla\mathbf{v})^T\right) = \begin{pmatrix} 0 & 0 & \frac{\kappa_0}{2} \\ 0 & 0 & 0 \\ \frac{\kappa_0}{2} & 0 & 0 \end{pmatrix}, \tag{6.24}$$

and

$$\mathbf{W} = \frac{1}{2}\left(\nabla\mathbf{v} - (\nabla\mathbf{v})^T\right) = \begin{pmatrix} 0 & 0 & \frac{\kappa_0}{2} \\ 0 & 0 & 0 \\ -\frac{\kappa_0}{2} & 0 & 0 \end{pmatrix}. \tag{6.25}$$

Substituting (6.22) and (6.25) into (6.3), we obtain

$$\mathbf{N} = \begin{pmatrix} -\frac{\kappa_0}{2}\sin\theta - \theta'\sin\theta \\ 0 \\ \frac{\kappa_0}{2}\cos\theta - \theta'\sin\theta \end{pmatrix}, \tag{6.26}$$

and

$$\mathbf{M} = \begin{pmatrix} -\frac{\kappa_0}{2}\cos\theta - \theta'\sin\theta \\ 0 \\ -\frac{\kappa_0}{2}\sin\theta - \theta'\sin\theta \end{pmatrix}. \tag{6.27}$$

We can see from (6.14) that $\tilde{t}_{ij}$ does not depend on any spatial variables, then [78]

$$\tilde{t}_{ij,j} = 0.$$

Therefore, substituting (6.23) into the equation (6.11) gives

$$p_{,x} = -\rho\frac{\partial v}{\partial t}, \quad p_{,y} = 0, \quad p_{,z} = 0. \tag{6.28}$$

For the term $\tilde{g}_i^n$, substituting (6.22) into (6.12) gives

$$\tilde{g}_1^n = \kappa m_1 + \gamma n_1 = \gamma\cos\theta - \kappa\sin\theta, \tag{6.29}$$

$$\tilde{g}_2^n = 0, \tag{6.30}$$

$$\tilde{g}_3^n = \kappa m_3 + \gamma n_3 = \gamma\sin\theta + \kappa\cos\theta. \tag{6.31}$$

Also, substituting (6.22), (6.24) and (6.26) into (6.15) gives

$$\tilde{g}_1^n = \left[(\gamma_1+\gamma_3)\,\theta' + \frac{a\omega}{2d}\cos(\omega t)\,(\gamma_1 - \gamma_2 + \gamma_3 + \gamma_4\cos(2\theta)\right]\sin\theta, \tag{6.32}$$

$$\tilde{g}_3^n = -\left[(\gamma_1+\gamma_3)\,\theta' + \frac{a\omega}{2d}\cos(\omega t)\,(\gamma_1 + \gamma_2 + \gamma_3 + \gamma_4\cos(2\theta)\right]\cos\theta. \tag{6.33}$$

Similar to g_i^m, substituting $(6.22)_2$ into (6.13) gives

$$\tilde{g}_1^m = \tau m_1 + \kappa n_1 = -\tau\sin\theta + \kappa\cos\theta, \tag{6.34}$$

$$\tilde{g}_2^m = 0, \tag{6.35}$$

$$\tilde{g}_3^m = \tau m_3 + \kappa n_3 = \tau\cos\theta + \kappa\sin\theta. \tag{6.36}$$

Also, substituting (6.22), (6.24) and (6.27) into (6.16) gives

$$\tilde{g}_1^m = \Big[\lambda_1\theta' + \frac{a\omega}{2d}(\lambda_1 - \lambda_2)\cos(\omega t)\Big]\cos\theta, \tag{6.37}$$

$$\tilde{g}_3^m = \Big[\lambda_1\theta' + \frac{a\omega}{2d}(\lambda_1 + \lambda_2)\cos(\omega t)\Big]\sin\theta. \tag{6.38}$$

Eliminating γ, κ and τ from (6.86), (6.88),(6.34) and (6.36), we have

$$(\tilde{g}_1^m - \tilde{g}_3^n)\cos\theta + (\tilde{g}_1^n + \tilde{g}_3^m)\sin\theta = 0. \tag{6.39}$$

Now substituting (6.32), (6.33), (6.37) and (6.38) into (6.39), we find the governing dynamic equation

$$\overline{\gamma_1}\theta' + \Big[\overline{\gamma_1} + \overline{\gamma_2}\cos(2\theta)\Big]\frac{a\omega}{2d}\cos(\omega t) = 0, \tag{6.40}$$

where,

$$\begin{gathered}\overline{\alpha_2} = \alpha_2 - \beta_3 + \mu_1, \quad \overline{\alpha_3} = \alpha_3 - \beta_2 + \mu_2,\\ \overline{\gamma_1} = (\overline{\alpha_3} - \overline{\alpha_2}) = \gamma_1 + \gamma_3 + \lambda_1, \quad \overline{\gamma_2} = (\overline{\alpha_2} + \overline{\alpha_3}) = \gamma_2 + \gamma_4 - \lambda_2,\end{gathered} \tag{6.41}$$

and

$$\begin{gathered}\gamma_1 = \alpha_3 - \alpha_2, \quad \gamma_2 = \alpha_2 + \alpha_3, \quad \gamma_3 = \mu_2 - \mu_1, \quad \gamma_4 = \mu_1 + \mu_2,\\ \lambda_1 = \beta_3 - \beta_2, \quad \lambda_2 = \beta_2 + \beta_3.\end{gathered} \tag{6.42}$$

Notice that $\overline{\gamma_1} = \overline{\alpha_3} - \overline{\alpha_2} > 0$, whereas $\overline{\gamma_2} = \overline{\alpha_2} + \overline{\alpha_3}$ is indeterminate in sign. The equation (6.40) can be rewritten as

$$\frac{d\theta}{dt} = -\Big[\sin^2\theta - \alpha\cos^2\theta\Big]A\omega\cos(\omega t), \tag{6.43}$$

where

$$\alpha = \frac{\overline{\alpha_3}}{\overline{\alpha_2}}, \quad \text{and} \quad A = \frac{|\overline{\alpha_2}|\,a}{\overline{\gamma_1}d}. \tag{6.44}$$

This is analogous to the nematic equation [78] that arises in the oscillatory shear

of nematic. The solution is easily found by separation of variables [78]:

$$\theta(t) = \tan^{-1}\{\delta \tanh\left(A\delta \sin(\omega t)\right)\}, \quad \delta = \sqrt{\alpha}, \quad \text{when} \quad \alpha > 0, \tag{6.45}$$

$$\theta(t) = -\tan^{-1}\{\delta \tan\left(A\delta \sin(\omega t)\right)\}, \quad \delta = \sqrt{|\alpha|}, \quad \text{when} \quad \alpha < 0. \tag{6.46}$$

We note that A and δ are dimensionless, and we can produce some qualitative plots of these solutions, see Figures 6.2 and 6.3.

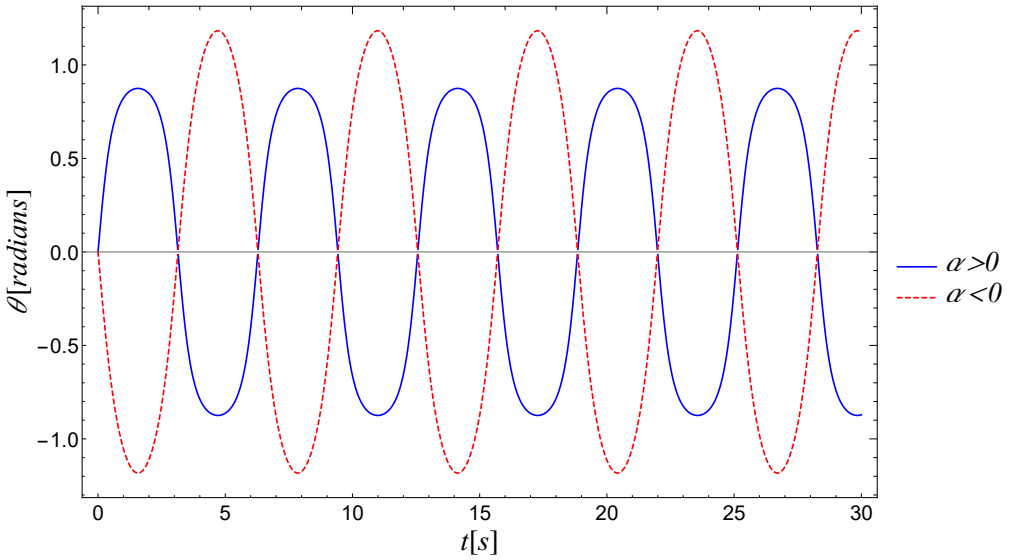

Figure 6.2: The solutions (6.45) and (6.46) where, for demonstration purposes, we have chosen $A = \frac{\pi}{2}$, $\delta = \frac{2}{\pi}$ and $\omega = 1$.

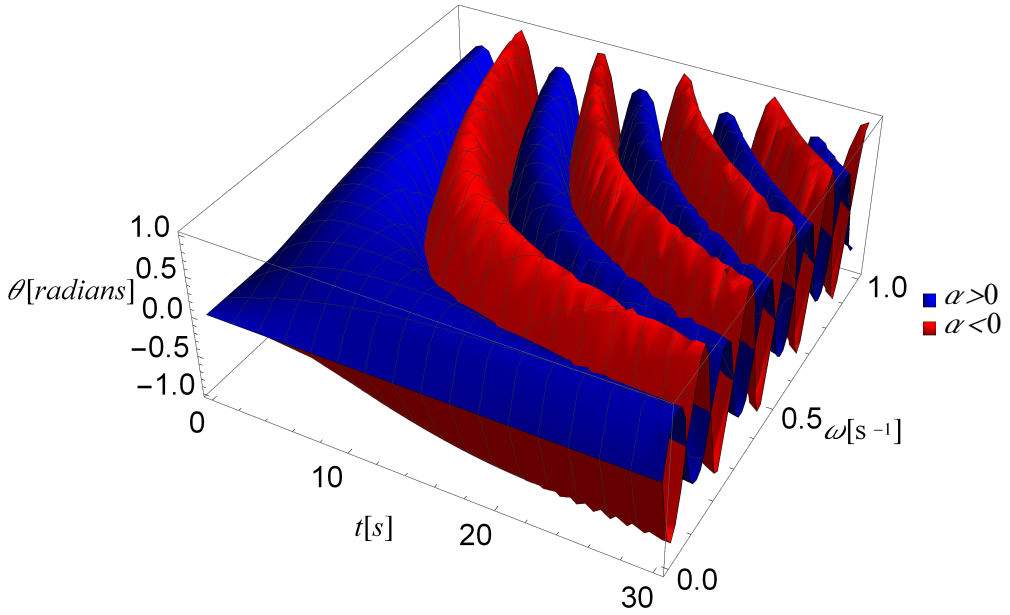

Figure 6.3: The solutions (6.45) and (6.46) where, as before, $A = \frac{\pi}{2}$, $\delta = \frac{2}{\pi}$.

6.2.1.1 Adding a perturbation

A non-linear analysis of the nematic solutions has been carried out elsewhere [51, 78]. We now examine the linear stability of these solutions, which were not considered elsewhere. This will guide our analysis for the linear stability of the analogous biaxial nematic problem. Firstly, let $\theta_1(t)$ be given by (6.45) and set

$$\theta(t) = \theta_1(t) + \epsilon(t), \tag{6.47}$$

where $\epsilon(t) << 1$.

Substitution of (6.47) into (6.40) gives

$$\overline{\gamma_1}\,(\theta_1' + \epsilon') + \frac{a\omega}{2d}\Big[\overline{\gamma_1} + \overline{\gamma_2}\cos(2\theta_1 + 2\epsilon)\Big]\cos(\omega t) = 0, \tag{6.48}$$

$$\Rightarrow \overline{\gamma_1}\theta_1' + \Big[\overline{\gamma_1} + \overline{\gamma_2}\cos(2\theta_1)\Big]\frac{a\omega}{2d}\cos(\omega t) + \overline{\gamma_1}\epsilon' - \overline{\gamma_2}\epsilon\sin(2\theta_1)\frac{a\omega}{d}\cos(\omega t) = 0. \tag{6.49}$$

The last equation can be reduced by using (6.40) to

$$\overline{\gamma_1}\epsilon' - \overline{\gamma_2}\epsilon\sin(2\theta_1)\frac{a\omega}{d}\cos(\omega t) = 0. \tag{6.50}$$

From (6.45), we can write

$$\sin(2\theta_1) = 2\sin\theta_1\cos\theta_1 = \frac{2\delta\tanh\{A\delta\sin(\omega t)\}}{1+\delta^2\tanh^2\{A\delta\sin(\omega t)\}}. \tag{6.51}$$

Substitution of (6.51) into (6.50), we have

$$\overline{\gamma_1}\epsilon'(t) - \frac{a\omega\overline{\gamma_2}\cos(\omega t)\sin\{2\tan^{-1}(\delta\tanh(A\delta\sin(\omega t)))\}}{d}\epsilon(t) = 0. \tag{6.52}$$

The general solution of the equation (6.52) is

$$\epsilon(t) = c_1\Big[1-\delta^2+(\delta^2+1)\cosh\left(2A\delta\sin(\omega t)\right)\Big]^{\dfrac{a\overline{\gamma}_2}{Ad\,(1+\delta^2)\,\overline{\gamma}_1}}, \tag{6.53}$$

where c_1 is a constant. It is now clear that $\epsilon(t)$ is bounded and hence $\theta_1(t)$ is linearly stable.

Also, we can set the second solution as θ_2 from (6.46) and set

$$\theta(t) = \theta_2(t) + \epsilon(t). \tag{6.54}$$

Substitution of (6.54) into (6.40) gives

$$\overline{\gamma_1}\epsilon' - \overline{\gamma_2}\epsilon \sin(2\theta_2)\frac{a\omega}{d}\cos(\omega t) = 0. \tag{6.55}$$

From (6.46), we can write

$$\sin(2\theta_2) = 2\sin\theta_2\cos\theta_2 = -\frac{2\delta\tan\left[A\delta\sin(\omega t)\right]}{1+\delta^2\tan^2\left[A\delta\sin(\omega t)\right]}. \tag{6.56}$$

Substitution of (6.56) into (6.55) gives

$$\overline{\gamma_1}\epsilon'(t) + \frac{a\omega\overline{\gamma_2}\cos(\omega t)\sin\{2\tan^{-1}(\delta\tan(A\delta\sin(\omega t)))\}}{d}\epsilon(t) = 0. \tag{6.57}$$

The general solution of the equation (6.57) is

$$\epsilon(t) = c_2\Big[1+\delta^2+(1-\delta^2)\cos\Big(2A\delta\sin(\omega t)\Big)\Big]^{\frac{a\overline{\gamma}_2}{Ad\,(1-\delta^2)\,\overline{\gamma}_1}}, \tag{6.58}$$

where c_2 is a constant. We can see, as before, that the perturbed solution (6.58) is bounded. In this instance, $\delta < 1$ is a necessary requirement and this is physically meaningful, and by using the definitions in (6.41) and $(6.44)_1$, this requirement can be checked via data from experiments (which are not yet presently available); nevertheless, for nematics, where the β and μ terms are absent, this inequality is valid for MBBA, PAA and 5CB nematic liquid crystals [78, p.330].

Therefore, we conclude that the solutions (6.45) and (6.46) are linearly stable, although not asymptotically stable.

6.3 Stability and instability

6.3.1 An alternative linear stability of nematics

The nematic non-linear stability has been analysed by Leslie [49, 78] for a 2-dimensional perturbation. We inspect a linear analysis for this particularly more

sophisticated perturbation as a precursor to the biaxial linear stability case following an alternative perturbed solution in two dimensions. Firstly, we investigate the nematic linear stability to compare with the biaxial linear stability case. We seek the stability of the solutions of the form

$$\begin{aligned} \mathbf{n} &= \Big(1, \phi(t), \theta(t)\Big), \\ \mathbf{v} &= \Big(\kappa_0(t)z, \tau_0(t)z, 0\Big), \quad \kappa_0(t) = a\frac{\omega}{d}\cos(\omega t). \end{aligned} \tag{6.59}$$

where $\phi(t)$ and $\theta(t)$ are small time-dependent perturbations and note that the constraint requirement $\mathbf{n}\cdot\mathbf{n} = 1$ is satisfied to the second order when $|\phi(t)| \ll 1$ and $|\theta(t)| \ll 1$.

We will use a reformulated version of the dynamic equations where the dissipation function is applied. The dissipation function is calculated to be, for this particular problem, [78],

$$\hat{\mathcal{D}} = \frac{1}{4}\left[(\alpha_3 + \alpha_4 + \alpha_6)\xi^2 + \alpha_4\zeta^2\right] + \alpha_3\xi\frac{d\theta}{dt}, \tag{6.60}$$

where we define

$$\xi = \kappa + \tau\phi, \quad \zeta = \kappa\phi - \tau. \tag{6.61}$$

The balance law for linear momentum and the balance law for angular momentum equations are then

$$\rho\dot{v}_i = -p_{,i} + t_{ij,j}, \tag{6.62}$$

$$\tilde{g}_i = \lambda n_i, \tag{6.63}$$

respectively. The constitutive equations for the viscous stress $\tilde{t}_{ij}$ and the vectors

$\tilde{g}_i^n$ are given by [78]

$$\begin{aligned}
\tilde{t}_{ij} =&\alpha_1 n_k A_{kp} n_p n_i n_j + \alpha_2 N_i n_j + \alpha_3 n_i N_j + \alpha_4 A_{ij}, \\
&+ \alpha_5 n_j A_{ik} n_k + \alpha_6 n_i A_{jk} n_k, \\
\tilde{g}_i =& -\gamma_1 N_i - \gamma_2 A_{ip} n_p, \\
\gamma_1 =&\alpha_3 - \alpha_2 \geq 0, \\
\gamma_2 =&\alpha_3 + \alpha_2 = \alpha_6 - \alpha_5, \\
A_{ij} =&\frac{1}{2}\left(v_{i,j} + v_{j,i}\right), \\
N_i =&\dot{n}_i - W_{ij} n_j, \quad W_{ij} = \frac{1}{2}\left(v_{i,j} - v_{j,i}\right).
\end{aligned} \tag{6.64}$$

The dynamic equations for the balances of angular momentum and linear momentum above can be written as [78]

$$\frac{\partial \hat{\mathcal{D}}}{\partial \dot{\theta}} = 0, \quad \frac{\partial \hat{\mathcal{D}}}{\partial \dot{\phi}} = 0, \tag{6.65}$$

and

$$\rho \dot{v}_i = \left(\frac{\partial \hat{\mathcal{D}}}{\partial v_{i,j}}\right)_{,j}, \quad i = 1, 2, 3. \tag{6.66}$$

respectively, where [78],

$$\tilde{g}_i = -\frac{\partial \hat{\mathcal{D}}}{\partial \dot{n}_i}, \quad \tilde{t}_{ij} = \frac{\partial \hat{\mathcal{D}}}{\partial v_{i,j}}. \tag{6.67}$$

Inserting the dissipation function (6.60) into (6.65) and we obtain

$$\gamma_1 \frac{d\theta}{dt} + \alpha_3(\kappa + \tau\phi) = 0, \tag{6.68}$$

$$\gamma_1 \frac{d\phi}{dt} + \alpha_2 \tau\theta = 0. \tag{6.69}$$

The fluid inertial contribution $\dot{v}_i = \dfrac{\partial v_i}{\partial t}$ may be neglected. Integrating (6.66) we have [78]

$$\tilde{t}_{13} = \frac{\partial \widehat{\mathcal{D}}}{\partial \kappa} = \sigma_1(t), \quad \tilde{t}_{23} = \frac{\partial \widehat{\mathcal{D}}}{\partial \tau} = \sigma_2(t), \tag{6.70}$$

where,

$$\tilde{t}_{13} = \frac{1}{2}\left[(\alpha_3 + \alpha_4 + \alpha_6)\,\kappa + (\alpha_3 + \alpha_6)\,\tau\phi + 2\alpha_3\frac{d\theta}{dt}\right], \tag{6.71}$$

which, of course, must be equivalent to

$$\frac{\partial\widehat{\mathcal{D}}}{\partial\kappa} = \frac{1}{2}\left[(\alpha_3 + \alpha_4 + \alpha_6)\kappa + (\alpha_3 + \alpha_6)\tau\phi + 2\alpha_3\frac{d\theta}{dt}\right]. \tag{6.72}$$

Therefore, the equation $(6.70)_1$ then takes the form

$$\alpha_3\frac{d\theta}{dt} + \frac{1}{2}(\alpha_3 + \alpha_4 + \alpha_6)\kappa + (\alpha_3 + \alpha_6)\tau\phi = \sigma_1(t). \tag{6.73}$$

As is common practice, suppose that the transverse component $\sigma_2(t)$ of the stress is zero [78], then

$$\frac{\partial\widehat{\mathcal{D}}}{\partial\tau} = \frac{1}{2}\Big[\alpha_4\tau + (\alpha_3 + \alpha_6)\,\kappa\phi\Big] = 0. \tag{6.74}$$

By elimination of τ and κ from (6.68) and (6.73), we obtain

$$K\frac{\mathrm{d}\theta}{\mathrm{dt}} = 2\alpha_3\sigma_1, \tag{6.75}$$

where $K = 2\alpha_3^2 - \gamma_1(\alpha_3 + \alpha_4 + \alpha_6) \neq 0$.

Also by eliminating of τ from (6.69) and (6.74), we obtain

$$\gamma_1\frac{d\phi}{dt} = 0. \tag{6.76}$$

In equation (6.76), α_3, α_4 and γ_1 are nonzero, therefore,

$$\phi(t) = \phi_0, \tag{6.77}$$

where ϕ_0 is a constant. We can see that $\phi(t)$ is a constant and, therefore, bounded and stable.

The solution of the equation (6.75) can be written in the form,

$$\theta(t) = \int_{t_0}^{t} \frac{2\alpha_3\sigma_1(s)}{K}\,ds + \theta_0, \tag{6.78}$$

where θ_0 is a constant. We can see from (6.78) that there are two cases,

Case 1: $\sigma_1(t)$ is a nonzero constant, therefore $\theta(t) \to \infty$ and therefore $\theta(t)$ is unstable.

Case 2: $\sigma_1(t)$ is zero or a bounded and oscillatory function, then $\theta(t)$ is bounded and oscillatory and therefore $\theta(t)$ is stable.

Physically, we would expect $\sigma_1(t)$ not to be a nonzero constant (otherwise, this would mean a constant force present in the z-direction). This is based on the usual interpretation of surface forces arising from a consideration of the viscous stress tensor component $\sigma_1(t) \equiv \tilde{t}_{13}$ (see Appendix A). The linear solutions are, therefore, stable but not asymptotically stable. This linear stability result is in accordance with the non-linear result in [78] but is a new observation that will guide the linear analysis for a biaxial nematic below.

6.3.2 Linear stability of biaxial nematic

Given the level of complexity for the non-linear analogue of the nematic case for biaxial nematic, we state the dissipation function for reference at the end of this Section and for future work, and now concentrate on a linear analysis which is guided by the novel linear analysis we carried out above for nematics. We denote the original positions of $\mathbf{n}$ and $\mathbf{m}$ by

$$\mathbf{n}_0 = (1, 0, 0), \quad \mathbf{m}_0 = (0, 0, 1). \tag{6.79}$$

Now, to examine the linear stability of these solutions, we set

$$\mathbf{n} = \Big(1, \phi(t), \theta(t)\Big), \quad \mathbf{m} = \Big(-\theta(t), 0, 1\Big), \tag{6.80}$$

$$\mathbf{v} = \Big(\kappa_0(t)z, \tau_0(t)z, 0\Big), \quad \kappa_0(t) = a\frac{\omega}{d}\cos(\omega t), \quad \tau_0(t) = b\omega\cos(\omega t), \tag{6.81}$$

where $b > 0$ is a constant. In all the calculations that follow, we will be deriving governing linear equations to first order in $\phi(t)$ and $\theta(t)$, i.e., we will ignore second and higher order contributions that involve these functions; of course, the energies

involved and the dissipation function when required will correspondingly be taken to second order, as will be seen below, because functional derivatives of these entities arise for obtaining the linear dynamic equations.

Now, substituting (6.80) into (6.2), then

$$\mathbf{A} = \frac{1}{2}\Big(\nabla\mathbf{v} + (\nabla\mathbf{v})^T\Big) = \begin{pmatrix} 0 & 0 & \frac{\kappa_0}{2} \\ 0 & 0 & \frac{\tau_0}{2} \\ \frac{\kappa_0}{2} & \frac{\tau_0}{2} & 0 \end{pmatrix}, \tag{6.82}$$

and

$$\mathbf{W} = \frac{1}{2}\Big(\nabla\mathbf{v} - (\nabla\mathbf{v})^T\Big) = \begin{pmatrix} 0 & 0 & \frac{\kappa_0}{2} \\ 0 & 0 & \frac{\tau_0}{2} \\ -\frac{\kappa_0}{2} & -\frac{\tau_0}{2} & 0 \end{pmatrix}. \tag{6.83}$$

Substituting (6.80) and (6.83) into (6.3), we obtain

$$\mathbf{N} = \begin{pmatrix} -\frac{\kappa_0}{2}\theta \\ \phi' - \frac{\tau_0}{2}\theta \\ \frac{\kappa_0}{2} + \theta' + \frac{\tau_0}{2}\phi \end{pmatrix}, \tag{6.84}$$

and

$$\mathbf{M} = \begin{pmatrix} -\frac{\kappa_0}{2} - \theta' \\ -\frac{\tau_0}{2} \\ -\frac{\kappa_0}{2}\theta \end{pmatrix}. \tag{6.85}$$

For the term $\tilde{g}_i^n$, substituting (6.80) into (6.12) gives

$$\tilde{g}_1^n = \gamma - \kappa\theta, \tag{6.86}$$

$$\tilde{g}_2^n = \gamma\phi, \tag{6.87}$$

$$\tilde{g}_3^n = \kappa + \gamma\theta. \tag{6.88}$$

Also, substituting (6.80), (6.82) and (6.84) into (6.15) gives

$$\tilde{g}_1^n = \frac{1}{2}\Big(\gamma_1 - \gamma_2 + \gamma_3 + \gamma_4\Big)\kappa_0\theta, \tag{6.89}$$

$$\tilde{g}_2^n = \frac{1}{2}\Big(\gamma_1 - \gamma_2\Big)\tau_0\theta - \gamma_1\phi', \tag{6.90}$$

$$\tilde{g}_3^n = -\Big(\gamma_1 + \gamma_3\Big)\theta' - \frac{1}{2}\Big(\gamma_1 + \gamma_2 + \gamma_3 + \gamma_4\Big)\Big(\kappa_0 + \tau_0\phi\Big). \tag{6.91}$$

Similar to g_i^m, substituting $(6.80)_1$ and $(6.80)_2$ into (6.13) gives

$$\tilde{g}_1^m = \kappa - \tau\theta, \tag{6.92}$$

$$\tilde{g}_2^m = \kappa\phi, \tag{6.93}$$

$$\tilde{g}_3^m = \kappa\theta + \tau. \tag{6.94}$$

Also, substituting $(6.80)_2$, (6.82) and (6.85) into (6.16) gives

$$\tilde{g}_1^m = \frac{1}{2}\kappa_0\left(\lambda_1 - \lambda_2\right) + \lambda_1\theta', \tag{6.95}$$

$$\tilde{g}_2^m = \frac{1}{2}\left(\lambda_1 - \lambda_2\right)\tau_0, \tag{6.96}$$

$$\tilde{g}_3^m = \frac{1}{2}\kappa_0\left(\lambda_1 + \lambda_2\right)\theta. \tag{6.97}$$

From (6.86)-(6.88) and (6.89)-(6.91), we can write

$$\gamma = \kappa\theta + \frac{1}{2}\Big(\gamma_1 - \gamma_2 + \gamma_3 + \gamma_4\Big)\kappa_0\theta, \tag{6.98}$$

$$\gamma\phi = \frac{1}{2}\Big(\gamma_1 - \gamma_2\Big)\tau_0\theta - \gamma_1\phi', \tag{6.99}$$

$$\kappa = -\gamma\theta - \Big(\gamma_1 + \gamma_3\Big)\theta' - \frac{1}{2}\Big(\gamma_1 + \gamma_2 + \gamma_3 + \gamma_4\Big)\Big(\kappa_0 + \tau_0\phi\Big). \tag{6.100}$$

Substituting (6.98) into (6.99) and (6.100), respectively, we obtain

$$2\gamma_1\phi' + \Big(\gamma_2 - \gamma_1\Big)\tau_0\theta = 0, \tag{6.101}$$

$$\kappa = -\Big(\gamma_1 + \gamma_3\Big)\theta' - \frac{1}{2}\Big(\gamma_1 + \gamma_2 + \gamma_3 + \gamma_4\Big)\Big(\kappa_0 + \tau_0\phi\Big). \tag{6.102}$$

From (6.92)-(6.94) and (6.95)-(6.97), we can write

$$\kappa = \tau\theta + \frac{1}{2}\kappa_0\Big(\lambda_1 - \lambda_2\Big) + \lambda_1\theta', \tag{6.103}$$

$$\kappa\phi = \frac{1}{2}\Big(\lambda_1 - \lambda_2\Big)\tau_0, \tag{6.104}$$

$$\tau = \frac{1}{2}\Big[\left(\lambda_1 + \lambda_2\right)\kappa_0 - 2\kappa\Big]\theta. \tag{6.105}$$

Substituting (6.105) into (6.103), we have

$$\kappa = \frac{1}{2}\kappa_0\left(\lambda_1 - \lambda_2\right) + \lambda_1\theta'. \tag{6.106}$$

Substituting (6.106) into (6.104), we have

$$\phi(t) = \frac{\tau_0}{\kappa_0} = \frac{bd}{a}. \tag{6.107}$$

From equations (6.102) and (6.106), we have

$$2\Big(\gamma_1 + \gamma_3 + \lambda_1\Big)\theta' + \Big(\gamma_1 + \gamma_2 + \gamma_3 + \gamma_4 + \lambda_1 - \lambda_2\Big)\kappa_0 + \Big(\gamma_1 + \gamma_2 + \gamma_3 + \gamma_4\Big)\tau_0\phi = 0. \tag{6.108}$$

Note that when we have θ solution in (6.108), the κ in (6.102) must be identical to κ in (6.106).

Now, substituting (6.106) into (6.98) and (6.102) into (6.105) respectively, we have

$$\gamma = \frac{1}{2}\Big[\gamma_1 - \gamma_2 + \gamma_3 + \gamma_4 + \lambda_1 - \lambda_2\Big]\kappa_0\theta, \tag{6.109}$$

$$\tau = \frac{1}{2}\Big[\gamma_1 + \gamma_2 + \gamma_3 + \gamma_4 + \lambda_1 + \lambda_2\Big]\kappa_0\theta. \tag{6.110}$$

Now, we have three equations in two variables θ and ϕ, and

$$\phi = \frac{bd}{a}, \tag{6.111}$$

$$2\Big(\gamma_1 + \gamma_3 + \lambda_1\Big)\theta' + \Big(\gamma_1 + \gamma_2 + \gamma_3 + \gamma_4\Big)\Big(\tau_0\phi + \kappa_0\Big) + \Big(\lambda_1 - \lambda_2\Big)\kappa_0 = 0, \tag{6.112}$$

$$2\gamma_1\phi' = \Big(\gamma_1 - \gamma_2\Big)\tau_0\theta. \tag{6.113}$$

Now we have two cases to consider;

Case 1: $\tau_0 \neq 0$, then the equations (6.111) and (6.113) show that θ must be zero, which means that there is no consistent solution for the system above because if $\theta = 0$ and using the equation (6.111), the equation (6.112) becomes

$$\Big(\gamma_1 + \gamma_2 + \gamma_3 + \gamma_4\Big)\frac{b^2 d}{a} + \Big(\gamma_1 + \gamma_2 + \gamma_3 + \gamma_4 + \lambda_1 - \lambda_2\Big)\frac{a\omega}{d} = 0. \tag{6.114}$$

We can see that the last equation is not true, in general, because a and b are given by the experimentations. Therefore, there is generally no oscillatory transverse flow. However, in exceptional situations, the terms $\gamma_1 + \gamma_2 + \gamma_3 + \gamma_4$ and $\gamma_1 + \gamma_2 + \gamma_3 + \gamma_4 + \lambda_1 - \lambda_2$ could have the same sign: this means that there is a particular $\omega \neq 0$ for which there exists transverse oscillatory flow at that frequency.

Case 2: $\tau_0 = 0$, then equation (6.113) is true for any value for θ. On the other hand, the equation (6.112) becomes

$$2\left(\gamma_1 + \gamma_3 + \lambda_1\right)\theta' + \left(\gamma_1 + \gamma_2 + \gamma_3 + \gamma_4 + \lambda_1 - \lambda_2\right)k_0 = 0. \tag{6.115}$$

Substituting $(6.81)_2$ into (6.115), we obtain

$$2\left(\gamma_1 + \gamma_3 + \lambda_1\right)\theta' + \left(\gamma_1 + \gamma_2 + \gamma_3 + \gamma_4 + \lambda_1 - \lambda_2\right)\frac{a\omega}{d}\cos(\omega t) = 0, \tag{6.116}$$

and its solution is given by

$$\theta(t) = \theta_0 - \frac{a\left(\gamma_1 + \gamma_2 + \gamma_3 + \gamma_4 + \lambda_1 - \lambda_2\right)}{2d\left(\gamma_1 + \gamma_3 + \lambda_1\right)}\sin(\omega t), \tag{6.117}$$

where θ_0 is a constant. Recall that θ_0 and the coefficient of $\sin(\omega t)$ in (6.117) have the dimensions of radians.

Note that $\tau_0 = 0$ implies that $b = 0$, therefore, from equation (6.111), we can see in this case that $\phi(t) = 0$ and then bounded. Also, from equation (6.117), θ is oscillatory and bounded. Therefore, the biaxial nematic linear case solutions are oscillatory and bounded. Then the solutions are linearly stable but not asymptotically stable.

The Lagrange multipliers γ, τ and κ have some physical meaning. So, identifying them tells us about the constraints we have imposed on the modelling. For example, the magnitude of κ can be interpreted as indicating how difficult it is for the vector $\mathbf{m}$ to remain as a unit vector. Similarly, the magnitude of γ tells us how difficult it is for $\mathbf{n}$ to remain as a unit vector. So the modulus of the ratio $\left|\frac{\gamma}{\kappa}\right|$, for example, tells us which director is the more constrained in an approximate sense in mechanics, as we will now proceed to discuss.

Now we have

$$\left|\frac{\tau}{\kappa}\right| = |\chi\psi|\,|\theta_0 - B\sin(\omega t)|\,, \tag{6.118}$$

$$\left|\frac{\gamma}{\kappa}\right| = |\psi|\,|\chi - 2(\gamma_2+\lambda_2)|\,|\theta_0 - B\sin(\omega t)|\,, \tag{6.119}$$

$$\left|\frac{\gamma}{\tau}\right| = \left|1 - \frac{2(\gamma_2+\lambda_2)}{\chi}\right| = constant, \tag{6.120}$$

where,

$$\chi = \gamma_1+\gamma_2+\gamma_3+\gamma_4+\lambda_1+\lambda_2, \tag{6.121}$$

$$\psi = \frac{\gamma_1+\gamma_3+\lambda_1}{(\gamma_2+\gamma_4)\,\lambda_1 + (\gamma_1+\gamma_3)\,\lambda_2}, \tag{6.122}$$

$$B = \frac{a\,(\gamma_1+\gamma_2+\gamma_3+\gamma_4+\lambda_1-\lambda_2)}{2d\,(\gamma_1+\gamma_3+\lambda_1)}. \tag{6.123}$$

We can see that if $\left|\frac{\tau}{\kappa}\right| < 1$ then,

$$|\theta_0 - B\sin(wt)| < \frac{1}{|\psi\chi|}, \tag{6.124}$$

but

$$|\theta_0 - B\sin(\omega t)| \geqslant |\theta_0| - |B\sin(\omega t)| \tag{6.125}$$

$$\geqslant |\theta_0| - |B|, \tag{6.126}$$

therefore,

$$|\theta_0| < \frac{1}{|\psi\chi|} + |B| \equiv \theta_1^c, \tag{6.127}$$

and if $\left|\frac{\tau}{\kappa}\right| > 1$ then,

$$|\theta_0 - B\sin(wt)| > \frac{1}{|\psi\chi|}, \tag{6.128}$$

but

$$|\theta_0 - B\sin(\omega t)| \leqslant |\theta_0| + |B|, \tag{6.129}$$

therefore,

$$|\theta_0| > \frac{1}{|\psi\chi|} - |B| \equiv \theta_1^{cc}. \tag{6.130}$$

Similar for $\left|\frac{\gamma}{\kappa}\right|$, $\left|\frac{\gamma}{\kappa}\right| < 1$ if

$$|\theta_0| < \frac{1}{|\chi - 2(\gamma_2 + \lambda_2)|\,|\psi|} + |B| \equiv \theta_2^c, \tag{6.131}$$

and $\left|\frac{\gamma}{\kappa}\right| > 1$ if

$$|\theta_0| > \frac{1}{|\chi - 2(\gamma_2 + \lambda_2)|\,|\psi|} - |B| \equiv \theta_2^{cc}. \tag{6.132}$$

However, $\left|\frac{\gamma}{\tau}\right| < 1$ if $0 < \frac{\gamma_2 + \lambda_2}{\chi} < 1$ and $\left|\frac{\gamma}{\tau}\right| > 1$ if $\frac{\gamma_2 + \lambda_2}{\chi} < 0$ or $\frac{\gamma_2 + \lambda_2}{\chi} > 1$.

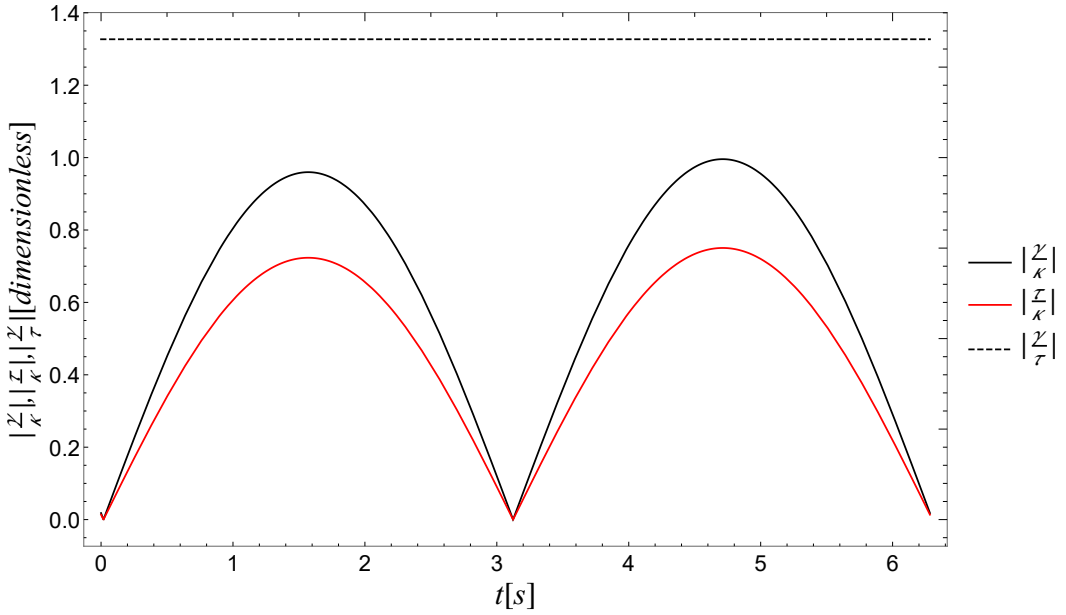

Figure 6.4: These graphs represent the ratios $\left|\frac{\gamma}{\kappa}\right|$, $\left|\frac{\gamma}{\tau}\right|$ and $\left|\frac{\tau}{\kappa}\right|$ for the Lagrange multipliers γ, τ and κ where, $\gamma_1 = 0.0777,\ \gamma_2 = -0.0848,\ \gamma_3 = -0.05,\ \gamma_4 = 0.02,\ \lambda_1 = -0.04,\ \lambda_2 = 0.03,\ a = d = 10^{-4},\ \omega = 1$ and $\theta_0 = 0.08$.

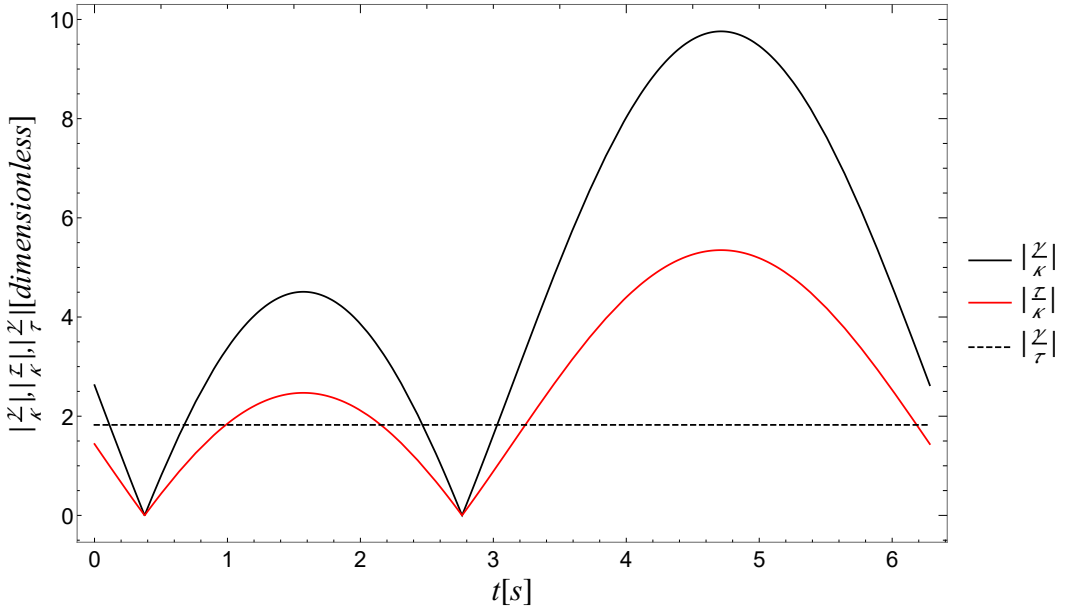

Figure 6.5: These graphs represent the ratios $\left|\frac{\gamma}{\kappa}\right|$, $\left|\frac{\gamma}{\tau}\right|$ and $\left|\frac{\tau}{\kappa}\right|$ for the Lagrange multipliers γ, τ and κ where, $\gamma_1 = 0.0777$, $\gamma_2 = -0.0848$, $\gamma_3 = 0.05$, $\gamma_4 = 0.02$, $\lambda_1 = 0.04$, $\lambda_2 = 0.03$, $a = d = 10^{-4}$, $\omega = 1$ and $\theta_0 = 0.08$.

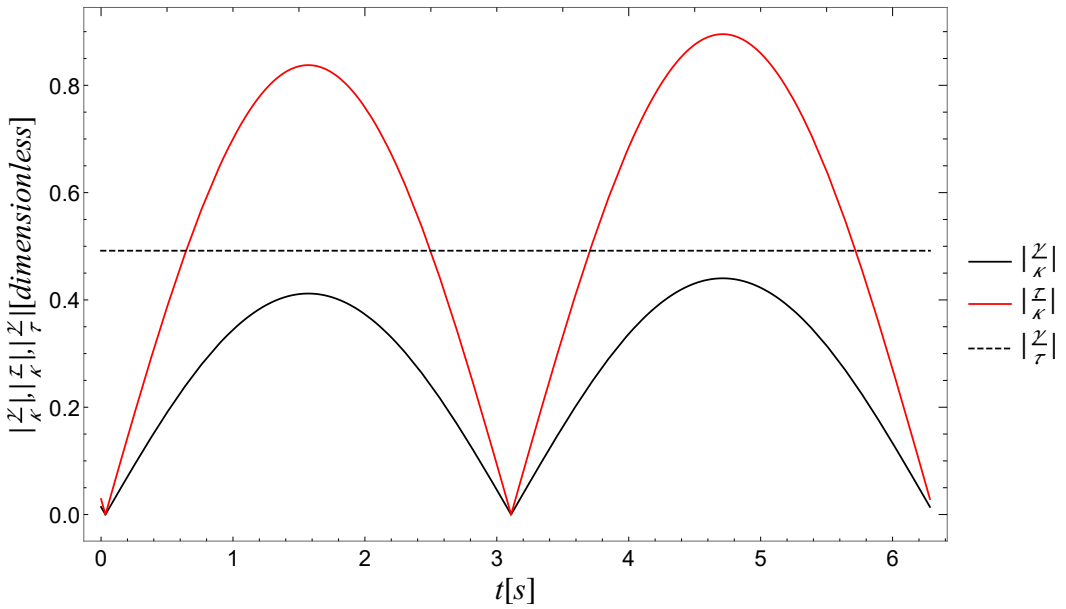

Figure 6.6: These graphs represent the ratios $\left|\frac{\gamma}{\kappa}\right|$, $\left|\frac{\gamma}{\tau}\right|$ and $\left|\frac{\tau}{\kappa}\right|$ for the Lagrange multipliers γ, τ and κ where, $\gamma_1 = 0.0777$, $\gamma_2 = -0.0848$, $\gamma_3 = -0.01$, $\gamma_4 = -0.01$, $\lambda_1 = -0.09$, $\lambda_2 = -0.01$, $a = d = 10^{-4}$, $\omega = 1$ and $\theta_0 = 0.08$.

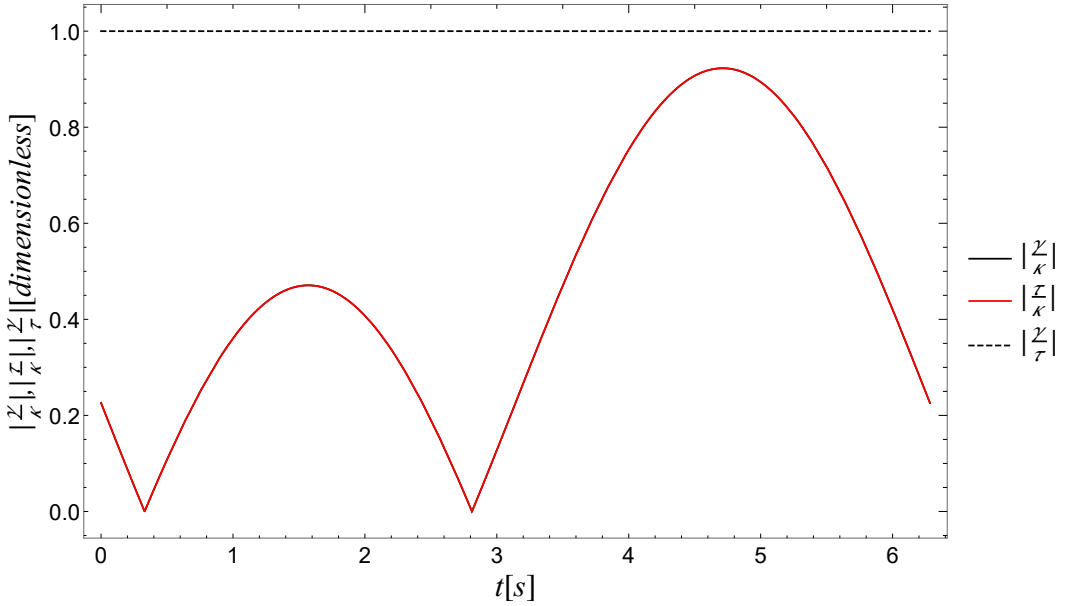

Figure 6.7: These graphs represent the ratios $\left|\frac{\gamma}{\kappa}\right|$, $\left|\frac{\gamma}{\tau}\right|$ and $\left|\frac{\tau}{\kappa}\right|$ for the Lagrange multipliers γ, τ and κ where, $\gamma_1 = 0.0777,\ \gamma_2 = -0.0848,\ \gamma_3 = -0.0777,\ \gamma_4 = 0.03,\ \lambda_1 = -0.03,\ \lambda_2 = -0.07,\ a = d = 10^{-4},\ \omega = 1$ and $\theta_0 = 0.08$.

We can see from equations (6.118)-(6.120) that the magnitude of the Lagrange multipliers γ, κ and τ (which keeps $\mathbf{n}$ and $\mathbf{m}$ orthogonal) are sinusoidal functions to the first order solution. The ratio $\left|\frac{\tau}{\kappa}\right|$ shows that the multiplier τ for keeping $\mathbf{n}$ and $\mathbf{m}$ to be orthogonal is more highly constrained than κ that keeps $\mathbf{m}$ as a unit vector if $|\theta_0| < \theta_1^{cc}$, whereas keeping $\mathbf{m}$ as a unit vector is more constrained than $\mathbf{n}$ and $\mathbf{m}$ to be orthogonal if $|\theta_0| < \theta_1^{c}$. On the other hand, the ratio $\left|\frac{\gamma}{\kappa}\right|$ shows that the Lagrange multiplier γ for keeping $\mathbf{n}$ as a unit vector is much larger than for κ that constrains $\mathbf{m}$ to be a unit vector if $|\theta_0| < \theta_2^{cc}$. However, the constraint that fixes $\mathbf{m}$ to be a unit vector is larger than that for fixing $\mathbf{n}$ to be a unit vector if $|\theta_0| < \theta_2^{c}$. Moreover, we see that $\left|\frac{\gamma}{\tau}\right|$ is a constant; therefore, the multiplier τ is a scalar multiplier of γ. Also, the multiplier γ for constraining $\mathbf{n}$ as a unit vector is much larger than τ that constrains $\mathbf{n}$ and $\mathbf{m}$ to be orthogonal if $\frac{\gamma_2+\lambda_2}{\chi} < 0$ or $\frac{\gamma_2+\lambda_2}{\chi} > 1$, and τ for keeping $\mathbf{n}$ and $\mathbf{m}$ to be orthogonal is much larger than γ for fixing $\mathbf{n}$ as a unit vector if $0 < \frac{\gamma_2+\lambda_2}{\chi} < 1$. Figures 6.4-6.7 show some of the cases above.

6.4 An exploration of the dissipation function

In this section, we carry out a basic investigation of the associated dissipation function for the problem discussed in the previous section. This may give insight to the physical interpretation of the results (e.g., a priori inequalities for the viscosity coefficients, etc.).

From (6.80) and (6.81) in the previous section, we can write:

$$\mathbf{n} = (1, \phi(t), \theta(t)) = \mathbf{n}_0 + (0, \phi(t), 0) + (0, 0, \theta(t)), \tag{6.133}$$

$$\mathbf{m} = (-\theta(t), 0, 1) = \mathbf{m}_0 + (-\theta(t), 0, 0,), \tag{6.134}$$

$$\mathbf{v} = (\kappa_0(t)z, \tau_0(t)z, 0)\,, \quad \kappa_0(t) = a\frac{\omega}{d}\cos(\omega t), \quad \tau_0(t) = b\omega\cos(\omega t). \tag{6.135}$$

We made small angular perturbations to these constant state solutions. Because they are linearly stable but not asymptotically stable, a future non-linear analysis may be required to look for non-linear stability and instability criteria. Therefore, the biaxial nematic non-linear case can be investigated by deploying the dissipation function of biaxial nematic liquid crystals, which has been found by Leslie and Carlsson [51]. A non-linear stability analysis, such as that carried out by Leslie [49] for nematics, may be feasible in biaxial as we can see the important role of the dissipation function to study the stability for the non-linear case. Therefore, the dissipation function should be included in the non-linear biaxial stability case, which can be investigated in future work. It is known that the rate of viscous dissipation $\hat{\mathcal{D}}$ of biaxial nematic liquid crystals is given by [51].

$$\begin{aligned}\hat{\mathcal{D}} = &\alpha_1(n_k n_p A_{kp})^2 + \alpha_4 A_{kp}A_{kp} + \beta_1(m_k m_p A_{kp})^2 + (\mu_3+\mu_4)(m_k n_p A_{kp})^2 \\ &+ (\alpha_5+\alpha_6)A_{kp}n_p A_{kq}n_q + (\beta_5+\beta_6)A_{kp}m_p A_{kp}m_q + 2\gamma_2 A_{kp}N_k n_p \\ &+ \gamma_1 N_p N_p + \lambda_1 M_p M_p + \gamma_3(N_p m_p)^2 + 2\lambda_2 A_{kp}M_k m_p + 2\gamma_4 N_k m_k m_p n_q A_{qp} \\ &+ \tau_{ij}A_{ij},\end{aligned} \tag{6.136}$$

where,

$$\begin{aligned}2\tau_{ij} =&\alpha\left(N_i n_j + N_j n_i\right) + \beta\left(M_i m_j + M_j m_i\right) + \mu N_p m_p\left(m_i n_j + m_j n_i\right) \\ &+ 2\mu_5 m_k m_p A_{kp} n_i n_j,\end{aligned} \tag{6.137}$$

and

$$\alpha = \alpha_3 + \alpha_2 - \gamma_2, \quad \beta = \beta_3 + \beta_2 - \lambda_2, \quad \mu = \mu_1 + \mu_2 - \gamma_4. \tag{6.138}$$

The dissipation function for biaxial nematic liquid crystals is complicated; it requires extensive calculations and is beyond the scope of this thesis, see Appendix C. Nevertheless, here we consider the dissipation function to first order in θ and

ϕ; we find its terms are

$$\alpha_1(n_k n_p A_{kp})^2 = 0, \tag{6.139}$$

$$\alpha_4 A_{kp} A_{kp} = \frac{\alpha_4 \omega^2 \left(a^2 + b^2 d^2\right)}{2d^2} \cos^2(\omega t), \tag{6.140}$$

$$\beta_1(m_k m_p A_{kp})^2 = 0, \tag{6.141}$$

$$(\mu_3 + \mu_4)(m_k n_p A_{kp})^2 = \frac{a\left(\mu_3 + \mu_4\right)\omega^2(a + 2bd\phi)}{4d^2} \cos^2(\omega t), \tag{6.142}$$

$$(\alpha_5 + \alpha_6) A_{kp} n_p A_{kq} n_q = \frac{a\left(\alpha_5 + \alpha_6\right)\omega^2(a + 2bd\phi)}{4d^2} \cos^2(\omega t), \tag{6.143}$$

$$\begin{aligned}(\beta_5 + \beta_6) A_{kp} m_p A_{kp} m_q =& \frac{\left(\beta_5 + \beta_6\right)\omega^2\left[a^2 + b^2 d^2 - \left(2a^2 + b^2 d^2\right)\theta\right]}{4d^2} \\ & \times \cos^2(\omega t),\end{aligned} \tag{6.144}$$

$$2\gamma_2 A_{kp} N_k n_p = \frac{a\gamma_2\omega\left[\omega(a + 2bd\phi)\cos(\omega t) + 2d\theta'\right]}{2d^2} \cos(\omega t), \tag{6.145}$$

$$\gamma_1 N_p N_p = \frac{a\gamma_1\omega\left[\omega\cos(\omega t)(a + 2bd\phi) + 4d\theta'\right]}{4d^2} \cos(\omega t), \tag{6.146}$$

$$\lambda_1 M_p M_p = \frac{\lambda_1\omega\left[\omega\left(a^2 + b^2 d^2\right)\cos(\omega t) + 4ad\theta'\right]}{4d^2} \cos(\omega t), \tag{6.147}$$

$$\gamma_3(N_p m_p)^2 = \frac{a\gamma_3\omega[\omega(a + 2bd\phi)\cos(\omega t) + 4d\theta']}{4d^2} \cos(\omega t), \tag{6.148}$$

$$2\lambda_2 A_{kp} M_k m_p = -\frac{\lambda_2\omega\left[\omega\left(a^2 + b^2 d^2\right)\cos(\omega t) + 2ad\theta'\right]}{2d^2} \cos(\omega t), \tag{6.149}$$

$$2\gamma_t e 4 N_k m_k m_p n_q A_{qp} = \frac{a\gamma_4\omega\left[\omega(a + 2bd\phi)\cos(\omega t) + 2d\theta'\right]}{2d^2} \cos(\omega t), \tag{6.150}$$

$$\begin{aligned}\tau_{ij} A_{ij} =& \Big\{\omega\Big[-bd\beta + a(\alpha - \beta + \mu) + (\alpha + \mu)(a + bd)\phi \\ & (bd(-\alpha + \beta) - 2a\mu_5)\theta\Big]\cos(\omega t) + 2d\Big[(\alpha - \beta + \\ & \mu)\theta' + \alpha\phi'\Big]\Big\}\frac{\omega}{2d^2}(a + bd)\cos(\omega t),\end{aligned} \tag{6.151}$$

$$\hat{\mathcal{D}} = p_0 + p_1 + p_2 + p_3 + p_4, \tag{6.152}$$

where,

$$p_0 = \frac{\omega^2}{4d^2}\Big[a^2\left(2\alpha + 2\alpha_4 + \alpha 5 + \alpha 6 - 2\beta + \beta_5 + \beta_6 + \gamma_1 + 2\gamma_2 + \gamma_3 + 2\gamma_4 + \lambda_1\right.$$

$$-2\lambda_2 + 2\mu + \mu_3 + \mu_4) + b^2d^2\,(2\alpha_4 - 2\beta + \beta_5 + \beta_6 + \lambda_1 - 2\lambda_2)$$
$$+ 2abd(\alpha - 2\beta + \mu)\Big]\cos^2(\omega t), \tag{6.153}$$

$$p_1 = -\frac{\omega^2}{4d^2}\Big[2a^2\,(\beta_5 + \beta_6 + 2\mu_6) + 2abd\,(\alpha - \beta + 2\mu_6) + b^2d^2(2\alpha - 2\beta + \beta_5$$
$$+ \beta_6)\Big]\cos^2(\omega t)\theta, \tag{6.154}$$

$$p_2 = \frac{\omega^2}{2d^2}\Big[a^2(\alpha + \mu) + abd(2\alpha + \alpha 5 + \alpha 6 + \gamma_1 + 2\gamma_2 + \gamma_3 + 2\gamma_4 + 2\mu + \mu_3$$
$$+ \mu_4) + b^2d^2(\alpha + \mu)\Big]\cos^2(\omega t)\phi, \tag{6.155}$$

$$p_3 = \frac{\omega}{d}\Big[a\,(\alpha - \beta + \gamma_1 + \gamma_2 + \gamma_3 + \gamma_4 + \lambda_1 - \lambda_2 + \mu) + bd(\alpha - \beta + \mu)\Big]$$
$$\times \cos(\omega t)\theta', \tag{6.156}$$

$$p_4 = \frac{\alpha\omega}{d}(a + bd)\cos(\omega t)\phi'. \tag{6.157}$$

We can see that it is complicated to check the positivity of the dissipation function in (6.152) for the non-linear case. However, in the previous section, we found that the solutions of (6.79)-(6.81) in the linear case can be taken in the forms

$$\theta(t) = \theta_0 - B\sin(\omega t), \quad \phi(t) = 0. \tag{6.158}$$

Substituting these solutions into (6.152), we obtain

$$\hat{\mathcal{D}} = \frac{1}{4d^2}\omega^2\Big[s_1\theta_0 + s_2 + s_3\sin(\omega t)\Big]\cos^2(\omega t), \tag{6.159}$$

where,

$$s_1 = -2a^2\,(\beta_5 + \beta_6 + 2\mu_5)\,, \tag{6.160}$$

$$s_2 = a^2\Big[2\alpha + 2\alpha_4 + \alpha_5 + \alpha_6 - 2\beta + \beta_5 + \beta_6 + \gamma_1 + 2\gamma_2 + \gamma_3 + 2\gamma_4 + \lambda_1$$
$$- 2\lambda_2 + 2\mu \quad + \mu_3 + \mu_4\Big] - 4aBd\Big[\alpha - \beta + \gamma_1 + \gamma_2 + \gamma_3 + \gamma_4 + \lambda_1 -$$
$$\lambda_2 + \mu\Big], \tag{6.161}$$

$$s_3 = 2a^2B\,(\beta_5 + \beta_6 + 2\mu_5)\,. \tag{6.162}$$

We can make $\hat{\mathcal{D}}$ positive by choosing an appropriate value for the arbitrary constant

θ_0. This value must obey the following conditions,

$$s_1\theta_0 + s_2 \geq 0, \quad s_1\theta_0 + s_2 \geq |s_3|. \tag{6.163}$$

The linear solutions obey the dissipation function positivity requirement (a necessary condition). This checks that we have viable physical perturbations for the selected viscosities; see Figures 6.8 and 6.9.

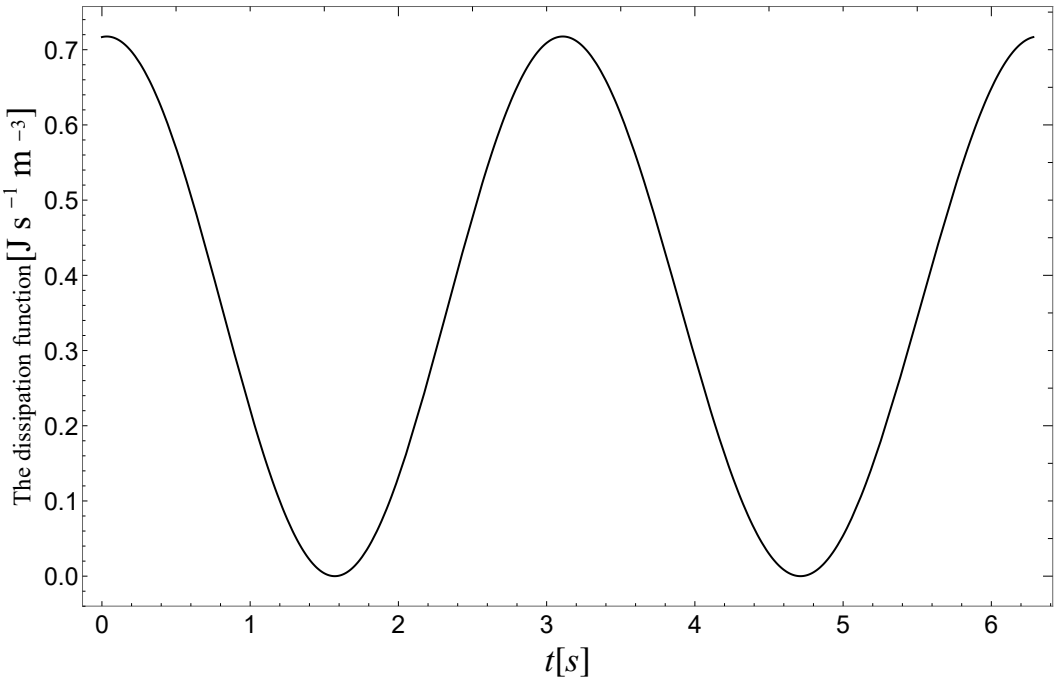

Figure 6.8: The dissipation function for the linear case, which is given by (6.159) in 2D under conditions (6.163).

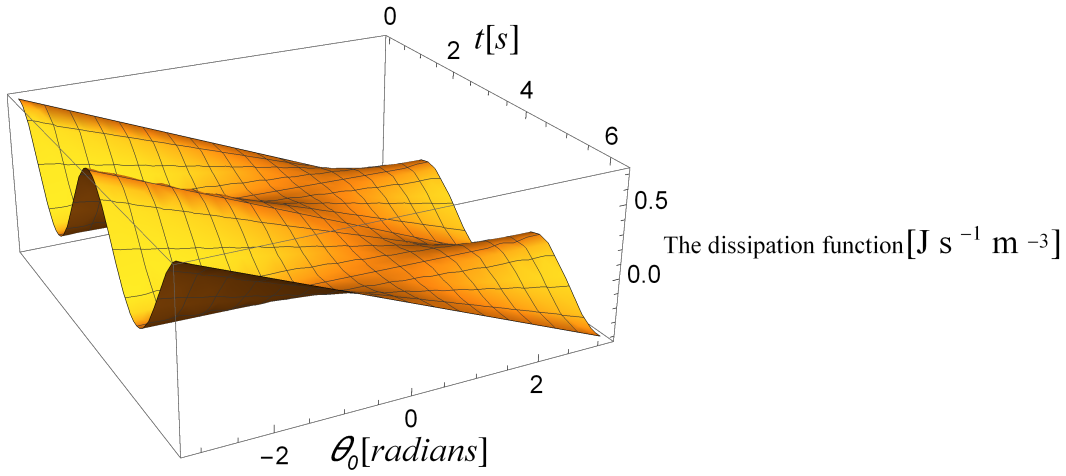

Figure 6.9: The dissipation function for the linear case, which is given by (6.159) in 3D under conditions (6.163).

Now we look for second order expansion of the dissipation function. The linear solutions (6.158) are substituted into the dissipation function for biaxial nematic liquid crystal; we obtain its terms,

$$\alpha_1(n_k n_p A_{kp})^2 = \alpha_1 \kappa_0^2 \Big(\theta_0 - B\sin(t\omega)\Big)^2, \tag{6.164}$$

$$\alpha_4 \kappa_0^2 A_{kp} A_{kp} = \frac{1}{2}\alpha_4 \left(H^2+1\right), \tag{6.165}$$

$$\beta_1(m_k m_p A_{kp})^2 = \beta_1 \kappa_0^2 \Big(\theta_0 - B\sin(t\omega)\Big)^2, \tag{6.166}$$

$$\begin{aligned}(\mu_3+\mu_4)(m_k n_p A_{kp})^2 =& -\frac{1}{4}\kappa_0^2\Big[2\left(\theta_0 - B\sin(t\omega)\right)^2 - \left(H^2+1\right)^2\Big]\times \\ & (\mu_3+\mu_4),\end{aligned} \tag{6.167}$$

$$\begin{aligned}(\alpha_5+\alpha_6)A_{kp}n_p A_{kq}n_q =& \frac{1}{4}\kappa_0^2\left(\alpha_5+\alpha_6\right)\left(H^2+1\right)\kappa_0^2\Big[\Big(\theta_0 - B\sin(t\omega)\Big)^2 + \\ & H^2+1\Big],\end{aligned} \tag{6.168}$$

$$\begin{aligned}(\beta_5+\beta_6)A_{kp}m_p A_{kp}m_q =& \frac{1}{4}\left(\beta_5+\beta_6\right)\kappa_0^2\Big[B\sin(t\omega)-\theta_0+1\Big]\Big[B\sin(t\omega) - \\ & \theta_0 + H^2 + 1\Big],\end{aligned} \tag{6.169}$$

$$\begin{aligned}2\gamma_2 A_{kp}N_k n_p =& \frac{1}{2}\gamma_2\kappa_0\left(1+H^2\right)\Big[\kappa_0\Big(1+H^2-\left(\theta_0 - B\sin(\omega t)\right)^2\Big) \\ & - 2B\cos(\omega t)\Big],\end{aligned} \tag{6.170}$$

$$\begin{aligned}\gamma_1 N_p N_p =& \frac{1}{4}\gamma_1\Big\{\Big[\kappa_0\left(1+H^2\right) - 2B\cos(\omega t)\Big]^2 + \kappa_0^2\left(1+H^2\right) \\ & \times\Big[\theta_0 - B\sin(\omega t)\Big]^2\Big\},\end{aligned} \tag{6.171}$$

$$\begin{aligned}\lambda_1 M_p M_p =& \lambda_1\Big\{\frac{1}{4}\kappa_0^2\Big(1+H^2+\left(\theta_0 - B\sin(\omega t)\right)^2\Big) + B\cos(\omega t) \\ & \times\Big(B\cos(\omega t) - \kappa_0\Big)\Big\},\end{aligned} \tag{6.172}$$

$$\begin{aligned}\gamma_3(N_p m_p)^2 =& \frac{1}{4}\gamma_3\Big\{2\kappa_0^2\Big(\theta_0 - B\sin(\omega t)\Big)^2 + \Big(\kappa_0\left(1+H^2\right) - 2B \\ & \times\cos(\omega t)\Big)^2\Big\},\end{aligned} \tag{6.173}$$

$$\begin{aligned}2\lambda_2 A_{kp}M_k m_p =& \frac{1}{2}\kappa_0\lambda_2\Big\{\kappa_0\Big[1+H^2-\Big(\theta_0 - B\sin(\omega t)\Big)^2\Big] - 2B \\ & \times\cos(\omega t)\Big\},\end{aligned} \tag{6.174}$$

$$2\gamma_4 N_k m_k m_p n_q A_{qp} = \frac{1}{2}\gamma_4\kappa_0\left(H^2+1\right)\Big[\left(H^2+1\right)\kappa_0 - 2B\omega\cos(\omega t)\Big], \quad (6.175)$$

$$\begin{aligned}\tau_{ij}A_{ij} = &-\frac{1}{2}\kappa_0(1+H)\Big\{\kappa_0 B^2\Big[\alpha(1+H)-\beta+4\mu_5\Big]\sin^2(\omega t) + \Big[-B\Big(\kappa_0 H(-\beta \\ &+ 2\alpha(1+\theta_0)+\mu+4\mu_5) + 2\kappa_0(\mu_5+\theta_0(\alpha-\beta+4\mu_5))\Big) - 2B^2(\alpha+\beta) \\ &\times\cos(\omega t)\Big]\sin(\omega t) + 2B\Big[\beta(-1+\theta_0)+\alpha(1+H+\theta_0)+(1+H)\mu\Big] \\ &\times\cos(\omega t) - \kappa_0\Big[\beta(-1+\theta_0)(1+H+\theta_0)+\alpha(1+H+\theta_0)(1+H^2 \\ &-(1+H)\theta_0)+\mu+H\left(1+H+H^2-\theta_0\right)\mu - 2(1+2H+2\theta_0) \\ &\times\theta_0\mu 5\Big]\Big\} \end{aligned} \quad (6.176)$$

where $H = \dfrac{bd}{a}$.

Then we can write $\hat{\mathcal{D}}$ in this form

$$\hat{\mathcal{D}} = \left[r_0\theta_0^2 + p_0\theta_0 + p_1\right]\cos^2(\omega t), \quad (6.177)$$

where,

$$p_0 = \left(r_1 + r_2\sin(\omega t)\right), \quad (6.178)$$

$$p_1 = r_3\left(r_4 + r_5\sin(\omega t) + r_6\cos(2\omega t)\right), \quad (6.179)$$

and

$r_0, r_1, r_2, r_3, r_4, r_5$ and r_6 are functions of the viscosities. The dissipation function that is given by (6.177) is plotted for some values of θ_0 in Figures 6.10-6.12.

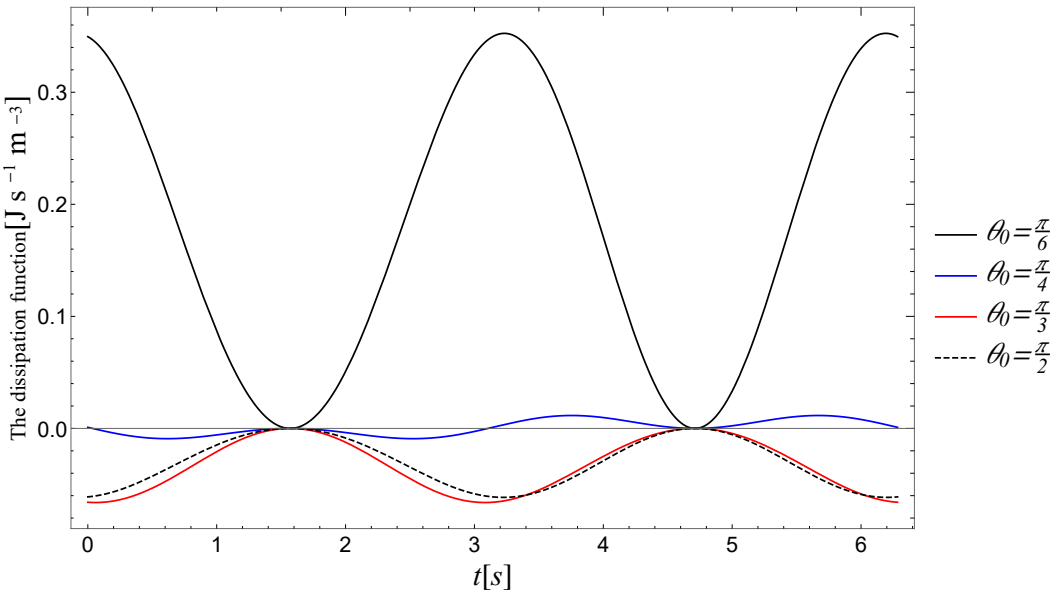

Figure 6.10: The dissipation function for the second order case, which is given by (6.177) for positive values of θ_0.

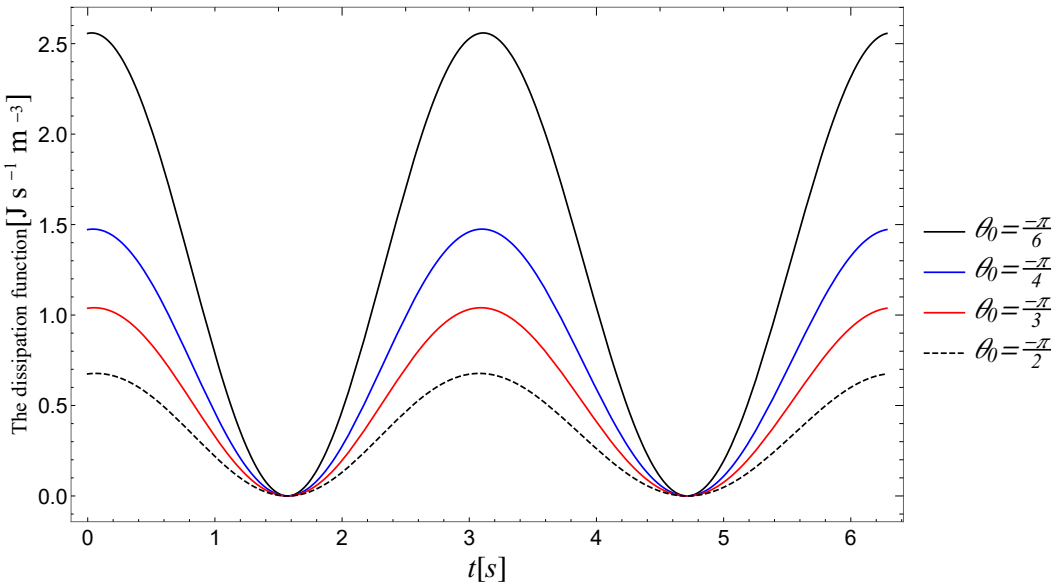

Figure 6.11: The dissipation function for the second order case, which is given by (6.177) for negative values of θ_0.

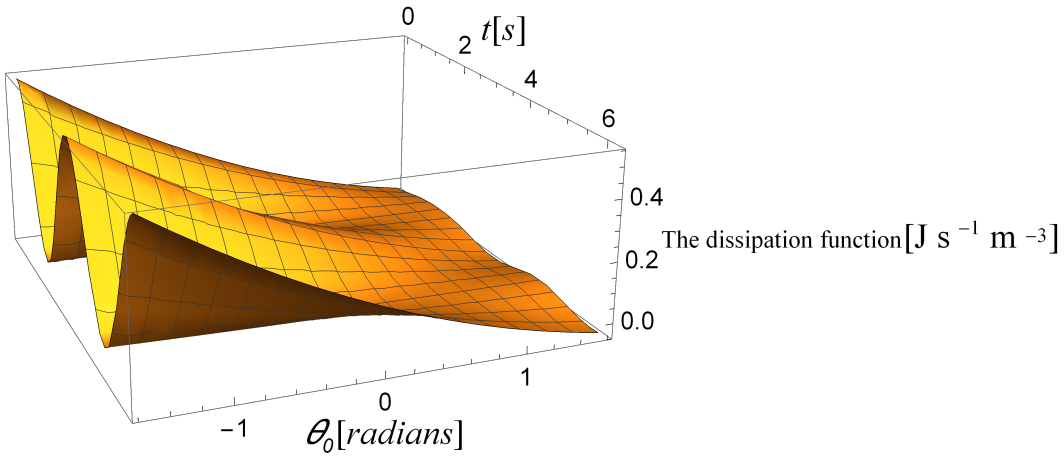

Figure 6.12: The dissipation function for the second order case, which is given by (6.177) when $\frac{-\pi}{2} \leq \theta_0 \leq \frac{\pi}{2}$.

In conclusion, as an approximation when linearisation is around $\theta_0 = 0$, we can presume that the non-linear behaviour will be similar if we restrict $\mid \theta_0 \mid \leq \frac{\pi}{2}$, in the first instance e.g., $-\frac{\pi}{2} \leq \theta_0 \leq \frac{\pi}{2}$. This means that the key result from Figure 6.10 is valid for a positive value of θ_0 and for the selected viscosities where the dissipation function is no longer positive; hence, θ_0 must be negative; see Figure 6.11. Both cases are illustrated in 3D in Figure 6.12. Physically, the director in (6.133) will favour a component in the negative $z-$direction. Thus, taking the dissipation function to second order reveals the anticipated perturbation to the director for maintaining stability.

A key future project is to derive the analogous equations for a biaxial; the extent of the work is beyond the scope of this thesis.

6.5 Conclusions and comments

In Section 6.1, we introduced biaxial nematic liquid crystals and the biaxial nematic dynamic equations. In Subsection 6.2.1, we obtained oscillatory shear flow solutions by using the biaxial nematic dynamic equations. These solutions are plotted in Figures 6.2 and 6.3. Then we added a perturbation to these solutions to study the linear stability of these solutions. We found that these solutions are linearly stable but not asymptotically stable. In Subsection 6.3.1, we studied the stability and instability of nematics by investigating the dynamic equations (6.65) and (6.66). We found that the solutions (6.77) and (6.78) are stable. In Subsection 6.3.2, we looked at the linear stability of biaxial nematic liquid crystals using the dynamic equations of biaxial nematics. We concluded that the solutions $\theta(t)$ and $\phi(t)$ are linearly stable but not asymptotically stable. We also investigated the Lagrange multipliers γ, τ and κ by looking at the ratios $\left|\frac{\tau}{\kappa}\right|, \left|\frac{\gamma}{\kappa}\right|$ and $\left|\frac{\gamma}{\tau}\right|$, and investigated their behaviour, detailed and graphically displayed at the end of Sec-

tion 6.3. In Section 6.4, we investigated the dissipation function that was required to study non-linear stability and instability of biaxial nematic liquid crystals. We found that the dissipation function for biaxial nematic liquid crystals is complicated for the non-linear case. Then we considered the dissipation function for first order and substituted the solutions from the linear case in equations (6.158), from which we found that the dissipation function can be positive under some conditions, see Figures 6.8 and 6.9. We also examined second order expansions of the dissipation function by substituting the linear solutions (6.158) into the dissipation function for biaxial nematic liquid crystals. We concluded that if $|\theta_0| \leqslant \frac{\pi}{2}$, then the dissipation function is positive for only negative values of θ_0.

Chapter 7

Conclusions and future work

Chapter 1 introduced a brief history of liquid crystals and their discovery. This chapter also provided some brief details on the physical descriptions of the three main types of liquid crystalline phases: nematic, cholesteric and smectic. We also discussed viscosity and elasticity in liquid crystals and concluded with an outline of this thesis.

Chapter 2 discussed the development of the continuum theory of liquid crystals. We considered both the static and dynamic theory of nematics and introduced the classical equations that arise from the continuum theory. In conjunction with this work, relevant context around the classical Freedericksz transition was also summarised in Appendix A, variants of which are used in everyday display devices for 'switching' pixels on flat panel displays. This required the introduction of describing and modelling the applied electric and magnetic fields used in Freedericksz transitions. A brief mention of defects was also made.

In Chapter 3, we considered the known phenomenon of the Helfrich-Hurault

effect in SmA. We discussed the classic effect of an electric field applied to a SmA sample when the director **n** and the layer normal **a** are coincident. The influence of the layer compression coefficient B_0 upon the critical electric field strength is evident through the identified classical Helfrich-Hurault transition threshold. This chapter concluded with an exploration of the influence of the layer compression coefficient, B_0 and the wave number threshold q_x^c for both the classical transition and the transition when **n** and **a** may be uncoupled.

Chapter 4 is an important chapter of developed novel work. We applied the dynamic theory for SmA liquid crystals, which was developed by Stewart [79], in which the layer normal **a** and the director **n** are not necessarily parallel. The stability of initially planar alignments of SmA liquid crystal samples was considered here. We first started with the simplest case where it is presumed that flow is negligible. We then extended the analysis to problems with included flow and the incorporation of more sophisticated and relevant combinations of appropriate viscosities.

Chapter 5 extended work from Chapter 4 in different directions. In this chapter, the dynamic continuum theory for SmA was used when an applied electric field is included. We discussed the consequent revisions to the previously identified critical threshold when an electric field is applied to smectic layers. We found the conditions for stability and instability to small perturbations for an alignment of SmA, which is initially planar. The response time was also considered in both stability and instability cases. Moreover, we extended the problem in this chapter to include the dynamic contribution $\tilde{g}_i$ in order to investigate the stability and instability of the initial planar alignment of a SmA sample.

In Chapter 6, we considered the stability and instability in the dynamics of

an incompressible biaxial nematic liquid crystals by applying the continuum theory of biaxial nematic liquid crystals. We also considered by assuming, at first, no elastic contributions. We focused only on the linear stability case because it quickly became evident that the fully non-linear case became mathematically intractable and beyond the scope of this thesis; despite this, some progress was made in the derivation of the non-linear equations and their analysis, albeit very limited. Nevertheless, a linear analysis was successfully undertaken. Firstly, for background context, we looked at the linear stability of nematics that has been studied by Stewart [78] in non-linear stability analysis. This study guided us in the investigation of a linear stability analysis of biaxial nematics for the reasons highlighted in the text. It revealed that the dissipation function can be applied here to gain useful results and information in the linear case. The Lagrange multipliers were investigated by comparing the ratios $\left|\frac{\gamma}{\kappa}\right|$, $\left|\frac{\gamma}{\tau}\right|$ and $\left|\frac{\tau}{\kappa}\right|$. We concluded this chapter with ideas for future work, especially looking into anticipated applications of the dissipation function $\tilde{\mathcal{D}}$ for biaxial nematic liquid crystals. We calculated the dissipation function $\tilde{\mathcal{D}}$ explicitly to the first and second orders. Some novel, but limited, information was obtained, and it was seen that the calculations are complicated, but tractable, and that a more extended non-linear approach to stability was clearly beyond the scope of this thesis. Nevertheless, the linear analyses presented new results as they appear in Chapter 6.

Appendix A

A.1 Notation and conventions

In this thesis, we will use the classical notation that is adopted by Stewart and is common throughout continuum mechanics [78]. There are two important relations, the Kronecker delta δ_{ij} and the alternator ϵ_{ijk} which are defined by

$$\delta_{ij} = \begin{cases} 1 & \text{if } i = j, \\ 0 & \text{if } i \neq j, \end{cases} \tag{A.1}$$

and

$$\epsilon_{ijk} = \begin{cases} 1 & \text{if } i, j \text{ and } k \text{ are unequal and in cyclic order,} \\ -1 & \text{if } i, j \text{ and } k \text{ are unequal and in non-cyclic order,} \\ 0 & \text{if any two of } i, j \text{ or } k \text{ are equal,} \end{cases} \tag{A.2}$$

where, $i, j, k = 1, 2, 3$.

We denote the partial derivative of a quantity p with respect to the i^{th} variable by $p_{,i}$. Scalar and vector products, gradient, divergence and curl in Cartesian notation are defined respectively by

$$\mathbf{a} \cdot \mathbf{b} = a_i b_i, \tag{A.3}$$

$$\mathbf{a} \times \mathbf{b} = \mathbf{e}_i \epsilon_{ijk} a_j b_k, \tag{A.4}$$

$$\nabla p = \mathbf{e}_i p_i, \tag{A.5}$$

$$\nabla \cdot \mathbf{a} = a_{i,i}, \tag{A.6}$$

$$\nabla \times \mathbf{a} = \mathbf{e}_i \epsilon_{ijk} a_{kj}. \tag{A.7}$$

where $\mathbf{a}, \mathbf{b}$ and $\mathbf{c}$ are vectors in $\mathbb{R}^3$ and p is a scalar field. The dyadic product (or tensor product) of two vectors $\mathbf{a}$ and $\mathbf{b}$ is denoted by the symbol $\otimes$ and is defined as matrix with components given by

$$[\mathbf{a} \otimes \mathbf{a}]_{ij} = a_i b_j. \tag{A.8}$$

We shall define the divergence of a second order T_{ij} by

$$T_{ij,j}. \tag{A.9}$$

As mentioned by Stewart [78], if the tensor T_{ij} is symmetric, that is, $T_{ij} = T_{ji}$, then this convention coincides with that given by Goodbody [33], among others. However, care needs to be exercised in liquid crystal theory because the stress tensor, a second order tensor, is in general not symmetric: its divergence, therefore, has to be treated carefully and consistently. Note: the original work on liquid crystal theory by Leslie in 1966 [45] used a different notational convention.

A.2 Freedericksz transition and defects

When an external electric or magnetic field is applied to a finite sample of liquid crystals, the director $\mathbf{n}$ will change its orientation within layers except at the surface or boundary when there is strong anchoring. For example, when a magnetic field $\mathbf{H}$ is applied to a thin sample of nematic liquid crystal where the

magnetic anisotropy satisfies $\chi_a > 0$, the director $\mathbf{n}$ then changes its direction to be parallel to the field when the magnitude field $H = |\mathbf{H}|$ is greater than a specific value, say, H_c, called the critical field strength. This means that the director will be influenced by the magnetic field and change its orientation to be parallel to $\mathbf{H}$ only when $H > H_c$. Similar ideas apply when an electric field is applied except that the electric field requires more care in the analysis because the electric field itself can be influenced by the presence of the liquid crystal. The classical Freedericksz transition in nematics can be classified in three cases: splay, twist and bend geometries (for more details, see the review by Stephen and Straley [76]).

It is known that the orientation of $\mathbf{n}$ can be discontinuous [21, 78]. This case can give rise to defect structures. These defects can be a point, line or a sheet on a surface. For more details on point and line defects, see [78], and for sheet defects see de Gennes and Prost [21]. In this thesis, we are only concerned with defect-free surface alignments of smectic samples. Nevertheless, it is important to be aware of the complex internal structures that can arise when constraints or perturbations are made. These can lead to defect structures and other complex behaviour under dynamics which will not be considered here.

A.3 The Ericksen-Leslie dynamic equations for nematics

This is a summary [78] of the Ericksen-Leslie dynamic equations for nematics in the incompressible isothermal theory when the director inertial term is neglected. The director $\mathbf{n}$ and the velocity vector must fulfil the constraints,

$$n_i n_i = 1, \quad v_{i,i} = 0, \tag{A.10}$$

and the balance laws equations which arise from linear and angular momentum respectively take the forms

$$\rho\dot{v}_i = \rho F_i - (p + w_F)_{,i} + \tilde{g}_j n_{j,i} + G_j n_{j,i} + \tilde{t}_{ij,j}, \tag{A.11}$$

$$\left(\frac{\partial w_F}{\partial n_{i,j}}\right)_{,j} - \frac{\partial w_F}{\partial n_i} + \tilde{g}_i + G_i = \lambda n_i, \tag{A.12}$$

where F_i is the external body force per unit mass, G_i is the generalised body force, ρ is the density, p is the pressure, and w_F is the elastic energy density for nematics. The superposed dot denotes the usual material time derivative defined in equation (2.15). The scalar function λ is a Lagrange multiplier which can usually be eliminated or evaluated by taking the scalar product of equation (A.12) with $\mathbf{n}$. The constitutive equations for the viscous stress $\tilde{t}_{ij}$ and the vector $\tilde{g}_i$ are

$$\tilde{t}_{ij} = \alpha_1 n_k A_{kp} n_p n_i n_j + \alpha_2 N_i n_j + \alpha_3 n_i N_j + \alpha_4 A_{ij}, \tag{A.13}$$

$$+ \alpha_5 n_j A_{ik} n_k + \alpha_6 n_i A_{jk} n_k, \tag{A.14}$$

$$\tilde{g}_i = -\gamma_1 N_i - \gamma_2 A_{ip} n_p, \tag{A.15}$$

$$\gamma_1 = \alpha_3 - \alpha_2 \geq 0, \tag{A.16}$$

$$\gamma_2 = \alpha_3 + \alpha_2 = \alpha_6 - \alpha_5, \tag{A.17}$$

$$A_{ij} = \frac{1}{2}\left(v_{i,j} + v_{j,i}\right), \tag{A.18}$$

$$N_i = \dot{n}_i - W_{ij} n_j, \quad W_{ij} = \frac{1}{2}\left(v_{i,j} - v_{j,i}\right), \tag{A.19}$$

where $\alpha_1, \alpha_2, \ldots, \alpha_6$, are the Leslie viscosities, A_{ij} is the rate of strain tensor, W_{ij} is the vorticity tensor, N_i is the co-rotational time flux of the director $\mathbf{n}$ and a superposed dot again represents the material time derivative.

A.4 Electric field and associated energies

It is common practice to apply a magnetic or an electric field to align samples of liquid crystals. This was known and applied by researchers from the beginning of

liquid crystals research. The aim of this idea is to force the director to be parallel or perpendicular to the field for the majority of the nematics and many cholesterics. In fact, electric and magnetic fields produce energies, called the electric energy (produced by an electric field) and the magnetic energy (produced by a magnetic field). A brief description of these energies is given in this section. For more details, see [78]. There is a phenomenon that is produced by applying an electric field $\mathbf{E}$ to a sample of liquid crystal. This phenomenon is called polarisation, denoted by $\mathbf{P}$. There is a relation between the polarisation and the electric field; it is given by the equation

$$\mathbf{P} = \epsilon_0 \chi_e \mathbf{E}, \quad \chi_e = \begin{bmatrix} \chi_{e_\perp} & 0 & 0 \\ 0 & \chi_{e_\perp} & 0 \\ 0 & 0 & \chi_{e_\parallel} \end{bmatrix}, \tag{A.20}$$

where χ_e is called the electric susceptibility tensor, ϵ_0 (unitless) is the permittivity of free space, $\chi_{e_\perp}$ and $\chi_{e_\parallel}$ represent the electric susceptibilities parallel and perpendicular to the director, respectively. It is assumed that $\mathbf{n}$ is parallel to the $z-$direction, $\mathbf{n} = \mathbf{n}_0 = (0, 0, 1)$. The electric displacement $\mathbf{D}$ induced by $\mathbf{E}$ and $\mathbf{P}$ is defined by

$$\mathbf{D} = \epsilon_0 \mathbf{E} + \mathbf{P} = \epsilon_0 \epsilon_1 \mathbf{E} + \epsilon_0 \epsilon_a \left(\mathbf{n}_0 \cdot \mathbf{E}\right) \mathbf{n}_0, \quad \epsilon_a = \epsilon_\mu - \epsilon_\perp, \tag{A.21}$$

where $\epsilon_\parallel$ and $\epsilon_\perp$ are called dielectric Permittivities (known as the dielectric constants) of liquid crystals when the field and director are parallel and perpendicular, respectively. The quantity ϵ_a can be negative or positive. When ϵ_a is positive, the director attempts to be parallel to the field and perpendicular to the field when ϵ_a is negative [78]. The total electric energy, w_{elec} is given by

$$w_{elec} = -\frac{1}{2}\mathbf{D} \cdot \mathbf{E} = -\frac{1}{2}\epsilon_0 \epsilon_\perp E^2 - \frac{1}{2}\epsilon_0 \epsilon_a (\mathbf{n} \cdot \mathbf{E})^2, \tag{A.22}$$

where $\mathbf{E} = |E|$. Here, the term $-\frac{1}{2}\epsilon_0\epsilon_\perp E^2$ can be ignored because it is independent of the director $\mathbf{n}$. Therefore, the electric energy density takes the form

$$w_{elec} = -\frac{1}{2}\epsilon_0\epsilon_a(\mathbf{n}\cdot\mathbf{E})^2. \tag{A.23}$$

The Maxwell equations must be satisfied on the electric field $\mathbf{E}$ and the electric displacement $\mathbf{D}$. The polarisation can influence on the electric field in a liquid crystals sample. This interaction is strong with liquid crystals. In general, the electric field $\mathbf{E}$ is not constant and obeys the relevant reduced Maxwell equations,

$$\nabla\cdot\mathbf{D} = 0, \quad \nabla\times\mathbf{E} = 0. \tag{A.24}$$

It is known to make calculations easier to start by studying a simple case which needs some assumptions should be imposed. Suppose the influence of the liquid crystals on the electric field is ignored, then the Maxwell equations are given by

$$\nabla\cdot\mathbf{E} = 0, \quad \nabla\times\mathbf{E} = 0, \tag{A.25}$$

where ϵ_a is small.

A.5 Magnetic fields and the magnetic energy

The application of a magnetic field $\mathbf{H}$ across a liquid crystal sample induces a magnetisation $\mathbf{M}$ in the liquid crystal due to the weak magnetic dipole moments imposed upon the molecular alignment by the magnetic field. Similar analogues for the displacement $\mathbf{D}$ in the electric field, the magnetic induction $\mathbf{B}$ is defined by

$$\mathbf{B} = \mu_0\mu_\perp\mathbf{H} + \mu_0\Delta\chi(\mathbf{n}\cdot\mathbf{H})\mathbf{n}, \tag{A.26}$$

where,

$$\mu_\perp = 1+\chi_{m_\perp}, \quad \mu_\parallel = 1+\chi_{m_\parallel}, \quad \Delta\chi = \mu_\parallel - \mu_\perp = \chi_{m_\parallel} - \chi_{m_\perp}. \tag{A.27}$$

The quantity $\Delta\chi$ is called the magnetic anisotropy, $\chi_{m_\parallel}$ and $\chi_{m_\perp}$ denote the diamagnetic susceptibilities (negative) when the field and the director are parallel and perpendicular, respectively. Similar analogues in the electric field case, when $\chi_{m_\perp}$ is positive, the director attempts to be parallel to the magnetic field, whereas it is perpendicular to the magnetic field when $\chi_{m_\perp}$ is negative. The relevant energy density follows by an argument that is completely analogous to that for obtaining the electric energy density w_{elec} in equation (A.23). We have that the magnetic energy density is given by

$$w_{mag} = -\frac{1}{2}\mathbf{B}\cdot\mathbf{H} = -\frac{1}{2}\mu_0\mu_\perp H^2 - \frac{1}{2}\mu_0\Delta\chi(\mathbf{n}\cdot\mathbf{H})^2, \tag{A.28}$$

and the simplest magnetic energy density employed in calculations involving a finite sample of nematic is defined by

$$w_{mag} = -\frac{1}{2}\mu_0\Delta\chi(\mathbf{n}\cdot\mathbf{H})^2. \tag{A.29}$$

In general, the magnetic induction $\mathbf{B}$ and magnetic field $\mathbf{H}$ must satisfy the relevant Maxwell field equations

$$\nabla\cdot\mathbf{B} = 0, \quad \nabla\times\mathbf{H} = \mathbf{0}. \tag{A.30}$$

Moreover, the liquid crystal sample is presumed to have no influence on the applied magnetic field. Suppose that $\Delta\chi$ is small, $\mathbf{B}$ can be considered as being parallel to the magnetic field $\mathbf{H}$ when considering Maxwell's equations. Therefore, the conditions in (A.30) are often replaced by the two equations

$$\nabla\cdot\mathbf{H} = 0, \quad \nabla\times\mathbf{H} = \mathbf{0}, \tag{A.31}$$

under this approximation.

Appendix B

Stress measures

This is a brief summary on stress in material systems. The force per unit area is called stress, the measure of the capacity of the material to carry loads. Stress at a point in a three-dimensional continuum can be measured in terms of nine quantities, three per plane (on three mutually perpendicular planes at the point). These nine quantities can be arranged into a two-dimensional stress tensor. Now, let $\hat{\mathbf{n}}$ be a unit normal to a given surface. The stress vector (or surface traction) is a point function of the unit normal $\mathbf{n}$, which denotes the orientation of the plane on which $\mathbf{t}$ acts. The stress vector is defined by (cf: equation (A.8))

$$\mathbf{t}^{(\hat{n})} = (\mathbf{t}_1 \otimes \hat{\mathbf{e}}_1 + \mathbf{t}_2 \otimes \hat{\mathbf{e}}_2 + \mathbf{t}_3 \otimes \hat{\mathbf{e}}_3) \cdot \hat{\mathbf{n}}, \tag{B.1}$$

where $\mathbf{t}_j$ denote the stress vectors that act on the faces that are perpendicular to the x_j coordinate axis of a point cube, respectively, as shown in Figure B.1. The terms $\mathbf{t}_1 \otimes \hat{\mathbf{e}}_1 + \mathbf{t}_2 \otimes \hat{\mathbf{e}}_2 + \mathbf{t}_3 \otimes \hat{\mathbf{e}}_3$ called stress tensor, denoted σ and defined by

$$\sigma = \mathbf{t}_1 \otimes \hat{\mathbf{e}}_1 + \mathbf{t}_2 \otimes \hat{\mathbf{e}}_2 + \mathbf{t}_3 \otimes \hat{\mathbf{e}}_3, \tag{B.2}$$

therefore

$$\mathbf{t} = \sigma \cdot \hat{\mathbf{n}} \quad \text{or} \quad t_i = \sigma_{ij} n_j. \tag{B.3}$$

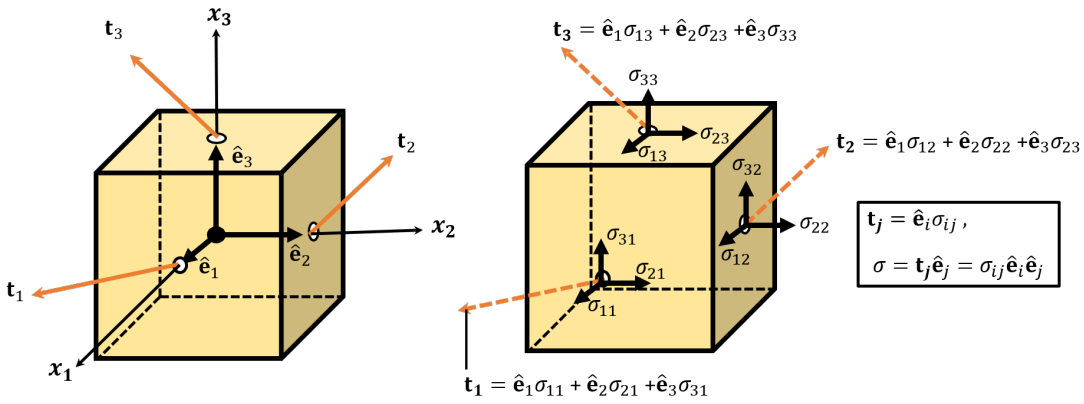

Figure B.1: Display of stress components in Cartesian rectangular coordinates [67].

We can write $\mathbf{t}_1, \mathbf{t}_2$ and $\mathbf{t}_3$ in their orthogonal components in the Cartesian system, see Figures B.1.

$$\mathbf{t}_j = \hat{\mathbf{e}}_i \sigma_{ij}, \quad i, j = 1, 2, 3, \tag{B.4}$$

and the stress tensor can be expressed as

$$\sigma = \mathbf{t}_j \hat{\mathbf{e}}_j = \hat{\mathbf{e}}_i \sigma_{ij} \hat{\mathbf{e}}_j.$$

The component σ_{ij} represents the stress in the x_i-coordinate direction and on a plane perpendicular to the x_j coordinate on the faces of a point cube. So, in matrix form, we can write

$$\mathbf{t}_1 = \hat{\mathbf{e}}_1 \sigma_{11} + \hat{\mathbf{e}}_2 e_{21} + \hat{\mathbf{e}}_3 \sigma_{31}, \tag{B.5}$$

$$\mathbf{t}_2 = \hat{\mathbf{e}}_1 \sigma_{12} + \hat{\mathbf{e}}_2 \sigma_{22} + \hat{e}_3 \sigma_{32}, \tag{B.6}$$

$$\mathbf{t}_3 = \hat{\mathbf{e}}_1 \sigma_{13} + \hat{\mathbf{e}}_2 \sigma_{23} + \hat{e}_{\mathbf{e}} \sigma_{33}. \tag{B.7}$$

In matrix form, we can write

$$\sigma = \begin{bmatrix} \sigma_{11} & \sigma_{12} & \sigma_{13} \\ \sigma_{21} & \sigma_{22} & \sigma_{23} \\ \sigma_{31} & \sigma_{32} & \sigma_{33} \end{bmatrix}. \tag{B.8}$$

We call σ_{11}, σ_{22} and σ_{33} the normal stresses, whereas the other components σ_{12}, σ_{13}, σ_{21}, σ_{23}, σ_{31} and σ_{32} are called shear stresses.

Appendix C

The dissipation function $\hat{\mathcal{D}}$ of biaxial nematic liquid crystals

Here we will calculate the terms of the dissipation function $\hat{\mathcal{D}}$ of biaxial nematic liquid crystals given by (6.136) for non-linear case to show that calculations are complicated. Further applications exploiting these expressions are beyond the scope of this thesis. Nevertheless, these results do reveal structural features of the influence of the material parameters.

$$\alpha_1(n_k n_p A_{kp})^2 = \alpha_1 \kappa_0^2 \theta^2 (1 + H\phi)^2, \tag{C.1}$$

$$\alpha_4 A_{kp} A_{kp} = \frac{1}{2}\alpha_4 \kappa_0^2 \left(1 + H^2\right), \tag{C.2}$$

$$\beta_1(m_k m_p A_{kp})^2 = \beta_1 \kappa_0^2 \theta^2, \tag{C.3}$$

$$(\mu_3 + \mu_4)(m_k n_p A_{kp})^2 = \frac{1}{4}\kappa_0^2 \left(\mu_3 + \mu_4\right) \Big[-1 + \theta^2 - H\phi \Big]^2, \tag{C.4}$$

$$(\alpha_5 + \alpha_6) A_{kp} n_p A_{kq} n_q = \frac{1}{4}\kappa_0^2 \left(\alpha_5 + \alpha_6\right) \Big[\left(1 + H^2\right)\theta^2 + (1 + H\phi)^2 \Big], \tag{C.5}$$

$$(\beta_5 + \beta_6) A_{kp} m_p A_{kp} m_q = -\frac{1}{4}\kappa_0^2 \left(\beta_5 + \beta_6\right) \left(1 + H^2 - \theta\right)(-1 + \theta), \tag{C.6}$$

$$2\gamma_2 A_{kp}N_k n_p = \frac{1}{2}\gamma_2\kappa_0\Big\{-\kappa_0(1+H^2)\theta^2 + (1+H\phi)\Big[\kappa_0(1+H\phi)+2\theta'\Big] + 2H\theta\phi'\Big\}, \tag{C.7}$$

$$\gamma_1 N_p N_p = \frac{1}{4}\gamma_1\Big\{\kappa_0^2\Big[1+\theta^2+H^2\theta^2+H^2\phi^2\Big] - 4\left(H\kappa_0\theta-\phi'\right)\phi' + 4\theta'\left(\kappa_0+\theta'\right) + 2H\kappa_0\phi\left(\kappa_0+2\theta'\right)\Big\}, \tag{C.8}$$

$$\lambda_1 M_p M_p = \frac{1}{4}\lambda_1\Big[\kappa_0^2(1+H^2+\theta^2)+4\theta'(\kappa_0+\theta')\Big], \tag{C.9}$$

$$\gamma_3(N_p m_p)^2 = \frac{1}{4}\gamma_3\Big[\kappa_0\left(1+\theta^2+H\phi\right)+2\theta'\Big]^2, \tag{C.10}$$

$$2\lambda_2 A_{kp}M_k m_p = -\frac{1}{2}\kappa_0\lambda_2\Big[\kappa_0\left(1+H^2-\theta^2\right)+2\theta'\Big], \tag{C.11}$$

$$2\gamma_4 N_k m_k m_p n_q A_{qp} = -\frac{1}{2}\gamma_4\kappa_0\Big[-1+\theta^2-H\phi\Big]\Big[\kappa_0(1+\theta^2+H\phi)+2\theta'\Big], \tag{C.12}$$

$$\begin{aligned}\tau_{ij}A_{ij} =& \frac{1}{2}\Big\{2\Big[\theta'\Big(\alpha-\beta+\mu+\theta(\alpha+\beta-\mu\phi)+(\alpha+\mu)\phi-\mu\theta^2\Big) \\ &+\alpha(\theta+\phi+1)\phi'\Big]-\kappa_0\Big[-\alpha+\beta+\beta H+\theta^2\Big(\alpha-\beta+\alpha H \\ &+(H-1)\mu\phi+4\mu_6(\phi+1)\Big)+\theta\Big(H(\alpha-\beta)+H\mu\phi^2+ \\ &(\alpha+\mu)\phi+2\mu_6(\phi+1)^2\Big)-H(\alpha+\mu)\phi^2-(H+1)(\alpha+\mu)\phi \\ &-\mu+\theta^3\Big(2\mu_6+\mu\phi\Big)+\mu\theta^4\Big].\end{aligned} \tag{C.13}$$

Then we can write the dissipation function $\hat{\mathcal{D}}$ of biaxial nematic liquid crystals in the form

$$\hat{\mathcal{D}} = p_1 + p_2 + p_3 + p_4 + p_5 + p_0, \tag{C.14}$$

where,

$$\begin{aligned}p_0 =& \frac{1}{4}\kappa_0\Big\{2(\alpha-(1+H)\beta+\mu)+\kappa_0\Big[\alpha_5+\alpha_6+\beta_5+\beta_6+\gamma_1+2\gamma_2+\gamma_3+2\gamma_4 \\ &+\lambda_1-2\lambda_2+\mu_3+\mu_4+2\alpha_4(1+H^2)+H^2\Big(\beta_5+\beta_6+\lambda_1-2\lambda_2\Big)\Big]\Big\},\end{aligned} \tag{C.15}$$

$$p_1 = (\gamma_1+\gamma_3+\lambda_1)\theta'^2, \tag{C.16}$$

$$p_2 = \gamma_1 \phi'^2, \tag{C.17}$$

$$p_3 = \Big\{ \kappa_0 \left[\gamma_1 + \gamma_2 + \gamma_3 + \gamma_4 + \lambda_1 - \lambda_2 + (\gamma_3 - \gamma_4)\,\theta^2 \right] + \alpha - \beta + \mu + (\alpha + \mu)\phi + \theta(\alpha + \beta - \mu\theta) + \Big[H\,(\gamma_1 + \gamma_2 + \gamma_3 + \gamma_4)\,\kappa_0 - \mu\theta \Big] \phi \Big\} \theta', \tag{C.18}$$

$$p_4 = \Big[\alpha + (\alpha + H\,(-\gamma_1 + \gamma_2)\,\kappa_0)\,\theta + \alpha\phi \Big] \phi', \tag{C.19}$$

$$\begin{aligned} p_5 = \frac{1}{4}\kappa_0 \Big\{ & \Big[-2\mu + \kappa_0\,(\gamma_3 - 2\gamma_4 + \mu_3 + \mu_4) \Big] \theta^4 - 2\,(2\mu_6 + \mu\phi)\,\theta^3 \\ & + \Big[-2 \Big((1+H)\alpha - \beta + (-1+H)\mu\phi + 4\mu_6(1+\phi) \Big) \kappa_0 \times \\ & \Big(4 + (1+H^2)\alpha_5 + \alpha_6 + 4\beta_1 + \beta_5 + \beta_6 + \gamma_1 - 2\gamma_2 + 2\gamma_3 + \lambda_1 + 2\lambda_2 \\ & - 2\mu_3 - 2\mu_4 + H\left(2\,(4 + \gamma_3 - \mu_3 - \mu_4)\,\phi + H\left(\alpha_6 + \gamma_1 - 2\gamma_2 + 4\phi^2 \right) \right) \Big) \Big] \theta^2 \\ & - \Big[2H\,(\alpha - \beta) + \left(2 + H^2\right)(\beta_5 + \beta_6)\kappa_0 + 4\mu_6\left(1 + \phi^2\right) + 2\phi(\alpha + \mu + H\mu\phi) \Big] \theta \\ & + \Big[2(1+H)(\alpha+\mu) + 2H(\alpha+\mu) + \kappa_0 H\,(2+\phi) \Big(\alpha_5 + \alpha_6 + \gamma_1 + 2\gamma_2 + \gamma_3 \\ & + 2\gamma_4 + \mu_3 + \mu_4 \Big) \Big] \phi \Big\}, \end{aligned} \tag{C.20}$$

and

$$H = \frac{bd}{a}.$$

Appendix D

A Dissipation inequality

For reference and convenience, in line with the comments on page 48, we quote the result from Appendix A in Stewart [79] with the Author's permission. The dissipation inequality in (2.25) can be reduced to

$$\alpha_4 A_{ij}A_{ij} + \tau_1 \left(a_i A_{ij} a_j\right)^2 + 2\tau_2 a_i A_{ij} a_p A_{pj} + \lambda_p \left(J_{i,i}\right)^2 = \mathcal{D} \geq 0. \tag{D.1}$$

Without loss of generality, set a $= (0, 0, 1)$. Note that incompressibility of the fluid means that $A_{ii} = 0$ and therefore $A_{33} = -\left(A_{11} + A_{22}\right)$. Inserting these results into the inequality (D.1) gives a quadratic form that must satisfy

$$\begin{aligned} &A_{11}^2 \left(2\alpha_4 + \tau_1 + 2\tau_2\right) + A_{22}^2 \left(2\alpha_4 + \tau_1 + 2\tau_2\right) + 2A_{11}A_{22} \left(\alpha_4 + \tau_1 + 2\tau_2\right) \\ &\quad + 2A_{12}^2 \alpha_4 + 2A_{13}^2 \left(\alpha_4 + \tau_2\right) + 2A_{23}^2 \left(\alpha_4 + \tau_2\right) + \lambda_p \left(J_{i,i}\right)^2 \geq 0. \end{aligned} \tag{D.2}$$

By (4.13), $\lambda_p \geq 0$, and by (D.2), we must necessarily have

$$\alpha_4 \geq 0, \quad \alpha_4 + \tau_2 \geq 0. \tag{D.3}$$

The first three terms in (D.2) can be written as a quadratic form $\mathbf{X}^T C \mathbf{X}$ where $\mathbf{X} = [A_{11}, A_{22}]$ and C is the unique symmetric matrix

$$C = \begin{bmatrix} 2\alpha_4 + \tau_1 + 2\tau_2 & \alpha_4 + \tau_1 + 2\tau_2 \\ \alpha_4 + \tau_1 + 2\tau_2 & 2\alpha_4 + \tau_1 + 2\tau_2 \end{bmatrix}. \tag{D.4}$$

This quadratic form is positive semi-definite if and only if the determinants of all the principal submatrices are non-negative. Therefore, we require

$$2\alpha_4 + \tau_1 + 2\tau_2 \geq 0 \quad \text{and} \quad \alpha_4 \left(3\alpha_4 + 2\tau_1 + 4\tau_2\right) \geq 0. \tag{D.5}$$

Given the result in $(\text{D.3})_1$, the second inequality in (D.5) is sharper than the first when $\alpha_4 > 0$ because it reduces to $\frac{3}{2}\alpha_4 + \tau_1 + 2\tau_2 \geq 0$.

Bibliography

[1] D. Andrienko. Introduction to Liquid Crystals. *J. Mol. Liq.*, 267:520–541, 2018.

[2] R. Aris. *Vectors, Tensors and the Basic Equations of Fluid Mechanics*. Dover, New York, 1989.

[3] R. J. Atkin and I. W. Theoretical studies of Freedericksz Transitions in SmC Liquid Crystals. *Eur. J. Appl. Math.*, 8:253–262, 1997.

[4] G. K. Auernhammer, H. R. Brand, and H. Pleiner. The undulation instability in layered systems under shear flow–a simple model. *Rheol. Acta*, 39:215–222, 2000.

[5] G. K. Auernhammer, H. R. Brand, and H. Pleiner. Shear-induced instabilities in layered liquids. *Physical Review E*, 66:061707, 2002.

[6] G. K. Auernhammer, H. R. Brand, and H. Pleiner. Erratum: Shear-induced instabilities in layered liquids. *Phys. Rev. E*, 71:049901, 2005.

[7] L. M. Blinov. *Electro-optical and magneto-optical properties of liquid crystals*. International Union of Crystallography (IUCr), 1983.

[8] V. Borshch, S. V. Shiyanovskii, and O. D. Lavrentovich. Nanosecond liquid crystalline optical modulator, US 9,400,412 B2, 26 July 2016.

[9] T. Carlsson, I. W. Stewart, and F. M. Leslie. Theoretical studies of smectic C liquid crystals confined in a wedge: Stability considerations and Frederiks transitions. *Liq. Cryst.*, 9:661–678, 1991.

[10] P. M. Chaikin and T. C. Lubensky. *Principles of condensed matter physics*. Cambridge University Press, Cambridge, 1995.

[11] S. Chandrasekhar. *Liquid crystals*. Cambridge University Press, Cambridge, 2nd edition, 1992.

[12] R. H. Chen. *Liquid crystal displays: fundamental physics and technology*. John Wiley & Sons, 2011.

[13] V. G. Chigrinov. *Liquid crystal devices: physics and applications*. 1999.

[14] J. S. R. Chisholm. *Vectors in Three-Dimensional Space*. Cambridge University Press, 1978.

[15] B. Climent-Ezquerra and F. Guillén-Donzález. A review of mathematical analysis of nematic and smectic-A liquid crystal models. *Eur. J. Appl. Math.*, 25:133–153, 2014.

[16] D. Collin, J. Gallani, and P. Martinoty. Abnormal sound damping in the smectic-c phase of terephthal-bis-p-p'-butylaniline (TBBA): Evidence for anharmonic effects. *Phys Rev Lett*, 58:254–257, 1987.

[17] P. J. Collings. *Liquid Crystals: Nature's Delicate Phase of Matter*. Adam Hilger, Bristol, 1990.

[18] P. J. Collings and M. Hird. *Introduction to Liquid Crystals.* Taylor and Francis, London, 1997.

[19] P. J. Collings and M. Hird. *Introduction to Liquid Crystals: Chemistry and Physics.* CRC Press, London, 2017.

[20] C. R. da Cruz, J. L. Figueirinhas, and P. J. Sebastião. *NMR of Liquid Crystal Dendrimers.* Jenny Stanford Publishing, 1st edition, 2016.

[21] P. G. de Gennes and J. Prost. *The Physics of Liquid Crystals.* Clarendon Press, Oxford, 2nd edition, 1993.

[22] W. H. De Jeu. *Physical properties of liquid crystalline materials.* CRC Press, 1980.

[23] R. De Vita and I. W. Stewart. Energetics of lipid bilayers with applications to deformations induced by inclusions. *Soft Matter*, 9:2056–2068, 2013.

[24] D. Demus, J. Goodby, G. Gray, H. Spiess, and V. Vill, editors. *Handbook of Liquid Crystals*, volume 1 , Fundamentals. Wiley-VCH, Weinheim, Germany, 1998.

[25] I. Dierking. *Textures of Liquid Crystals.* Wiley-VCH, Weinheim, Germany, 2003.

[26] D. Dunmur and T. Sluckin. *Soap, Science and Flat-Screen TVs: A History of Liquid Crystals.* Oxford University Press, Inc., New York, 2011.

[27] J. L. Ericksen. Conservation laws for liquid crystals. *Trans. Soc. Rheol.*, 5:23–34, 1961.

[28] J. L. Ericksen. Equilibrium theory of liquid crystals. *Adv. Liq. Cryst.*, 2:233–298, 1976.

[29] M. Fallahpour, S. McKee, and E. B. Weinmüller. Numerical simulation of flow in smectic liquid crystals. *Appl. Numer. Math.*, 132:154–162, 2018.

[30] F. C. Frank. Liquid crystals. On the theory of liquid crystals. *Discuss. Faraday Soc.*, 25:19–28, 1958.

[31] G. Friedel. Les états mésomorphes de la matière. *Ann. Phys. (Paris).*, 9:273–474, 1922.

[32] C. J. García-Cervera and S. Joo. Analytic description of layer undulations in amectic A liquid crystals. *Arch. Ration. Mech. Anal.*, 203:1–43, 2012.

[33] A. M. Goodbody. Cartesian Tensors, Ellis Horwood, Chichester, 1982.

[34] J. W. Goodby, P. J. Collings, T. Kato, C. Tschierske, H. F. Gleeson, and P. Raynes, editors. *Handbook of Liquid Crystals*, volume 1 , Fundamentals of Liquid Crystals. Wiley-VCH, Weinheim, Germany, 2014.

[35] C. Gu and P. Yeh. Liquid Crystal Display (LCD). In *Handbook of Digital Imaging*, pages 1–44. John Wiley Sons, Ltd, 2015.

[36] W. Helfrich. Electrohydrodynamic and dielectric instabilities of cholesteric liquid crystals. *J. Chem. Phys.*, 55:839–842, 1971.

[37] W. Helfrich and M. Schadt. Swiss Patent No.532,261, 4th December 1970.

[38] J. P. Hurault. Static distortions of a cholesteric planar structure induced by magnetic or ac electric fields. *J. Chem. Phys.*, 59:2068–2075, 1973.

[39] A. Jákli and A. Saupe. Field-induced thickness change of ferroelectric liquid crystal films. *Phys. Rev. E*, 53:5580–5583, 1996.

[40] J. T. Jenkins. Flows of nematic liquid crystals. *Annu. Rev. Fluid Mech.*, 10:197–219, 1978.

[41] H. Kelker. Survey of the early history of liquid crystals. *Mol. Cryst. Liq. Cryst. Inc. Nonlinear Opt.*, 165:1–43, 1988.

[42] I.-C. Khoo. *Liquid crystals*. John Wiley & Sons, 2nd edition, 2007.

[43] N. Koide. *Liquid Crystal Display Story*. Springer, 2016.

[44] S. Kumar. *Chemistry of Discotic Liquid Crystals*. CRC Press, London and New York, 2016.

[45] F. M. Leslie. Some constitutive equations for anisotropic fluids. *Q. J. Mech. Appl. Math.*, 19:357–370, 1966.

[46] F. M. Leslie. Some constitutive equations for liquid crystals. *Arch. Ration. Mech. Anal.*, 28:265–283, 1968.

[47] F. M. Leslie. Theory of flow phenomena in liquid crystals. *Adv. Liq. Cryst.*, 4:1–81, 1979.

[48] F. M. Leslie. Viscometry of nematic liquid crystals. *Mol. Cryst. Liq. Cryst.*, 63:111–127, 1981.

[49] F. M. Leslie. Liquid Crystal Devices. *Inst. Wiskd. Dienstverlening, Tech. Univ. Eindhoven*, 1992.

[50] F. M. Leslie and T. Carlsson. Flow alignment in biaxial and discotic nematics. *Mol. Cryst. Liq.*, 292:113–122, 1997.

[51] F. M. Leslie, J. S. Laverty, and T. Carlsson. Continuum theory for biaxial nematic liquid crystals. *Q. J. Mech. Appl. Math.*, 45:595–606, 1992.

[52] F. M. Leslie, I. W. Stewart, and M. Nakagawa. A continuum theory for smectic C liquid crystals. *Mol. Cryst. Liq. Cryst.*, 198:443–454, 1991.

[53] G. R. Luckhurst. Biaxial nematic liquid crystals: fact or fiction? *Thin Solid Films*, 393:40–52, 2001.

[54] G. R. Luckhurst. V-shaped molecules: new contenders for the biaxial nematic phase. *Angew. Chemie - Int. Ed.*, 44:2834–2836, 2005.

[55] P. C. Martin, O. Parodi, and P. S. Pershan. Unified hydrodynamic theory for crystals, liquid crystals, and normal fluids. *Phys. Rev. A*, 6:2401–2420, 1972.

[56] R. M. May. Stability and Complexity in Model Ecosystems. *J. Anim. Ecol.*, 44:931, 1975.

[57] S. Obayya, M. F. O. Hameed, and N. F. F. Areed. *Computational Liquid Crystal Photonics: Fundamentals, Modelling and Applications*. John Wiley & Sons, Ltd, 2016.

[58] H. Ockendon and J. R. Ockendon. *Viscous Flow*. Cambridge University Press, Cambridge, 1995.

[59] Orsay Group. Simplified elastic theory for smectics C. *Solid State Commun.*, 9:653–655, 1971.

[60] C. W. Oseen. *Beiträge zur Theorie der anisotropen Flüssigkeiten, Arkiv För Matematik, Astronomi Och Fysik, 19A, part 9, 1-19*. 1925.

[61] C. W. Oseen. The Theory of Liquid Crystals. *Trans. Faraday Soc.*, 29:883–899, 1933.

[62] P. Oswald and P. Pieranski. *Nematic and cholesteric liquid crystals: concepts and physical properties illustrated by experiments*. CRC press, 2005.

[63] P. Oswald and P. Pieranski. *Smectic and columnar liquid crystals: concepts and physical properties illustrated by experiments*. CRC press, 2005.

[64] S. V. Pasechnik, V. G. Chigrinov, and D. V. Shmeliova. *Liquid Crystals: Viscous and Elastic Properties*. John Wiley and Sons, 2009.

[65] A. Ramage and E. C. Gartland. A preconditioned nullspace method for liquid crystal director modeling. *SIAM J. Sci. Comput.*, 35:226–247, 2013.

[66] A. Rapini. Instabilités magnétiques d'un smectique C. *J. Phys.*, 33:237–247, 1972.

[67] J. N. Reddy. *An Introduction to Continuum Mechanics*. Cambridge University Press, Cambridge, 2nd edition, 2013.

[68] F. Reinitzer. Beitrage zur Kenntniss des Cholesterins. *Monatsh. C hem.*, 9:421–441, 1888.

[69] F. Reinitzer. Contributions to the knowledge of cholesterol. Translation of References [68]. *Liq. Cryst.*, 9:7–18, 1888.

[70] C. Reiter. Liquid crystals show potential for detection of neuro-degenerative disease. `https://news.uchicago.edu/story/liquid-crystals-show-potential-detection-neuro-degenerative-disease`, Sept. 2015.

[71] R. Ribotta and G. Durand. Mechanical instabilities of smectic-A liquid crystals under dilative or compressive stresses. *J. Phys.*, 38:179–204, 1977.

[72] M. Schadt and W. Helfrich. Voltage-dependent optical activity of a twisted nematic liquid crystal. *Applied Physics Letters*, 18(4):127–128, 1971.

[73] J. V. Selinger, J. Xu, R. L. Selinger, B. R. Ratna, and R. Shashidhar. Theory of chiral modulations and fluctuations in smectic-A liquid crystals under an electric field. *Phys. Rev. E*, 62:666–674, 2000.

[74] T. J. Sluckin, D. A. Dunmur, and H. Stegemeyer. *Crystals That Flow: Collected Papers from the History of Liquid Crystals*. Taylor and Francis, London and New York, 2004.

[75] T. Soddemann, G. K. Auernhammer, H. Guo, B. Dünweg, and K. Kremer. Shear-induced undulation of smectic-A: molecular dynamics simulations vs. analytical theory. *Eur. Phys. J. E*, 13:141–151, 2004.

[76] M. J. Stephen and J. P. Straley. Physics of Liquid Crystals. *Rev. Mod. Phys.*, 46:617–704, 1974.

[77] F. Stewart and I. W. Stewart. A novel method for measuring compression constants in smectics. *Mol. Cryst. Liq. Cryst.*, 478:23–32, 2007.

[78] I. W. Stewart. *The Static and Dynamic Continuum Theory of Liquid Crystals*. Taylor and Francis, London, 2004.

[79] I. W. Stewart. Dynamic Theory for Smectic A Liquid Crystals. *Contin. Mech. Thermodyn.*, 18:343–360, 2007.

[80] I. W. Stewart. Continuum theory of biaxial nematic liquid crystals. In G. R. Luckhurst and T. J. Sluckin, editors, *Biaxial Nematic Liquid Crystals: Theory, Simulation and Experiment*, pages 185–203. John Wiley & Sons, Chichester, England, 2015.

[81] I. W. Stewart and F. Stewart. Shear flow in smectic A liquid crystals. *J. Phys. Condens. Matter*, 21:465101, 2009.

[82] H. Takezoe and A. Eremin. *Bent-shaped liquid crystals: structures and physical properties*. CRC Press, 2017.

[83] E. G. Virga. *Variational Theories for Liquid Crystals*. Chapman and Hall/CRC, 1st edition, 1994.

[84] A. Walker and I. Stewart. Couette flow of a smectic a liquid crystal. *J. Phys. Condens. Matter*, 21:155101, 2009.

[85] E. Weinan. Nonlinear continuum theory of smectic-A liquid crystals. *Arch. Ration. Mech. Anal.*, 137:159–175, 1997.

[86] F. M. White. *Fluid mechanics*. McGraw-Hill Education, New York, 2016.

[87] P. J. Wojtowicz, P. Sheng, and E. Priestley. *Introduction to liquid crystals*. Springer, 1975.

[88] D. Yang and S. Wu. *Fundamentals of Liquid Crystal Devices*. John Wiley & Sons, Ltd, 2nd edition, 2014.

[89] J. You, J. Y. Jung, K. Rhie, V. M. Pergamenshchik, and S. T. Shin. Macroscopic properties of the nematic phase of boomerang-shaped C7: Evidence of biaxiality. *J. Korean Phys. Soc.*, 52:342–349, 2008.

[90] J. A. Zasadzinski, L. E. Scriven, and H. T. Davis. Liposome structure and defects. *Philos. Mag. A*, 51:287–302, 1985.

[91] H. Zocher. Über die Einwirkung magnetischer, elektrischer und mechanischer Kräfte auf Mesophasen. *Phys. Zietschr*, 28:790–796, 1927.

[92] H. Zocher. The effect of a magnetic field on the nematic state. *Trans. Faraday Soc.*, 29:945–957, 1933.